A study of bioreactor surfaces for cell interactions and sensing

-

Rachel Marina Khan, BSc (Hons)

School of Engineering and Materials Science

Queen Mary, University of London

Thesis submitted for the degree of Doctor of Philosophy

2013

Statement of originality

I certify that this thesis, and the work embodied within it is the product of my own research and has not been previously submitted for a degree in any other university. Any ideas or quotations from the work of others published or otherwise are fully acknowledged in accordance with standard referencing practices.

During the course of this degree, parts of the research have been presented in poster or oral form at various scientific conferences and meetings. Written articles also contributed for publication are listed in the appendices.

ABSTRACT

Polymeric hydrogels were used to create bio-smart hydrogels serving *multi-functional* roles interfacing with cells and enzyme substrates. Their value lies in their use as:

i) Stimuli- responsive membranes that directly transmute chemical potential energy into proportionate electrical signals, ii) as biomimetically inspired biocompatible coatings on stents and other implantable bionic devices, iii) as bio receptor hosting membranes for enzyme-based implantable biosensors. Biosensors use oxidoreductase enzymes such as glucose oxidase (GOx) and lactate oxidase (LOx) to confer specificity. Such enzymes may initiate more complex *in vivo* inflammatory response. In this thesis individual and combined effects of different enzymes (GOx, Superoxide dismutase (SOD), and catalase) were studied to achieve hydrogel-enzyme systems, which in theory may mitigate against adverse cell outcomes.

The incorporation of enzymes into bioactive hydrogels was investigated, and revealed effects on the growth, viability and attachment of surface dependant RMS13 human muscle fibroblasts and B50 rat neuronal cells. Agarose and p(HEMA)-based hydrogels were prepared with fibrinogen 5% (w/v) to promote integrin-mediated cellular attachment and also with different combinations of glucose oxidase (GOx), catalase (CAT) and superoxide dismutase (SOD). Cell viability was maintained best on catalase hydrogels. The presence of GOx within hydrogels membrane compromised cell viability in both hydrogel types, presumably due to accumulation of H_2O_2 confirmed by amperometric detection using fabricated platinum needle electrodes. Hydrogels prepared with GOx and CAT showed

improved cell viability, further suggesting the negative influence of H_2O_2. High temperature treatment of the enzyme-hydrogel membranes, resulting in enzyme denaturation, returned all constructs to control levels of viability, confirming the relationship of cell viability with enzyme activity.

An additional study was undertaken into the viability and growth of B50 cells on crosslinked protein membranes of fibrinogen and albumin as a potential bioreactor surface. The use of crosslinked fibrinogen to facilitate cell growth within microfluidic channels appears to have been realized. Fabrication and use of miniaturized gold-filled silica recess and inlaid disc electrodes, compared with the use of agarose gels in the recesses was investigated to improve stabilization of an amperometric H_2O_2 electrode. From this, a microfluidic device with an integrated inner diameter working and counter / reference electrode was fabricated which showed feasibility of more rapid amperometric detection of H_2O_2 in miniature flow channels.

Acknowledgements

I will forever be indebted for the support and guidance provided to me by my supervisor Professor Pankaj Vadgama; without your insightful knowledge and persistent faith in me, this thesis would not be possible. I am grateful to you for motivating me to strive for perfection. Secondly, I would like to thank Professor Anthony Guiseppi-Elie from Clemson University (South Carolina) and Dr Annette Guiseppi-Elie, for giving me the opportunity to present my research internationally. I have learned a lot from our stimulating discussions that have enabled me to develop myself as a scientist, thank you for never allowing me to lose sight of the task at hand. Dr. Andrei Sapelkin from the Department of Physics, my second supervisor for whom I am grateful for providing me the use of his laboratory and cell culture facilities.

I would also like to thank Shafir Iqbal and Chris Mole for your advice on cell culture techniques. Michaela Egertova from the school of biological and chemical sciences for all the help and advice provided on confocal microscopy.

I am grateful for the administrative support provided by Jonathan Hills and the extremely helpful Catherine Jones; your words of wisdom will most definitely be remembered! To my colleagues; Dr. Hong Chang, Hussein Eshadi-oskoi, Dr. Zimei Rong, Dr. Wenjun Zhang, Zhencheng Xu, I am grateful to you for your encouragement and advice. A special thanks to Dr. Salzitsa Anastasova and

Dr. Anna-Maria Spehar-Deleze for all your guidance particularly in the last few months of my project. Without the wealth of knowledge between you I would have been lost, you are both excellent mentors.

My fantastic, supportive, friends Jayshree and Abira; without your stimulating and consistent pep talks I would not have been able to focus and persevere through my studies.

I am truly thankful to my family, my incredibly ambitious and inspirational brother and sister-in-law, Louis and Danya; for all your advice, motivation and for believing in me. Louisa, for being such a wonderful big sister and for listening to my rants (no pun intended). To my beautiful niece Leonie and nephew Nathaniel, thank you for keeping me entertained and for being a wonderful distraction from my studies every time I visit. My extended marital family, grandparents Gurdial and Rachhpal Dhillon, Harinder Bajwa (my second mother) and Ricky (my brother from another mother) for all your reprographic assistance! Thank you for welcoming me into the family.

I am infinitely grateful to my amazing husband Taj for providing me with unconditional love and support throughout. Thank you for being so considerate of my ambitions and dreams, even when at times it meant neglecting you!

Last but by no means least I would like to dedicate this thesis to two of the most influential people in my life, my parents Mickey and Dorothy. Thank you for planting the seeds of wisdom in my mind and for encouraging me to be the best that I can be. Without your continued support I would not be the person I am today, nor would I have been able to accomplish such a momentous achievement.

Table of Content

List of Figures

List of Tables

List of symbols and abbreviations

PDMS: Poly(dimethylsiloxane)

PMMA: Poly(methylmethacrylate)

BSA: Bovine serum albumin

TCL: Terephthaloyl chloride

BioMEMs: Biomedical microelectromechanical systems

t: Time

PBS: Phosphate buffer saline

DMEM: Dulbecco's Modified Eagle's Medium

FBS: Fetal Bovine Serum

DPBS: Dulbecco's Phosphate buffered Saline

SEM: Scanning Electron Microscopy

GOx: Glucose oxidase

SOD: Superoxide dismutase

CAT: Catalase

Pt: Platinised

ECM: Extracellular matrix

FN: Fibronectin

RGD: Arginine-glycine aspartate

CAMs: Cell adhesion molecules

FAK: Focal adhesion kinase

HA: hyaluronic acid

hGH: human growth hormone

PGA: Poly gycolic acid

GAG: glycosaminoglycan

HEMA: 2-hydroxyethyl methacrylate

MPC: 2-metacryloyloxyethyl phosphorycholine

DMAEMA: N-N-(dimethyl(amino) ethylmethacrylate

TEGDA: tetraethyleneglycol

K_m: Michaelis constant

V_{max}: Maximum velocity

K_{cat}: Catalytic turnover

AA: Acetaminophen

AC: Ascorbic acid

DAMP's: Damage associated molecular patterns

CHAPTER 1

-

Introduction

1.0 Introduction

1.1 Background and motivation

Biomaterial interactions influence cell-cell communication, which affect the maintenance of normal tissue function [1]. Extra cellular matrix proteins facilitate cellular attachment, cell spreading and the formation of focal adhesions *via* integrins [2]. Studies have revealed that the lack of cellular attachment can initiate adverse biological responses. In recent years we have seen a rise in the development of various biocompatible micro devices for applications from biosensors throughout tissue engineering. These devices exploit the use of both natural and synthetic materials to increase biocompatibility. In particular, biomimetic hydrogels have been proposed as bioreceptor hosting materials used in implantation [3]. This is mainly due to the stabilizing nature of hydrogels on the activity of bio molecules such as enzymes [4] and antibodies [5].

The relationship between microfluidics and hydrogels can be established through understanding the significance of these devices and constructs within the following disciplines:

- Bioreactor engineering

  Whole cell bioreactors within the field of bioreactor engineering promote the transformation of pharmaceutically relevant biomolecules from various biochemicals to extend viability and proliferation of cells grown within hydrogels [6].

- Regenerative medicine

The development of 3-D constructs such as hydrogels for use as artificial tissues and organs [7] require the use of perfused constructs for efficiency in the delivery of nutrients and removal of waste products. Therefore understanding the processes of flow and diffusion are of importance for use as 3-D scaffolds and matrices for cell/tissue growth.

- Implantable biosensors

Biosensors are subject to microflows of extracellular fluids in the vicinity of implantable devices. Understanding the properties of cell binding and adhesion at the biointerface of implantable biosensors is of vital importance in evaluating biocompatibility.

Amperometric enzyme biosensors provide accurate and precise measurement of analytes such as glucose and lactate *in vitro*. Since the development of the first described biosensor [8], there has been little success in the commercialization of long term implantable biosensors [9], with a typical loss in sensitivity observed following 1-2 months of implantation [10]. Failure of these implantable devices can occur as a result of the following:

1) Foreign body response, where the device becomes encapsulated by fibrous collagens, preventing the transport of analytes across the otherwise functioning device [11].

2) Protease degradation of the immobilized enzyme [12]

3) Denaturation of the immobilized enzyme by the molecular environment, which induces protein unfolding, resulting in the loss of biorecognition [13].

4) Changes in membrane properties as a result of temperature/ time leading to the

lack of transport.

5) Materials failure such as changes in electrical connectivity or delamination of membranes [14].

6) Electrode surface passivation by small molecules present in tissue in the case of electrochemical biosensors [15]

Despite the development of biocompatible hosting materials, degradation of the biorecognition layer of these devices persists, which may be due to the lack of biomaterial biocompatibility [16]. This thesis investigates whether oxidative stress induced by the interaction of the immobilized bioreceptor (Glucose oxidase) with its substrate (glucose) is responsible for the viability of RMS13 human muscle fibroblasts and B50 rat neuronal cells cultured on host compatible p(HEMA) and agarose hydrogels. In addition to this the fabrication and stabilization of recess and non-recess electrodes is investigated with the use of agarose gel as a potential stabilization matrix. Also explored is the viability and growth of crosslinked protein membranes to enhance cell attachment of B50 cells. The final objective of the study was to design and fabricate a sensor integrated microfluidic device for the amperometric detection of analytes.

1.2 Organisation of thesis

The second Chapter of this thesis discusses basic concepts related to the study, and provides an overview of cell surface interactions and biomimemtic surfaces such as agarose and p(HEMA) hydrogels and the use and the methods of cellular immobilization within these matrices. Also discussed is the concept of enzymology and the history and development of biosensors. Concluding with an overview of the area of microfluidics, including the history and development, applications and general fabrication techniques. Chapter 3 describes the experimental techniques used in the synthesis of enzyme encapsulated p(HEMA) and agarose hydrogels. As well as the methods used to form crosslinked protein membranes. The fabrication and development of recessed and non-recessed electrodes and microfluidic devices used in this study is also discussed. Chapter 4 investigates the viability of RMS 13 and B50 cells on enzyme encapsulated hydrogels, with the detection of H_2O_2 produced from the enzymatic activity of GOx gels reported in Chapter 5. Also investigated is the stabilization of recess and non-recess electrodes using agarose gel as the stabilizing medium. The final results Chapter, Chapter 6 studies cell growth and viability on crosslinked protein membranes. Concluding this, chapter seven provides a general discussion of the results obtained with the advantages and disadvantages outlined, and the main findings highlighted. The future outlook of the research is also suggested.

CHAPTER 2

-

Literature review

2.1 Cell surface interactions

2.1.1 Basic membrane properties

All biological membranes have one common structure; each membrane has a very thin film of lipid and protein molecules held together by non-covalent interactions [17]. In general, cell membranes are dynamic structures, which enable the molecules within the structure to move within the plane of the membrane. Cell membranes are vital in the maintenance of the life of a cell; they define the boundaries of the cell's contents and help to maintain a balance between what is allowed inside the cell and what must remain exterior. Original research by Langmuir [18] suggested that the structure of biological membranes to be a lipid monolayer. He studied the behaviour of purified phospholipids by dissolving phospholipids in benzene and layering this solution onto the surface of water. Once the benzene had evaporated a lipid film approximately one molecule thick remained, thus comprising of a monolayer. Langmuir, like Singer and Nicolson concluded phospholipids to be amphipathic molecules possessing both hydrophobic and hydrophilic regions. The phospholipids are assembled into a bi-layer in which the hydrophilic heads of the phospholipids are on the outside of the bilayer and the hydrophobic tails form part of the internal structure of the bilayer. Figure 2.1 outlines the fluidic mosaic structure of a membrane as proposed by Singer and Nicolson in 1972. The key aspect of the model is that membranes are two-dimensional structures consisting of oriented phospholipids and globular proteins.

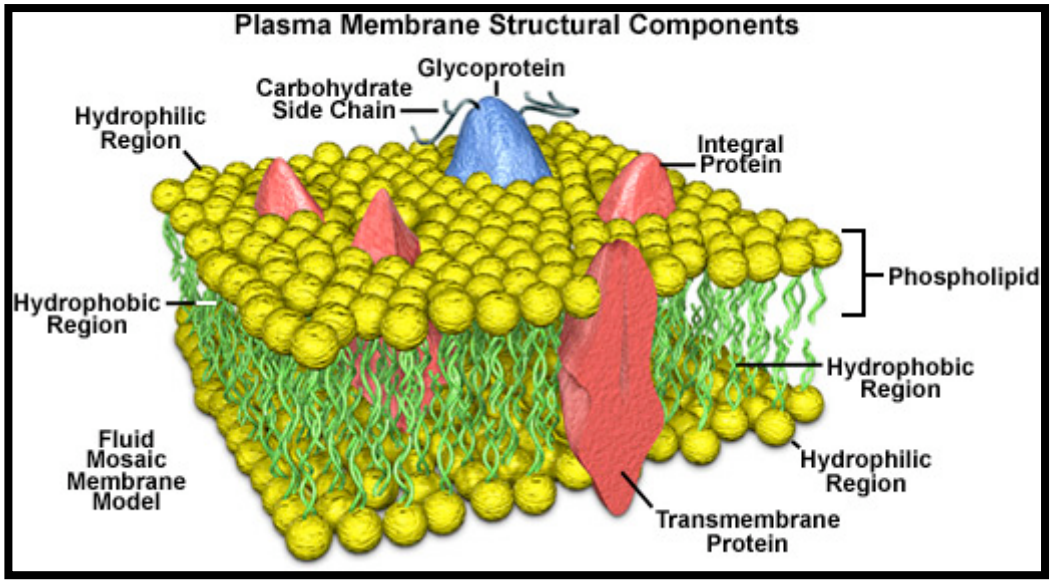

Figure 2.1: The fluid mosaic structure of a plasma membrane based on the Singer and Nicolson model. (Image obtained online from Michael W. Davidson, Florida State University Research Foundation).

Singer and Nicolson [19] proposed that the lipid bilayer had two main functions; one was to serve as a solvent for integral membrane proteins and the other as a permeability barrier. A membrane is able to do this because of its hydrophobic interior, which is effective in blocking hydrophilic molecules and ions. Molecules and structures embedded or localised within a membrane give rise to specific functions associated with them, proteins in particular code for specific functions within the body.

2.1.2 Membrane surface properties

The most obvious function of a membrane is its ability to define boundaries and compartments within a cell. Membranes also help in regulating the transport of substances that enter and exit a cell or a structure. Nutrients, ions and gases can be taken up through a membrane depending on its permeability. These substances move

partly in accordance with their concentration gradients; in the case of ions this occurs through charge and concentration gradients across the membrane. Molecules such as water, oxygen, and ethanol cross membranes through simple diffusion. Specific transport proteins through the process of facilitated diffusion aid other larger molecules such as amino acids. Biological membranes also consist of receptors found on the surface of the membrane; these receptors allow cells to detect and transmit electrical and chemical signals.

2.2 Biointerface and cell adhesion

The extracellular matrix (ECM) is a network through which cells are connected; it also further enhances cell movement during embryonic development. The interactions between the ECM and cells facilitate many cellular processes through cell signalling. Fibronectin (FN) is an essential protein component of the ECM that assembles into fibrillar form, thus allowing cellular attachment. Within the blood stream, fibronectin occurs in a compact form, which enables processes such as cellular tissue repair and blood clotting. RGD (arginine-glycine-aspartate) is a sequence motif within fibronectin that mediates cell attachment. Many proteins such as vitronectin, osteopntin, collagens, thrombospondin, fibrinogen and others including those of the ECM contain this tripeptide sequence which functions as a cell adhesion site recognized by cell surface receptors known as integrins [20], discussed in more detail in Section 2.2.1.

Cell adhesion molecules (CAMs) are proteins located on the surface of cells that interact and bind with other cells or the ECM enabling cellular adhesion. CAM's can be classified as transmembrane receptors composed of three subunits:

1) Intracellular – interacts with the cytoskeleton

2) Transmembrane – interacts with other CAMs of the same kind (homophillic binding)

3) Extracellular – interacts with CAMs of different kind or the ECM (heterophillic binding)

2.2.1 Integrin

Integrin proteins are known to be heterodimeric proteins consisting of two membrane subunits, alpha and beta, that penetrate the plasma membrane. Figure 2.2 demonstrates the interaction of fibronectin with cells at the surface through transmembrane proteins such as integrin. Fibrillogenisis is the transformation of proteins such as fibrinogen, fibronectin, and collagen from compact to fibrillar form. This is a highly regulated process that requires mechanical forces generated through cellular interactions.

Guan *et al* [21] described different combinations of alpha and beta subunits formed by differential splicing, which generated the formation of unique integrins.

The subunits of integrin proteins consist of cytoplasmic domains containing between 40-70 amino acids with a molecular mass varying from 90 – 160 kDa. Beta subunits consist of four cysteine amino acid sequences. Alpha and beta subunits also bind divalent cations, the cations of the beta subunits are involved in the coordination of ligand binding in integrins.

Integrins consisting of alpha chains that are included towards the N-terminal bind to collagens or act as cell –cell adhesion molecules. Integrins link the extracellular matrix of a cell to the cytoplasm, more specifically the microfilaments contained

within the cell. The ligand within the extracellular matrix that the integrin binds to is defined by the sequence of α and β subunits that make up the integrin itself. Integrins also mediate cell signalling by providing the cell with signals concerning the nature of its surroundings along with signals from receptors. These signals are vital in the cellular decision-making processes such as attachment, migration, and differentiation or programmed death.

Cell attachment occurs through a series of cell adhesion complexes. Cytoplasmic proteins such as talin, vinculin, paxillin and alpha-actin along with integrin work to regulate the kinases such as focal adhesion kinase (FAK) that are responsible for cell attachment, motility and survival. The series of adhesion complexes attach to the cell actin cytoskeleton enabling integrin to serve as a link between the extracellular matrix and the intracellular actin filamenteous system.

For tissue engineering integrins play a vital role in cell migration. Cells adhere to the manufactured substrate through integrins. During migration, cells attach to the substrate at its front and simultaneously release binding at its rear. During this process, the integrin molecules are taken back into the cell through the process of endocytosis and are transported to the cell to the front by the endocytic cycle where they emerge back into the surface. The outcome of this process is a form of recycling occurring at a cellular level that enables the cell to make fresh attachments at the leading front [22].

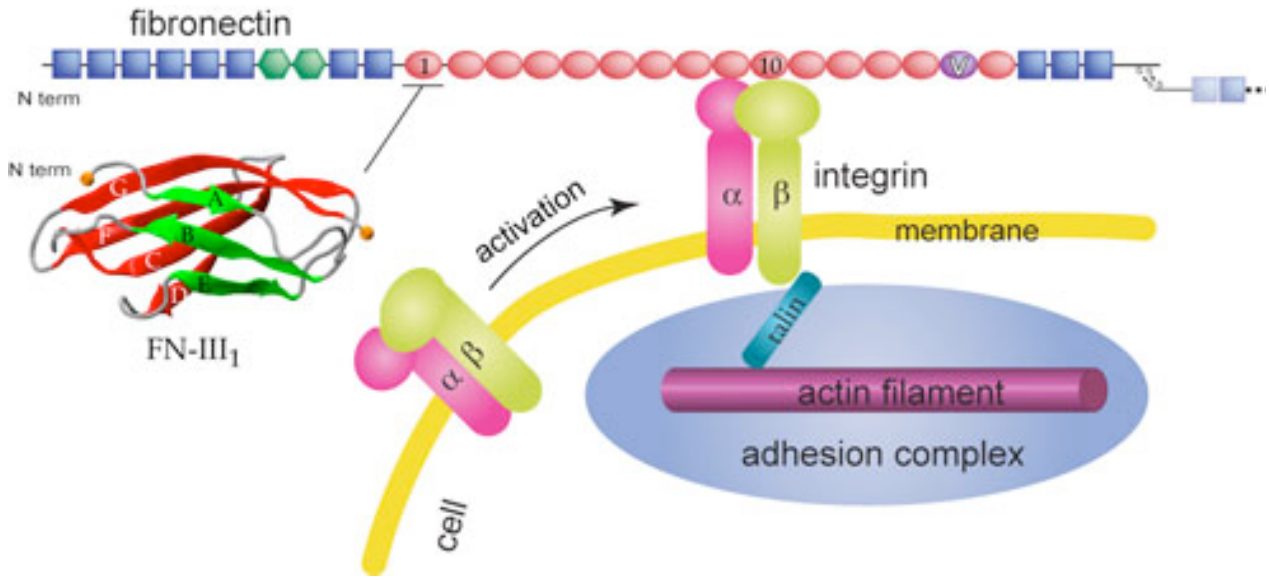

Figure 2.2: Schematic view of fibronectin bound to integrin at the cell surface. Image from Theoretical and computational Biophysics group, NIH Centre for Macromolecular Modeling & Bioinfomatics, University of Illinois at Urbana Campaign [23].

Research into the in vitro polymerization of fibronectin (FN) and its assembly into fibres by Ulmer *et al* [24] demonstrated the in vitro, formed fibres to be highly similar to a FN matrix produced by cultured fibroblasts. This was achieved through the use of high resolution scanning electron microscopy. Furthermore they showed the FN fibrils to support cell adhesion and to display antigenic epitopes, thus suggesting an ability of cells to mechanically make minor adjustments in the biological activity of the matrix through modulation of structure, surface properties and organization of fibrils

Ruoslahti *et al* [25] identified the use of more than ten RGD containing adhesion-promoting proteins for cell migration and for possible use as growth factors. When used alongside other cell growth factors such as collagen, fibronectin has been

known to anchor cells to the surface of collagen, thus increasing attachment properties. Other substances such as polylysine have also been used to enhance the growth of cells in tissue engineering. They work by altering the negatively charged surface of tissue culture flasks, formed from the plasma treatment of polystyrene, to a positive charge thus increasing the attachment of anchor dependant cells.

2.2.2 B50 cell line

The model cell line used within the current research was B50 rat hippocampal cells from an immortalised line. These cells were first established by Shubert *et al* [26] as clones of C1300 neuroblastoma cells. B50 cells have similar electrophysiological properties to nerve or nerve precursor cells. These cells have been described to grow in loose association with culture dish surfaces and consist of relatively spherical phase bright cell bodies. Due to the adhesive nature and ability of these cells to grow and proliferate on most untreated surfaces, it has been favourable to culture B50 cells on surfaces such as porous silicon as illustrated in Figure 2.3 [27]. Research to date has suggested that further investigations into changes in the morphology of the cells using growth factors are yet to be undertaken.

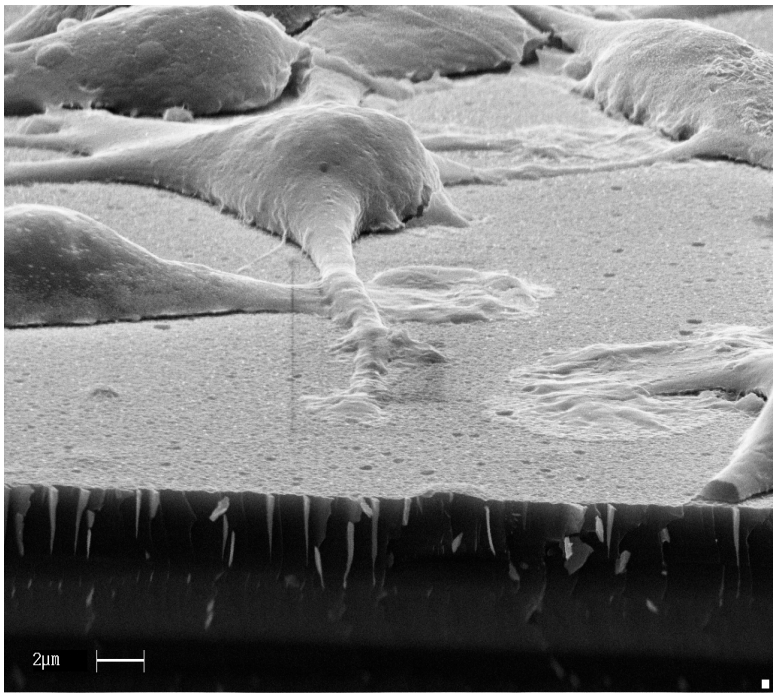

Figure 2.3: SEM image of B50 cell culture on porous Si wafer. Image from (Sapelkin *et al*) [27].

2.3 Biomimetic surfaces

2.3.1 Hydrogels

Hydrogels are networks of polymers that are hydrophilic and soluble; they are composed of super-absorbent natural or synthetic polymers that can absorb large quantities of water enabling them to give highly flexible gels, similar to natural tissue hence their being biocompatible [1]. Examples of synthetic materials for use as hydrogels include poly(ethyleneoxide) (PEO), poly(vinyl alcohol) (PVA), poly(acrylic acid) (PAA) and polypeptides. Naturally derived polymers used to form hydrogels include agarose, alginate, chitosan, collagen, fibrin, gelatin and hyaluronic acid (HA).

Common uses for hydrogels are:

- Scaffolds in tissue engineering - hydrogels may contain human cells in order to repair tissue.
- Environmentally sensitive hydrogels – sense changes in pH, temperature, or concentration of metabolites and release their load as result of such a change.
- Sustainable delivery systems
- In biosensors - responsive to molecules such as glucose or antigens
- In disposable diapers - to absorb urine
- Contact lenses – maintain flexibility and hydration of the eye
- Medical electrodes

2.3.2 Immobilisation of cells on hydrogels

Hydrogels can be engineered to be mechanically and chemically stable whilst ensuring their biocompatibility, which is essential for the successful culture of cells. The main methods for cellular immobilisation in hydrogels are adhesion, matrix entrapment and microencapsulation. In order for immobilization to be successful, the hydrogel must be permeable to enable sufficient diffusion and transport of oxygen and essential nutrients, metabolic waste and secretory products across the hydrogel network [28]. This is essential in sustaining the immobilized cells present. In general, a hydrogel should be non-toxic, inert and not interfere with cellular functions [28]. The biocompatibility of the hydrogel can be confirmed by cell viability and phenotypic expression of cells.

2.3.2.1 Adhesion

This method of immobilization for cells in hydrogels is based on the attachment of cells to the polymer substrate. It is generally used in the stabilisation of cells for culture or analytical procedures, providing structural support in directing cell growth and differentiation. This can be achieved by engineering hydrogels with bioadhesive properties. Another way in which cell adhesion is enhanced is through the addition of cell adhesive proteins or oligopeptides containing RGD motifs [25]. This preserves the permeability of the hydrogel whilst increasing cellular adhesion. Colloud *et al* [29] investigated the use of chitosan-loaded hydrogels for topical delivery of hexylaminolevulinate to epithelial cells in the oesophagus. Following the administration of chitosan gels loaded with the drug, fluorescence diagnosis confirmed the delivery of the drug to the epithelium after 10 min.

The physical characteristics of the hydrogel can also impact on adhesion affinity, therefore modification of the pore size and network structure of the gel can alter cell adhesion as well as impacting on the morphology and function of the cell. Oxley *et al* [30] demonstrated this through the fabrication of macro porous hydrogel membranes involving the polymerisation of a solution of monomers around a crystalline matrix. The method used was the freeze thaw technique involving the initial formation of ice based crystalline matrices. The second technique adopted was the porosigen method, whereby a crystalline compound such as sucrose was dispersed in the monomer solution prior to its polymerisation. It was noted that the composition of the copolymer and the polymerisation conditions were found to influence membrane morphology. With the adhesion method for cell immobilisation,

cells are usually cultured on the surface of the hydrogel and allowed to attach and migrate. Essential nutrients are supplemented via cell culture media.

2.3.2.2 Matrix entrapment

Matrix entrapment involves the physical constraint of cells within the hydrogel network. The technique can also be known as macroencapsulation when cells are isolated and protected by the gel matrix. The crosslink structures of synthetic and naturally derived hydrogels provide a 3-dimensional porous network which holds the cells in place whilst still permitting nutrients, waste, and essential molecules to be transported in the bulk fluid [28]. The key requirement of this method for cell immobilization is that a uniform cell distribution can be achieved and that the conditions for the formation of the cell –hydrogel matrix must be mild, without the use of harsh solvents, toxic monomers, U.V. radiation or high temperatures that could affect the viability or phenotypic expression of the cells. Awad *et al* [31] hypothesised that differentiation and growth of adult stem cells within engineered tissue constructs would be influenced by cell-biomaterial interactions. The study compared the chondrogenic differentiation of stem cells seeded in alginate and agarose hydrogels compared with porous gelatine scaffolds, as well as cartilage constructs. Cells that were encapsulated in the hydrogels exhibited spherical cell morphology, whilst cells in gelatine scaffolds were polygonal in shape. There was no indication that the difference in cell morphology hindered the chondrogenic differentiation of cells.

O'Connor *et al* [32] proposed the immobilization of embryonic day 18- rat cortical neurones maintained in culture for up to 24 days in agarose and type 1 collagen gels, to gain a better understanding of the interaction between neurones and ECM

equivalents. The live / dead staining of neuronal cultures in low-density collagen gels was monitored over a period of 3 weeks. The results revealed that at day 14 more than 50% of cells in collagen were viable compared with agarose, which indicated decreased cell viability. In-situ cell death detection showed the majority of dead cells in the gels underwent apoptosis. Collagen-trapped neurones exhibited normal neuronal polarity and developed long neurites estimated at over 500 μM. Overall it was concluded that collagen due to its major ECM matrix constituent, suppressed apoptosis and provided a suitable substrate for neuronal survival and differentiation.

2.3.2.3 Microencapsulation

The method of microencapsulation involves a thin microporous semi-permeable gel membrane surrounding a single cell or a small cluster of cells. The key requirement for cell encapsulation is that the hydrogel membrane is permeable, thus allowing transport of oxygen, nutrients and cellular products but inhibiting immune cell response [28].

Hydrogel capsules must also be able to withstand prolonged implantation without breaking or dissolving to prevent loss of the immunoprotective capability [33].

This is particularly useful in gene therapy as demonstrated by Chang *et al* [34] in the delivery of recombinant gene products using microencapsulated cells in vivo. Mouse Ltk^- cells transfected with human growth hormone (hGH) gene was encapsulated in immunoprotective permeably selective alginate microcapsules. Allogeneic mice that were implanted with the microcapsule demonstrated hGH within 2 weeks. Control studies carried out on mice without the implanted microcapsules confirmed the absence of significant hGH levels. After a period of 3 weeks, antibodies against hGH developed in microcapsule implanted mice. It was noted that the production of antibodies continued to rise for more than 3 months, but there was demonstration of

the continued delivery of growth hormone. The retrieval of the microcapsules showed an increase in viability, proliferation and production of hGH in transfected cells for up to 78-111 days. It was concluded there was feasibility of alginate microcapsules for use over prolonged periods, which is particularly useful in the application of gene therapy.

2.3.3 Hydrogels derived from natural materials

Hydrogels derived from natural materials have recently been investigated for tissue engineering. These materials include agarose, alginate, methylcellulose, hyaluronan (HA), collagen and chitosan. The key advantage to the use of naturally derived hydrogels within tissue engineering is the biocompatible nature of these materials. This is due to the components or macromolecular properties of these materials being similar to the ECM. For example collagen is the main protein of the ECM making up to 25% of protein mass in mammals [35]; 19 types of collagen exist. The basic structure of all collagens is three polypeptide chains which wrap around one another to form a three stranded single structure, held together by hydrogen and non-covalent bonds [36]. Collagen can also self aggregate to form stable fibres. These fibres along with collagen scaffolds can be created with their mechanical properties enhanced by the incorporation of crosslinkers such as glutaraldehyde, formalin and carbodimide [37]. Crosslinking by physical treatments such as U.V, freeze drying and heating can be used to combine collagen with other polymers such as HA, chitosan, poly gycolic acid (PGA) [38]. Collagen is degraded by metalloproteases such as collagenase, and synthesis controlled by cells or engineered tissues [36].

HA is a simple glycosaminoglycan (GAG) found in most mammalian tissue and fluids. Structurally it is a linear polysaccharide with a 1-3 repeating disaccharide and 1-4 linked β-d-glucuronic acid and *N*-acetyl-β-d-glucosamine units [39]. HA hydrogels are formed by covalent crosslinking with hydrazide derivatives, by esterification, or by annealing [40]. In addition to this, HA can be coploymerised with both collagen and alginate to form composite hydrogels [41]. Like most naturally derived hydrogels, HA can be easily degraded.

Chitosan is also structurally similar to GAGs and can be degradable by enzymes within the body. It also comprises a linear polysaccharide of 1-4 linked D-glucosamide and N-acetyl D-glucosamine residues derived from chitin [35]. Chitosan is soluble in dilute acid, once dissolved it can be gelled by increasing pH or extruding the solution to a non-solvent. Derivatives of chitosan can also be crosslinked, U.V irradiated or thermally varied through linkage with other polymers [42].

2.3.3.1 Agarose

Agarose is a purified linear galactan hydrocolloid obtained from agar that is isolated from a species of seaweed and is used in a variety of life science applications, especially in gel electrophoresis. Chemically it is a linear polysaccharide consisting of alternating D-galactose and 3,6-anhydro-L-galactose monomer units demonstrated in Figure 2.4.

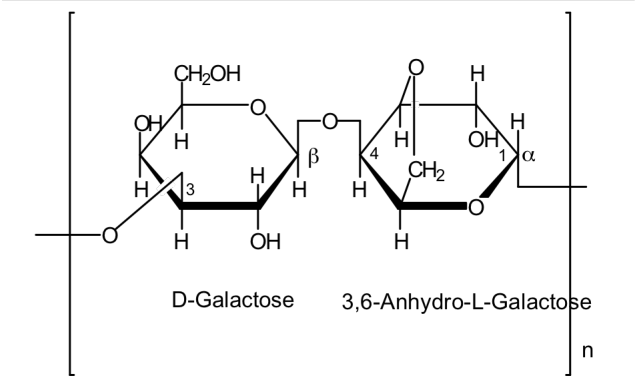

Figure 2.4: Structure of monomer repeat unit of agarose. Image obtained online from Sigma Aldrich Co.

Unlike many other hydrogels, agarose formation is not due to polymerization mechanisms but to non- covalent bonding. In aqueous solutions of approximately 35^{O}C the polymer strands are held together within the porous gel through non-covalent interactions such as hydrogen bonds and electrostatic interactions to form aggregates. When heat is applied these non-covalent interactions are broken thus resulting in separation of the strands and fluidisation. When cooled, the non-covalent interactions are re-established thus resulting in the formation of a gel.

The uses of agarose can be summarized as:

- Separation of nucleic acids through electrophoresis due to the larger pore size of agarose in comparison with polyacrylamide gels even at low concentration
- Demonstration of cross-reactions in immunoelectrophoresis (IEP)
- Formation of gel plates for cells in tissue culture
- Formation of gel matrices, beaded or crosslinked for chromatographic separations.

Agarose forms an inert matrix that is particularly utilized in separation techniques. Biological structures such as proteins easily affix to agarose, this is due to the double helical structure, which consists of multiple chain aggregates [43]. The thermo-reversible nature of agarose makes it a favourable choice for tissue engineering applications. Sakai *et al* [44] investigated the use of agarose as a biological scaffold for neurones and cartilage. More recently, research by Geckil *et al* [45] used agarose as a drug delivery vehicle by encapsulating live cells. Agarose contains very few moieties associated with cellular adhesion, which has resulted in low cell adhesion and proliferation. However, in recent years investigations have been carried out to enhance cellular adhesion to these hydrogels. Sreejalekshmi *et al* [46] introduced the idea of covalent coupling of cell adhesion peptides to agarose through modification of their chemical structure with laminin; the adhesion of cells to agarose was thus increased. Crompton *et al* [47] demonstrated a change in proliferation and growth of neurite cells on agarose by creating a copolymer with chitosan.

By lowering the mechanical stiffness of agarose, which can be achieved through using a low agarose concentration, it is possible to enable cell migration and proliferation. A similar method was investigated within this project in conjunction with the proteins fibrinogen and fibronectin known to enhance cellular adhesion and increase biocompatibility.

2.3.3.2 Synthetic polymer hydrogels

Synthetic hydrogels have been of interest within tissue engineering due to their reproducible and controllable chemical properties. Properties such as molecular weight, block structure, crosslinking mode and degradability can all be specified; this

in turn can determine gel formation dynamics and crosslinking density [3]. Examples of these are PEO and poly(ethylene gylcol) (PEG)

2.3.3.4 Poly(2-hydroxyethyl methacrylate)

The co-polymer of (2-hydroxyethyl methacrylate) (HEMA) and ethylene diamethacrylate was first developed by Wicherle and Lim in 1954 [48]. The polymerization of (HEMA) later developed to fabrication of the first soft hydrogel contact lens by Wicherle in 1961 [49]. This represented the first successful clinical application of hydrogel polymers. p(HEMA) hydrogels are not enzymatically degraded or hydrolysed by acidic or alkaline solutions which makes them attractive for some biomedical applications [50]. Studies have been conducted in which the structure of p(HEMA) has been modified to improve mechanical [51] and electro responsive properties [52] and to elicit better physiological responses [3].

Implantable integrated glucose and lactate biosensors were developed by Guiseppi-Elie [53] for use in monitoring during haemorrhage. Figure 2.5 demonstrates the constituents that make up the structure of p(HEMA) after polymerization through U.V. crosslinking. The fabricated devices comprised an amperometric biotransducer within a micro disc electrode array with immobilized glucose oxidase and lactate oxidase within biorecognition layers of 3 mol% TEGDA cross-linked p(HEMA-*co*-PEGMA-*co*-HMMA-*co*-SPA)-p(Py-*co*-PyBA) electro conductive hydrogels. The device was then coated with a bioactive hydrogel layer containing phosphoryl choline and polyethylene glycol pendant moieties [p(HEMA-*co*-PEGMA-*co*-HMMA-*co*-MPC). *In vitro* cell proliferation and viability studies confirmed both polymers to be non-cytotoxic, however, the PPy-based electro conductive hydrogels showed greater cell proliferation compared to the non-PPy controls. The glucose and lactate biotransducers revealed linear dynamic ranges of 0.10 - 13.0 mM glucose and

1.0 – 7.0 mM lactate. The overall stability of the biosensor showed 80% response after 5 days of continuous operation at 37°C.

The gels are generally synthesized by free radical polymerization of acrylate and methacrylate monomers, with the free radical initiator excited thermally or via U.V light, p(HEMA) gels are typically prepared through the mixing of monomers, crosslinkers, pre-polymer, deionized water and ethylene glycol to obtain a homogenous solution of controlled viscosity and density to which the initiator is added.

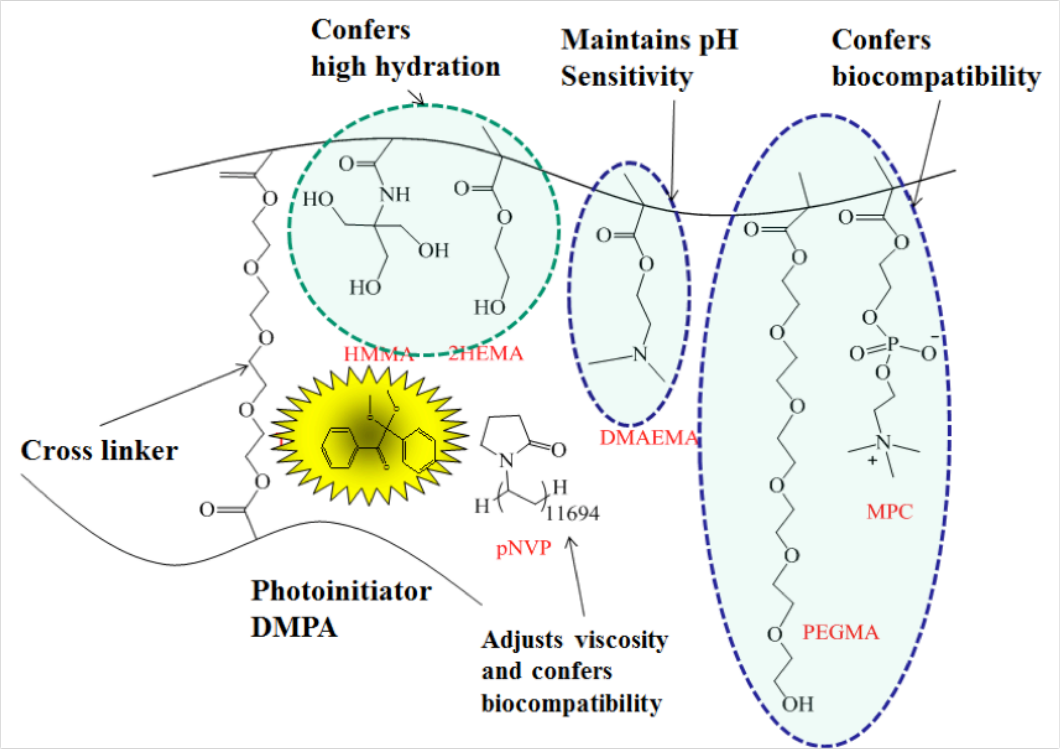

Key:
HMMA - ***N-[Tris(hydroxymethyl)methyl]acrylamide***
2HEMA - **2-Hydroxyethyl methacrylate**
DMAEMA- **2-(Dimethylamino)ethyl methacrylate**
pNVp - **Polyvinylpyrrolidone**
MPC - **2-(Methacryloyloxy)ethyl 2-(Trimethylammonio)ethyl Phosphate**
PEGMA - **Poly(ethylene glycol) methacrylate**

Figure 2.5: Partial p(HEMA) hydrogel structure. Image adaptation of Kotanen *et al*, Bioactive Electroconductive Hydrogels Yield Novel Biotransducers for Glucose (Wiley 2012) [54].

Controlling the mole percentage of the crosslinker relative to the reactive monomer allows for control of molecular weight between crosslinks. Kotanen *et al* [55] investigated the effect of cross-link density on the diffusivity of calcium ions through cell culture compatible p(HEMA) hydrogels. The gels each possessed 1.0% 2-metacryloyloxyethyl phosphorylcholine (MPC) and 5mol% N-N-(dimethyl(amino)ethylmethacrylate (DMAEMA) and ca. 17mol% n-butylacrylate (n-BA) To determine whether varying the crosslink density governs transport of calcium ions across hydrogel membranes, cross-linking density was varied by changing the composition of the crosslinker tetraethyleneglycol (TEGDA). The hydrogel membranes were cast on to track etched polycarbonate cell culture inserts before polymerization via U.V. light. The polymerized gels were then immersed in HEPES buffered calcium chloride solution and transport of calcium ions across the hydrogel monitored using a calcium ion selective electrode set within the insert. The resulting diffusion coefficients' were dependent on, and shown to exponentially decrease with increase in crosslink density.

A recent study into the effect of crosslink density of p(HEMA) gel influence on cell growth and proliferation was investigated by Guiseppi-Elie *et al* [56]. Adherent cells were cultured for 4,8,12 days on hydrogels consisting of crosslink densities between 1-12 mol% (TEGDA) and compared to silicone and agarose controls. The study revealed that short-term cell viability and long term proliferation of cells were favoured on low crosslink density hydrogels.

2.4 Enzymes as biological catalysts

Protein catalysts known as enzymes mediate cellular reactions and processes. In general all catalysts share three basic properties:

1) They increase the rate of a reaction by lowering the activation energy requirement, thus enabling a thermodynamically feasible reaction to occur at a reasonable rate without the need for thermal activation.

2) They form transient complexes with substrate molecules; the manner in which the binding occurs facilitates their interactions.

3) Only the rate at which equilibrium occurs is changed, there is no effect on the position of equilibrium [57].

The high level of catalytic efficiency of enzymes compared with chemical catalysts make the use of enzymes more favourable in industry [58]. In addition to this, the specificity of enzymes allows them to discriminate between reactions but also substrates (substrate specificity), similar molecules (regiospecificity) and optical isomers (stereospecificity).

2.4.1 Enzyme kinetics

Michaelis and Menten projected that a transition state forms when catalysis takes place and a substrate is converted to a product. The complex which is formed during the reaction is an enzyme substrate complex.

In the following equations, E = enzyme, S= substrate, ES= enzyme substrate complex, with k_1 and k_2 rate constants.

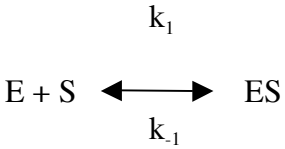

The enzyme-substrate complex then dissociates into the enzyme and product.

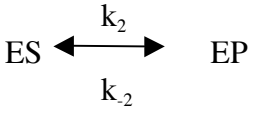

The rate constant k_1 refers to the conversion of an enzyme and a substrate to an enzyme-substrate complex. The reverse reaction is shown by k_{-1}, where the substrate is dissociated from the enzyme k_2 is the rate constant of the conversion of an enzyme-substrate complex into the enzyme and a final product [58].

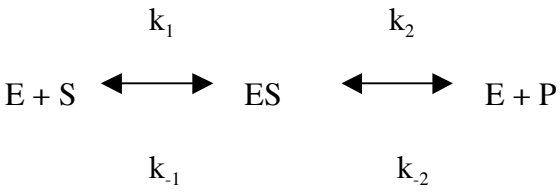

The rate of product formation is given by

$$\frac{d[P]}{dt} = k_2[ES]$$

The rate of formation of enzyme substrate complex is equal to the rate of its destruction, so the below expression can be derived

$d[ES]/dt = k_1[E][S]\ \ k_{-1}[ES] - k_2[ES] = 0$

The concentration of the enzyme substrate complex can be obtained by

$$[ES] = \frac{[E]_T[S]}{[S] + K_m}$$

Since the instantaneous enzyme concentration is equal to enzyme and enzyme substrate concentrations.

Therefore:

$$k_2[ES] = \frac{k_2[E]_T[S]}{[S] + K_m} \qquad \text{where } V_{max} = k_2[E]_T$$

Compared with chemical catalysts, enzymes operate under mild conditions of temperature, pressure and pH. However, unlike uncatalysed chemical reactions they display saturation kinetics. At given enzyme concentrations and low substrate concentrations, the reaction rate is said to be linear with respect to substrate concentration. Within the reaction process, enzyme molecules are free to catalyze the reaction. The increase in substrate concentration results in an increase in the rate at which the enzyme and substrate encounter. At high substrate concentrations the reaction rate reaches the theoretical maximum due to all the enzyme active sites being occupied by the substrate. The rate at which the reaction occurs is determined by the intrinsic turnover rate of the enzyme.

Figure 2.6 illustrates the general principal of enzyme kinetics. As larger amounts of substrate are added, the enzyme-binding site is limited to maximum velocity (V_{max}). Beyond this limit the enzyme is saturated with the substrate restricting the reaction rate from increasing. Knowing how quickly an enzyme is saturated with a particular substrate and the maximum rate of saturation is vital in the understanding of enzyme

behaviour in the cell and indicates how the enzyme responds to changes in its environment.

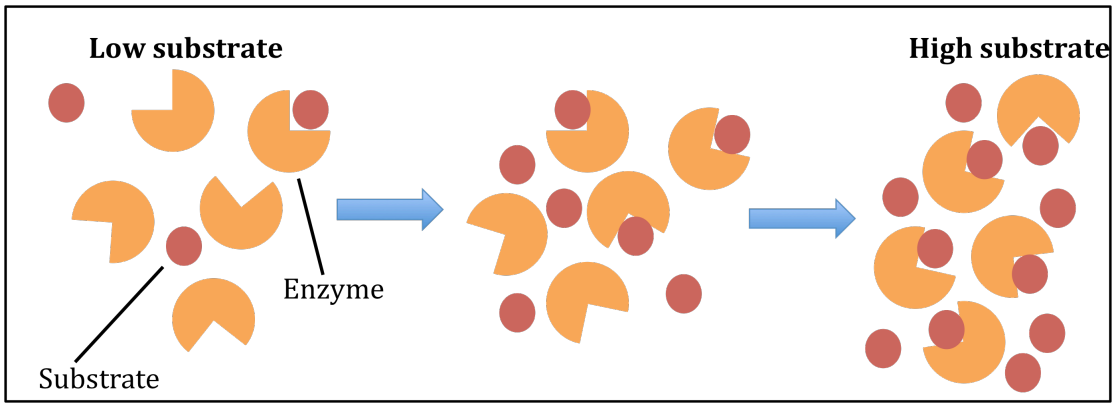

Figure 2.6: General principals of enzyme kinetics.

The Michaelis constant (K_m) is the substrate concentration at which the reaction rate is half of the maximum velocity (V_{max}). It is a measure of substrate affinity for the enzyme, shown in Figure 2.7. The value of K_m is dependant on the enzyme and substrate; a small K_m value indicates a high affinity, corresponding to an increase in the rate of reaction for a given concentration of substrate [59]. The value of K_m is therefore dependant on the enzyme and substrate in additional to experimental conditions such as pH and temperature.

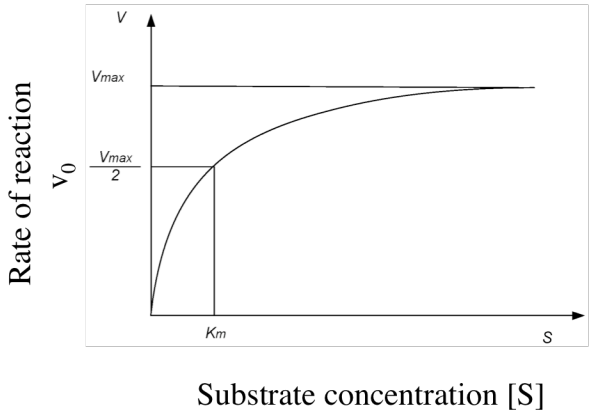

Figure 2.7: Michaelis-Menten plot of the reaction velocity (V_0) versus substrate concentration [S].

Each experimental point is obtained from a separate progress curve using the same concentration of enzyme. The shape of the curve is hyperbolic. At low substrate concentrations, the curve approximates to a straight line that rises steeply. In this region of the curve, the reaction is highly dependent on the concentration of substrate. At high concentrations of substrate, the enzyme is almost saturated, and the initial rate of the reaction does not change much when substrate concentration is further increased. The K_m value is useful in estimating where along the Michaelis-Menten plot an enzyme is functioning in a cell. This is based on the known normal substrate concentration in the cell. From this we can estimate at what fraction of the maximum velocity the enzyme-catalyzed reaction is preceding in the cell, therefore the K_m value is an indication of how effective an enzyme is [59].

2.4.2 Glucose Oxidase

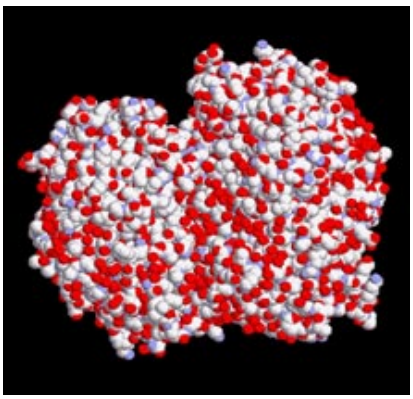

Figure 2.8: Atomic model of glucose oxidase. Image obtained online from Department of Chemistry, Cambridge University. Original source: Molecular dynamic simulation from the published crystal structure [60]**.**

Glucose oxidase (GOx) shown in Figure 2.8, is a flavoprotein oxidoreductase which catalyses the oxidation of β-D-glucose to produce D-glucono-1, 5-lactone and hydrogen peroxide. The catalysis involves two steps as outlined in Figure 2.9. Firstly the oxidation of B-D-glucose to D-gluconolactone is caused by a reductive half reaction with the transfer of protons and electrons of β-D-glucose to the enzyme.

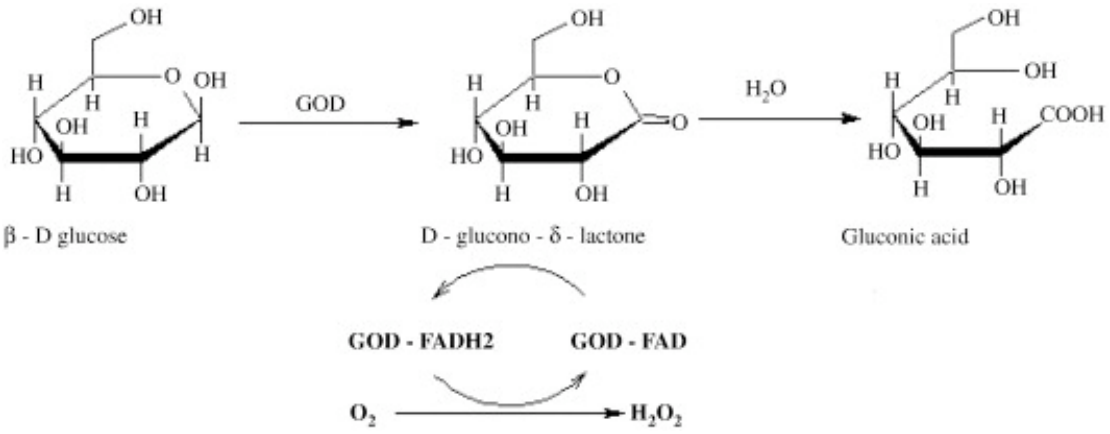

Figure 2.9: Reaction of glucose oxidase catalysed reaction. Image obtained from *Senel et al* [61].

The second step is when an oxidative half reaction takes place in which the enzyme gives up hydrogen peroxide when it is re-oxidised by molecular oxygen and D-gluconolactone is hydrolysed to gluconic acid [62].

Commercial uses of the enzyme include removal of small quantities of oxygen from food products and removal of glucose in food and drink for diabetics. Studies by Nakane *et al* [63] and Christofidou-Solomidou *et al* [64] proposed that glucose oxidase is an anticancer agent. Its hydrogen peroxide formation can cause damage to cancerous cells thus reducing the risk of the disease. It is also used in enzyme

immunoassays as an antibody and antigen marker and in medical applications for the quantitative determination of D-glucose in body fluids [65]. Following the development of the first reported biosensor by Updike and Hicks [8], which utilized the enzyme, in which the oxidation of glucose was detected through electrochemical techniques. This provides a useful application in diabetic patients [66].

2.4.2.1 General characteristics

Glucose oxidase is a relatively cheap and stable enzyme with a molecular weight ranging from 130 kDa to 175 kDa [67]. The unit Dalton quantifies the molar mass of a substance, i.e. equivalent to g/mol. The enzyme is specific to the β monomer substrate of D-glucose not the α monomer. Some of the inhibitors of the enzyme are Cu2+, hydrazine and sodium bisulphate.

Previous studies on the enzyme by Rando *et al* [68] and Hecht *et al* [69] have suggested that the optimum pH range of the enzyme is between 4 and 6. This is the pH at which the enzyme would have its maximum activity and the V_{max} would be high and K_m would be low. Glucose oxidase has an optimum temperature of 40-50^0 C but also works well enough at room temperature.

2.4.2.2 The use of GOx as an analytical reagent

The enzyme produces different product species, which can be used for the detection of the product in analysis. Kadish *et al* [70] and Wolfbeis *et al* [71] were one of the first researches to introduce glucose oxidase as an analytic reagent in homogeneous and heterogeneous assay applications. Kadish *et al* used the enzyme to quantify the concentration of glucose in urine. A spectrophotometric method was used to analyze

the coloured product at a wavelength of 436 nm when o-dianisidine coupled with peroxide. Another method proposed by Wolfbeis *et al* [71] was to use o-tolodine as a chromogenic oxygen acceptor with impregnated paper strips loaded with glucose oxidase and peroxidase. The paper strips were dried and immersed in test solution in order to compare with standard colour reactions of glucose oxidase. This method was used for determination of glucose in food and clinical samples. Witt *et al* [72] proposed a similar method to o-dianisidine but with another chromogenic substrate 2,2'-azino-bis(3-ethylbenzothiazoline-6-sulphonic acid (ABTS) which proved to be safer and more efficient [73]. Fourier transform infrared spectroscopy was used by Karmali *et al* [74] in which the kinetic properties of the enzyme were determined. The method was suggested to be useful since it monitors the reaction of both the substrate and product, which absorb at dissimilar frequencies.

2.4.3. Catalase

Virtually all living organisms exposed to oxygen contain catalase, which catalyzes the decomposition of hydrogen peroxide into water and oxygen according to, [75].

$2\ H_2O_2 \rightarrow 2\ H_2O + O_2$

The simplicity of the reaction of catalase can be broken down into two stages, however the mechanism of each stage is dependant on the type of catalase involved. In general, a single molecule of catalase has the ability to convert millions of molecules of hydrogen peroxide into water and oxygen, thus enabling catalase to have one of the highest turnover numbers of $2.25X10^7\ s^{-1}$ (K_{cat}) of all enzymes [75].

2.4.3.1 Structure and mechanism

Catalase exists as three classes of proteins that are not related in sequence or structure however they all exhibit catalase activity (Figure 2.10). The most common of the three is composed of monofunctional, heme-containing enzymes that are subdivided on the basis of large (>75 kDa) or small (<60 kDa) subunits. Klotz *et al* [76] studied the phylogenetic relationships among prokaryotic and eukaryotic catalase. It was concluded that two distinct classes or sub groupings of small subunit enzymes and one large class per subunit enzymes existed among mono-functional catalases.

The second class comprised bifunctional heme containing catalase-peroxidases closely related in sequence and structure to plant peroxidases. The third class included a non-heme or manganese (Mn) containing catalases.

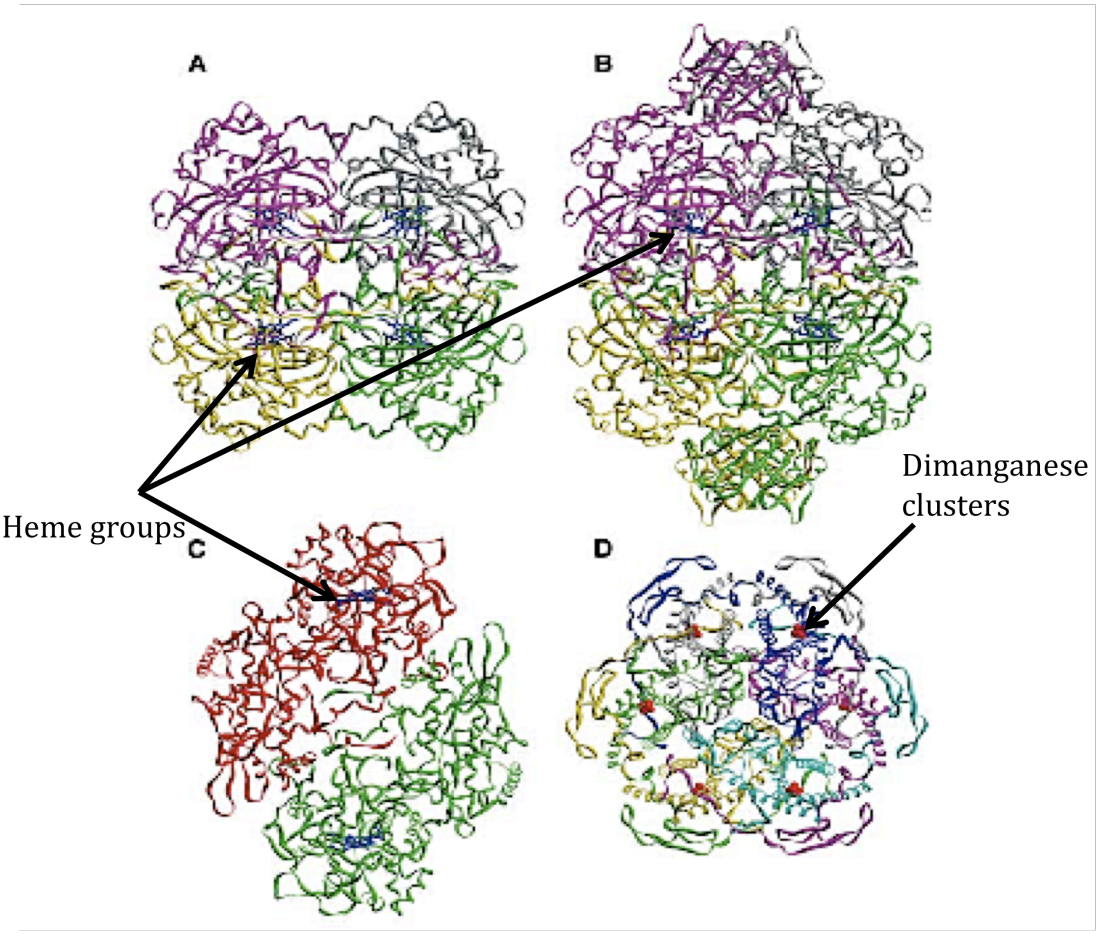

Figure 2.10: Ribbon structure of (A) tetrameric small subunit heme containing catalase, (B) large subunit catalase, (C) dimeric catalase-peroxidase and (D) hexameric diamanganese catalase. *The heme groups are represented in blue and dimanganese clusters in red. Image is an adaptation of Chelkani et al* [77].

The reaction of hydrogen peroxide with catalase occurs in two stages:

H_2O_2 + Fe(III)-E → H_2O + O=Fe(IV)-E(.+)

H_2O_2 + O=Fe(IV)-E(.+)→ H_2O + Fe(III)-E + O_2 [74]

The iron centre of the heme, represented above by Fe(III)-E is attached to the enzyme (E), in the reaction iron is not completely oxidized thus producing radical cations represented as (.+).

On entry to the heme cavity of the enzyme active site, hydrogen peroxide is sterically hindered and reacts with asparagine (Asn147) and histidine (His74) , at which the first stage of catalysis takes place. The transfer of a proton from one oxygen of peroxide to the other via His74 elongates and polarizes the O-O bond, which gradually breaks heterolytically as peroxide oxygen is coordinated to the iron centre (Fe) causing displacement of water and forming O+Fe(IV) plus a heme radical. The radical degrades in another one electron transfer to dispose of the radical electron, resulting in the heme ring being unaltered.

At the second stage a two electron transfer reaction of O=Fe(IV) with a second hydrogen peroxide produces Fe(III)E , water and a oxygen molecule. The efficiency of catalase may be due to the reaction of His74 and Asn147 with reaction intermediates. This mechanism is supported by experimental evidence indicating the modification of His74 with amino 1-2,4 triazole inhibits the enzyme by hindering substrate binding [78].

2.4.3.2 Cellular function

Many metabolic processes produce hydrogen peroxide as a by-product, which can be harmful and needs to be rapidly converted into less dangerous products. Catalase is therefore used to catalyze the decomposition of hydrogen peroxide into oxygen and water [75]. Studies by Ho *et al* demonstrated that mice that were genetically

engineered to lack catalase were still phenotypically normal [79]. This contradicts the theory by Laszlo *et al* [80] that a deficiency in catalase can lead to a probability of developing type II diabetes. Rao *et al* [81] conclude that hydrogen peroxide is used as an antimicrobial agent in infection. However pathogens in cells contain catalase, e.g. Mycobacterium tuberculosis, so microbial agents can deactivate the peroxide, enabling them to survive within the host.

Common uses for catalase in industry are:

- Removal of hydrogen peroxide from milk prior to the production of cheese
- Prevention of food oxidation from food wrappers
- Removal of peroxide from fabric
- In contact lens cleaning products to disinfect lens surfaces through decomposition of peroxide
- Skin care products combining catalase with hydrogen peroxide to increase cellular oxygenation of the upper layer of epidermis

2.4.4 Superoxide dismutase

Superoxide dismutase (SOD) is an enzyme which catalyses the disproportionation of superoxide free radicals through a specific redox reaction in which the superoxide molecule is simultaneously reduced and oxidized into oxygen and hydrogen peroxide:

$$2O_2^- + 2H_3O^+ \xrightarrow{\text{SOD}} O_2 + H_2O_2 + 2H_2O$$

Despite the importance of oxygen within the body, the presence of SOD is crucial as it serves as an important antioxidant defence system in virtually every cell exposed to oxygen. Early studies by Fridovich and Mc Cord [82] described SOD enzymes as various different metalloproteins with different functions. These exist as proteins cofactors with copper and zinc, iron, nickel or manganese.

The superoxide anion radical ($O_2^{\cdot}$-) is converted to O_2 and hydrogen peroxide (H_2O_2) at the rate of $\sim 10^5$ M^{-1} s^{-1} at pH 7. The order at which the anion is dismutated is second order with respect to the initial superoxide present. It has been shown that the half-life of superoxide is very short at high concentrations for example 0.05 seconds at 0.1 mM. However at low concentrations it is longer e.g. 14 h at 0.1nM.

The reaction of superoxide with SOD is first order with respect to the concentration of superoxide. The SOD catalytic efficiency (K_{cat}/K_M) is $\sim 7 \times 10^9$ $M^{-1}s^{-1}$ [83], this reaction rate is limited by diffusion of SOD towards the superoxide.

The reaction of superoxide, catalysed by SOD cofactors with metallic cation is demonstrated in the half- reactions written below:

$$M^{(n+1)+}\text{-SOD} + O_2^- \rightarrow M^{n+}\text{-SOD} + O_2$$
$$M^{n+}\text{-SOD} + O_2^- + 2H^+ \rightarrow M^{(n+1)+}\text{-SOD} + H_2O_2.$$

where M can be Cu (n=1); Mn (n-2) ; Fe (n=2); Ni (n=2)

Superoxide dismutase exists in three main groups that are determined by the metal cofactor to which they are bound. The structure and origin of these metal bound enzymes are outlined in Table 2.1.

Metal Cofactor	Copper and Zinc	Iron or Manganese	Nickel
Used by:	Eukaryotes	Prokaryotic, mitochondria, protists	Prokaryotic
Structure:	Eight stranded beta barrel. Active site held between the barrel and two subunits joined by hydrophobic and electrostatic interactions. Cu-zn-SOD also consist of six histidine and one asparate side chains.	Mn and Fe have same arrangement of alpha helices. Enzyme active sites also contain same arrangement of amino acid side chains.	Hexameric structure of right-handed 4-helix bundles, consisting of N-terminal hooks that chelate a Ni ion. Ni-hook contains the motif His-Cys-X-X-Pro-Cys-Gly-X-Tyr; it provides most of the interactions critical for metal binding and catalysis.

Table 2.1: Structure and type of metal cofactor SOD [84].

In humans there are three forms of SOD, SOD 1 is found in the cytoplasm and consists of two protein subunits bound to copper and zinc. This is a homodimer and converts superoxide radicals to molecular oxygen and hydrogen peroxide [83]. Clinical studies into mice lacking SOD 1 have revealed an increase in the early development of cataracts and other age related conditions, such as sarcopenia which is a degenerative loss of body mass [84].

SOD 2 is located in the mitochondria and is made up of four protein subunits with a manganese reactive centre. Similar to the other forms of SOD, SOD 2 transforms superoxide radicals formed as by-products in the mitochondrial electron transport

chain into diatomic oxygen and hydrogen peroxide [82]. Research by Van Rehman *et al* [85] opposes previous studies that indicate the deficiency of SOD enzymes results in shortened lifespan. However, it is revealed that 50% of studies conducted using mice deficient in SOD 2 showed there was a normal lifespan, but the mice suffered from increased DNA damage and an increased incidence of cancer.

SOD 3 is extracellular and is structurally similar to both SOD 1 and SOD 2. Like SOD 2, SOD 3 contains four protein sub-units and like SOD 1 is bound to both copper and zinc. Due to antioxidant properties, this product of the SOD genes is thought to protect the brain and lungs from oxidative stress [86].

2.5 Enzyme immobilization techniques

In recent years the catalytic properties of biological systems have been extensively exploited within the food industry and in particular medicine, in the development of microelectronic sensing devices. It is crucial that the fabrication of devices incorporating biological elements retain the stability of the biological component, thus the need for immobilization. A key benefit of immobilization is the ability to modify the behaviour of the biological element; the stability, specificity, and the kinetics can be modified for a more commercialized product.

Enzyme immobilization refers to physically confined or localized enzymes within a certain defined region of space, with retention of their catalytic activities and which can be used repeatedly and continuously [87]. The immobilization of enzymes has been of considerable interest particularly due to the beneficial effect of immobilized

enzymes over soluble enzymes. In particular, two key benefits of immobilized enzymes include the easy separation of the enzyme from the product, thus simplifying enzyme application and providing an efficient and reliable reaction. The second benefit being the ability to reuse the enzyme, which has proven to be cost effective. The first reported enzyme immobilization on a surface was carried out by Melson and Griffin in 1961 [88]. They bound a mixture of the enzyme invertase on to $Al(OH)_3$ and charcoal and proved the enzyme to be still catalytically active [88]. Following this the use of immobilized enzymes in industry in 1967 was achieved by Chibata *et al* [89] who immobilized *Aspergillus oryzae* animoacylase for the production of synthetic D-L amino acids. The main methods of enzyme immobilization as outlined in Figure 2. 11 include covalent coupling, entrapment, microencapsulation and cross linking.

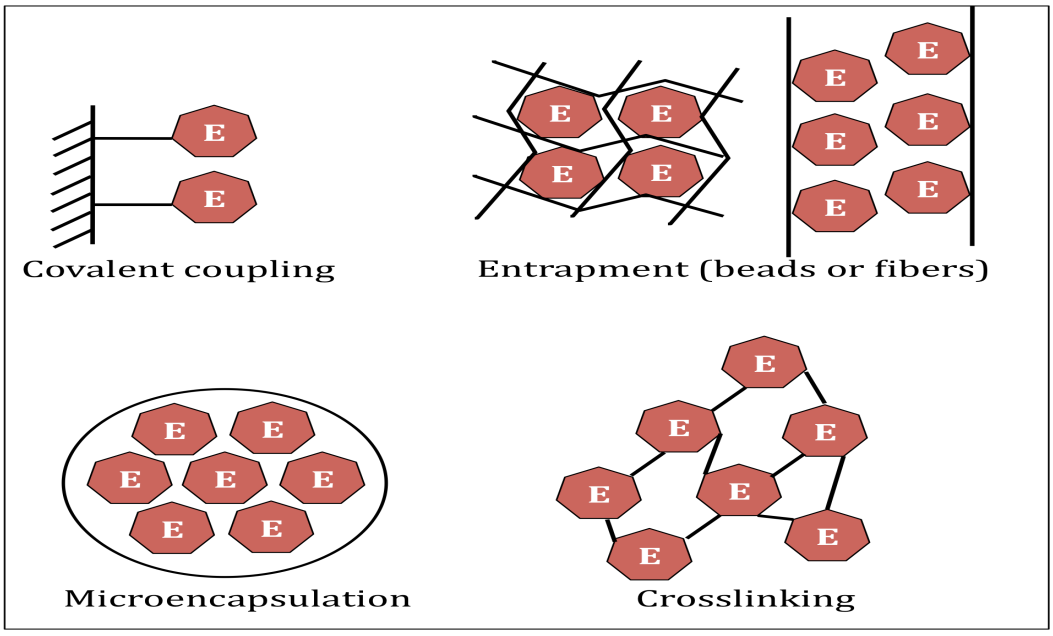

Figure 2.11: Methods of enzyme immobilization.

2.5.1 Adsorption and covalent coupling

The simplest method of enzyme immobilization is the adsorption of an enzyme onto an insoluble support. There are four main techniques used in which enzymes can be adsorbed, these include:

- Static procedure
- Electro-deposition
- Reactor loading process
- Mixing or shaking bath loading

Of the four techniques used, mixing is the most frequently used procedure.

This method involves mixing the enzyme with the support material under conditions appropriate for the enzyme; following the incubated period the insoluble material is separated from the soluble material by filtration or centrifugation. The main drawback of adsorption is that the enzyme is not bound firmly enough onto the support and changes with experimental conditions of temperature, pH, ionic strength, and the type of solvent used can give rise to desorption of the enzyme from the support. This is particularly noted in insoluble matrices such as DEAE-Sephadex, where the enzyme bound by salt linkages in the matrix are weakened [87]. Adsorption is a mild method of immobilization that has very little effect on catalytic activity; this is due to the binding consisting of mainly hydrogen bonds, multiple salt linkages and van der Waals forces, thus being similar to natural biological membranes [90]. Adsorption of the enzyme is also sometimes necessary in facilitating later covalent coupling.

The covalent coupling method of enzyme immobilization is based on the formation of a covalent bond between the enzyme and the support material. This method is the

most widely used method for enzyme immobilization due to the stability of the covalent bonds formed between the enzyme and matrix thus ensuring that the enzyme does not leech upon use. Some protein functional groups suitable for covalent binding include:

- alpha amino groups of chain ends and epsilon amino groups of lysine and arginine
- alpha carboxyl group of chain ends and beta and gamma carboxyl groups of aspartic and glutamic acids
- phenol ring of tyrosine
- thiol group of cysteine
- hydroxyl groups of serine and threonine
- imidazile group of histidine
- indole group of tryptophan

According to the linkage of the binding site, the method can be further classified into diazole, peptide or alkylation methods. Many in recent years have argued the effectiveness of covalent coupling. Garcia *et al* [91] argued that covalent binding of enzymes was a favourable method of immobilization as it prevented the removal of the enzyme from the surface particularly during the reaction and generally improved reusability of the enzyme. The benefit of covalent binding compared with free enzyme was demonstrated in studies carried out by Mao *et al* [92], who covalently immobilized cellulase and invertase. This resulted in the improved stability of the enzyme with respect to pH, temperature, reuse and storage compared to free enzyme in solution.

However, in contrast to this, it has also been observed that covalent binding can alter the structure and active site of the enzyme, thus resulting in a loss of activity and change to the substrate. Li *et al* [93] suggested that covalent attachment might result in the loss of activity compared to adsorption. Garcia *et al* [94] also reported a difference in the surface roughness and cross-sectional characteristics between substrates where cellulase was covalently immobilized and immobilized by adsorption. Despite the disadvantages of covalent coupling, the binding force between the enzyme and support material is strong enough to prevent leeching of the enzyme even in the presence of solutions or substrates of high ionic strength. The large range of binding reactions, and insoluble carriers with a variety of functional groups capable of covalent coupling makes this method of enzyme immobilization favourable.

2.5.2 Entrapment

The entrapment method of enzyme immobilization is the localization of the enzyme within a polymeric construct such as a lattice structure, gel, fibre, or membrane. In this method, the enzyme is retained whilst still allowing substrates and products to pass through [95]. This differs from coupling methods, as the enzyme is not bound to the matrix. Entrapment of enzyme is a cheap, fast and easy method of immobilization that requires mild conditions. The most widely used entrapment construct is based on polyacrylamide gels. A drawback of this form of immobilization for small soluble enzymes is that leeching of the enzyme can occur from the gel construct. This can be overcome by increasing the degree of cross-linking of the gel matrix thus reducing the pore size. However this can also decrease the likelihood of mass transfer and limit effective diffusion [95].

A review by Cosnier [96] into the entrapment of biomolecules to electrochemically polymerized films assessed the electrochemical procedure, involving the adsorption of amphiphilic monomers and biomolecules before the polymerization, it concluded biomolecule entrapment within electro polymerized films to be versatile and powerful in the fabrication of biosensors. Cosnier reported that biomolecules entrapped in electro-generated polymers such as polypyrole, polyanaline and polyphenol to be easily modulated by the monomer and electrolyte charge. It was noted that the one step procedure of entrapment ruled out the need for additional chemicals that can denature the biomolecules. Furthermore, the electro polymerisation of biomolecules on to pre-adsorbed amphiphilic pyrtole-protein coatings proved to be economical in the fabrication and control of the amount of entrapped biomolecule required.

Anwar *et al* [97] entrapped protease in calcium alginate beads using casein as a substrate. There was no reported change in the pH and temperature activity profile of the enzyme before and after immobilization. Also noted was an increase in the reaction time of the immobilized enzyme with respect to soluble enzyme. However, the enzyme activities decreased when the concentration of alginate was increased above 2%. It was concluded that the overall activity of the immobilized enzyme was retained for longer and it could be reused up to three times.

2.5.3 Microencapsulation

Microencapsulation of biomolecules such as enzymes has been of particular interest due to the simplicity of the methodology and the resulting freedom of the biomolecule. The process itself has proven to be straightforward and reproducible

[98]. It is based on the entrapment of a biomolecule within a polymer matrix with no covalent association between network and biomolecule. This restricts the rotation and unfolding movements of the enzyme but allows substrate recognition and binding as well enabling catalysis to take place. An advantage of this method is the permeability of these matrices allowing the transport of low molecular weight components without the leeching of the biomolecule.

Caruso *et al* [99] encapsulated the enzyme catalase in controlled multilayer coatings of bio crystals. This was achieved by sequential adsorption of oppositely charged polyelectrolytes onto the catalase crystal templates. This resulted in high enzyme loading within each polymer capsule with the enzymatic activity preserved. The polymer encapsulated enzyme proved to be stable against protease degradation compared to uncoated soluble catalase, which lost 90% activity within 100mins under the same conditions. The study concluded the importance of enzyme encapsulation to be useful in catalysis and drug delivery applications.

The advantages of biomimetic silica for enzyme immobilization were discussed by Betancor *et al* [100]. They reported immobilization to be simple and inexpensive without the need for chemical reagents. The immobilization itself occurred rapidly within seconds, under mild conditions (at room temperature and under neutral pH). The particles were nanosized, resulting in lower diffusion limitations and higher volumetric activities. The matrix was described as "smart matrix" meaning that the matrix could be dissolved to release the entrapped enzyme. Figure 2.12 demonstrates the structural hydration of silica through the bonding of H_20. The robust nature of silica makes its physical properties suitable in flow through applications, with its

polymorphous properties enabling structure to be tailored by varying the conditions of silica deposition.

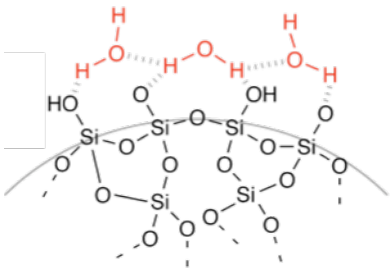

Figure 2.12: Structure of hydrating silica gel. *Image adaptation of Stephane Mons dry and hydrated silica gel* (commons.wikimedia.org).

It was concluded that silica was particularly stabilizing for enzyme encapsulation. Wang *et al* [101] also reported enzyme encapsulation in silica spheres resulting in high loading, high enzymatic activity and stability.

2.5.3 Crosslinking

Crosslinking is the formation of chemical bonds between two polymers to form infinite network [88]. Crosslinking increases the stability of an enzyme to denaturation by heat; organic solvents and proteolysis compared to soluble enzymes or lyophilised powder. One of the most widely used crosslinking agents is glutaraldehyde. The applications of glutaraldehyde range from histochemistry, microscopy, cytochemistry [102], enzyme technology, and chemical sterilization [103] and the biomedical and pharmaceutical industries [104]. Glutaraldehyde is a linear five-carbon dialdehyde that is soluble in water, alcohol, and organic solvents. It is generally available in acidic solutions of pH 3-4. Glutaraldehyde reacts rapidly

with amine groups at pH 1.7 making it more efficient than any other aldehyde in generating chemical crosslinks [105].

The first reported application of glutaraldehyde as a bifunctional reagent was by Zahn in 1950s. Following this, the chemistry of cross-linking with glutaraldehyde was investigated for the preparation of stable protein crystals for x-ray diffraction [106]. The use of glutaraldehyde as a crosslinking agent in the immobilisation of enzymes is favourable as reactions take place under aqueous conditions close to physiological pH, ionic strength and temperature [107].

2.6 The biosensor

Biosensors are devices, which contain biological components that are used in the detection of various analytes. [108] In 1962 Clark and Lyons proposed the immobilization of enzymes within electrochemical detectors to form enzyme electrodes. [109] Enzyme based biosensors are the most widely used biosensors in biomedical applications; one of the first biosensors to be designed targeted the measurement of glucose using glucose oxidase immobilized on a gel, over a polar graphic oxygen probe to measure the concentration of glucose in biological solutions and tissues, this work was illustrated by Updike and Hicks [8]. Both of the described electrodes were examples of or amperometric probes. Amperometric detection involves the measurement of current at a certain potential on a working electrode, when current is flowing through a system. In contrast, potentiometric detection involves the measurement of electrical potential (voltage) of an electrode when no

current is flowing. Guibault and Montalvo described the first reported potentiometric enzyme electrode for urea in 1969 [110].

The immobilization of enzymes as described in 2.4.2 is vital for reducing the amount of material required to perform an analysis and eliminate the need for repeated assay with the enzyme in order to obtain reproducible results. Furthermore the stability of the enzyme is improved when incorporated in a suitable matrix. In general, enzyme electrodes operate in five key processes:

1) The substrate must be transported to the surface of the electrode

2) The substrate must diffuse through the membrane to the active site

3) Reaction occurs at the active site

4) The product formed in the enzymatic reaction is transported through the membrane to the surface of the electrode

5) Product is measured at the electrode surface [111]

Glucose biosensors are commonly used by healthcare professionals to measure the glucose concentration in the blood of diabetic patients. Various enzymes can be used in the detection of glucose; however glucose oxidase (GOx) is usually used due to its stability and, as it does not require an enzyme cofactor that is required by some enzymes in order to complete a catalytic reaction.

2.6.1 Electrochemistry

Electrochemistry is the study of reactions in which charged particles in the form of ions or electrons, cross the interface between two phases of matter, typically a metallic phase (electrode) and a conductive solution or electrolyte.

The electrode processes takes place within the transition region between two phases or regions of charge unbalance known as the electrical double layer.

2.6.2 Reference electrodes

Within most electrochemical reactions the main area of interest focuses on only one of the electrode reactions. In order to improve the stability of electrochemical measurements it is common practice to use a reference electrode. The key feature of the reference electrode is the stability of the potential is known and the ease in which it is prepared and maintained. Stability is achieved by using an electrode reaction involving the saturated solution of an insoluble salt of the ion.

A widely used reference electrode is silver –silver chloride. It consists of a silver wire covered with a thin coating of silver chloride, which is insoluble in water. The electrode reaction involves the oxidation and reduction of silver:

$AgCl\ (s) + e^- \rightarrow Ag\ (s) + Cl^-\ (aq)$ - with standard hydrogen electrode (SHE)

$Ag\ (s) + Cl^-\ (aq) \rightarrow AgCl\ (s) + e^-$

2.6.3 Needle electrode biosensors

Schichiri [112] was the first to report glucose needle electrodes with platinum working electrode, a silver reference electrode and an outer polyurethane membrane. The sensor had a response time of 16 seconds and a linear range up to 27 mM glucose.

The needle electrode consists of five functional components:

1) Platinum wire - used as the working electrode. Under a polarising voltage of

+ 0.65 V *vs Ag/ Ag Cl*, hydrogen peroxide is oxidised at the platinum electrode as demonstrated in the equation below:

$H_2O_2 \rightarrow O_2 + 2H^+ + 2e^-$

2) Stainless steel tube – used as the pseudo reference electrode

3) Inner membrane - prevents oxidizable compounds reaching the working electrode due to electrical repulsion. It also provides a frame for the enzyme layer.

4) Enzyme layer – in this study glucose oxidase (GOx) is oxidized:

β-D-glucose + O_2 + H_2O → gluconic acid + H_2O_2

5) The outer membrane - protects the enzyme layer and controls glucose as well as oxygen permeability. The outer membrane also provides a barrier to micro-molecules and can be biocompatible for in vivo measurement.

Glucose molecules pass through the outer membrane and react with GOx. If the reaction of glucose with the enzyme is much slower than the transport of the glucose molecule through the membrane; the needle electrode is said to be working on a kinetic limit mode. However if the reaction of glucose is faster than the movement through the outer membrane; the needle electrode is said to be working on a mass transfer limit mode with the current passing through the electrode being proportional to the concentration of glucose [113].

The mean normal blood glucose concentration is said to be around 4 mM, however this fluctuates at different times of the day. The National Institute of Health and U.S reported normal human blood glucose levels to be 70-130 mg/dL before meals and > 180 mg/dL after meals. Cass *et al* [114] described the use of an amperometric enzyme electrode for the analysis of glucose, using a substituted ferric inium ion as a mediator of electron transfer between immobilized glucose oxidase and graphite

electrode. A linear current response proportional to the glucose concentration over a range commonly found in diabetic blood sample (1-30 mM) was observed.

2.6.4 Biocompatibility issues of biosensors

In vivo monitoring using electrochemical biosensors requires direct contact with the sample. One drawback of electrodes, as demonstrated in studies conducted by Judge *et al* [115] was the deposition of protein and cells from biological fluids that leads to fibrous encapsulation after chronic implantation.

The accumulation of cells and biological constituents such as proteins on the surface of the sensing area is known as 'biofouling'. This can be detrimental to the overall performance of the sensor [116]. This results in the need for frequent calibration of the electrode.

Polymeric materials and the active redox components used in the fabrication of biosensors are a contributing factor in the inflammation caused at the wound site. The main challenge in biocompatibility of biosensors is the anticipation of the biological response. The deposition of biological matter occurs within minutes and hours of implantation of sensors, during this time the accuracy and precision of the device is compromised.

The mechanical stability at the interface of the electrode with the body is vital in reducing motion artefacts found between the electrode and the surrounding tissue. This can been achieved through recessing electrodes in electrolyte solutions or gels.

Needle based recess electrodes devised by Anastasova *et al* [117] report the amperometric monitoring of oxygen and glucose *in vivo*. The needle like structure

consisted of a gold-filled silica capillary enclosed within stainless steel tubes that served as a counter / reference electrode. The surface of the working electrode was modified with different membranes to achieve selectivity to target analytes. The research revealed a linear working range for oxygen and glucose.

2.6.5 Applications of sensors

Due to the simplicity and cost effectiveness in fabrication, glucose needle electrodes as electrochemical biosensors have potential to be widely used in biotechnology, clinical practice and food industry [118]. In this study, glucose needle electrodes were to be constructed and integrated within a flow system to detect and monitor changes within different cell environments, for use as a bioreactor system. Later studies can investigate the development of these bioreactors for continuous long term *in vivo* monitoring. Rong *et al* [119] presented glucose needle electrodes with platinum working electrode, a stainless steel reference electrode and an outer polyurethane membrane. The sensor had a response time of 60 seconds and a linear range up to 70 mM. Pfeiffer [120] constructed glucose needle electrodes with a response time of 100 seconds and a lifetime of 6 days. Wilson [121] proposed needle electrodes in which the sensing element was located in the sensor body. An inner cellulose acetate membrane was used to reduce response to interferents, the sensor had a lifetime of 10 days. Chen [122] presented glucose needle electrodes with a lifetime of 25 days, in which an inner Nafion membrane and outer cellulose acetate membrane were used to diminish response to interferents. Moussy [123] used Nafion for outer membrane in the development of glucose needle electrodes, which was implanted subcutaneously in a dog with a lifetime of 14 days.

Studies by Rong *et al* [119] have seen the development of needle electrode biosensors to measure glucose concentration within a collagen gel, which is relevant to tissue engineering scaffolds. This electrode was based upon the classic H_2O_2 detection process as mentioned above. The main feature of this device was the ability to produce a rapid response enabling efficient tracking of glucose molecules and the formation of a membrane layer that restricts diffusion to minimise the glucose consumption that ensured more reliable results.

A second enzyme electrode developed by Rong *et al*. [124] was fabricated for lactate measurement *in vivo*, however an experimental *in vitro* model was developed first. Here a needle lactate electrode was inserted in a collagen gel to monitor the inward diffusion of lactate for determination of the lactate diffusion coefficient. Measurement of the diffusion coefficients of metabolites, help to gain valuable insight into the evaluation of the local tissue microenvironment, and the impact of tissue barriers.

There are two methods by which *in vivo* biosensors can be applied [125]; the first being the direct implantation of a sensor that is more suitable for measuring within a localised area. However, it is a more complex procedure to measure multiple analytes and it has proven to be harder to calibrate the sensor during each measurement. The second method by which biosensors can be applied is the development of a sensor, which is combined with an implanted sampling probe. This method reduces the response time in comparison with a conventional microelectrode based technique [126]. However, we are able to achieve higher selectivity and detect multiple analytes. The type of biosensor used in the present studies will be based

upon the needle enzyme electrodes produced within the research group stated in the above section. These electrodes will be used because they can be scaled down and accommodated within the microfluidic device with relative ease. Also, these needle electrodes described integrate well within the sidewalls of the microfluidic channels so that any membranes formed within the middle of the channel are not damaged.

2.7 Microfluidics

Microfluidics has been a rapidly growing field of research [127]. The last decade has seen the development of microsystems known as "lab on a chip" devices towards a largely expanding market [128]. These devices have been known to be particularly useful in biomedical applications such as drug delivery and *in vivo* monitoring [129]. Since the development of the first microfluidic device in the early 1970s, the new millennium has seen the progression of more advanced, inexpensive and time saving devices being developed to aid scientific research.

2.7.1 What are microfluidics?

Microfluidic devices contain one or more channels with cross-sectional dimensions typically ranging from 10-100 μM. They are commonly used to analyse fluid samples such as bacterial cell suspensions, protein and antibody solutions and simple buffers [129]. Figure 2.13 illustrates a Y channel Microfluidic system with a channel depth of 100 μM.

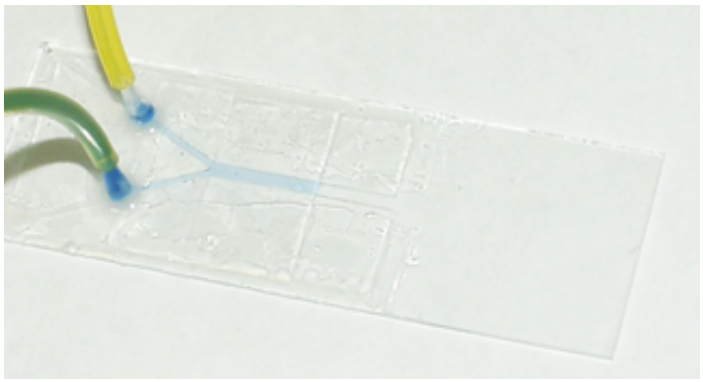

Figure 2.13: Microfluidic Y Channel fabricated in glass [130].

Microfluidics is a multidisciplinary field, which intersects engineering, physics, chemistry, micro technology and biotechnology. Its practical applications are revolutionizing molecular biology procedures for enzymatic analysis, DNA analysis and proteomics. [131] These devices are used to obtain a variety of measurements such as molecular diffusion coefficients [132], fluid viscosity pH, chemical binding coefficients and enzyme reaction kinetics [133]. In biomedical research, the use of microfluidic technology creates clinically significant advantages. The first major advantage is that the volume of fluid consumed within the channels is very small, thus the overall amounts of reagents and analytes used are small which can keep expenses to a minimum. Also general fabrication techniques are relatively inexpensive hence more elaborate multiplex devices can be readily mass-produced. Microfluidic technologies can also enable the fabrication of highly integrated devices, which can be used to perform several different functions within a single substrate chip or device. [134]

2.7.2 Development and background

Terry *et al* [135] developed the first fabricated microfluidic device in 1979. It involved the development of a gas chromatograph used to optimize the performance

of a fabricated sensor to enable the separation of gaseous hydrocarbon mixtures in less than 10 seconds. The components of the device were fabricated in silicon using photolithography and chemical etching techniques. The system consisted of a sample injection valve and a 1.5 mm long separating capillary column. The output thermal conductivity detector was batch fabricated and mounted on to the substrate wafer. Following this IBM developed ink jet printer nozzles etched in silicon [135]. The late 1990s gave rise to the development of microfluidic devices as analytical instruments, as dynamic cell separators [136], for surface patterning of cells and proteins [145], and as mass spectrometer delivery modules [137]. However the Yager group first developed a microfluidic device for use in chemical measurements. The fabrication of the resulting T-sensor exploited low Reynolds number flow conditions in microfluidic channels (described in 2.7.3.1). The chemical interaction of components from two or more input fluid streams was monitored optically, enabling the continuous measurement of analyte concentrations. The study was later optimized by Kamholz *et al* [138] to quantify analyte distribution using one and two-dimensional models. The results displayed the shape of the inter diffusion region in the T-sensor assay.

Microfabrication between 70s – 90s was based on silicon substrates that are expensive and generally require the use of complex facilities to process. A further disadvantage is opaqueness of the material that makes it unsuitable in optical detection. The late 90s has seen the development of microfluidic devices fabricated using polymeric materials such as silicone rubber, polyimide and more extensively poly(dimethylsiloxane) (PDMS) [139]. The main advantages of using materials such as PDMS for fabrication of microdevices are the optical transparency of the material

as well as the ability of the material to survive most non-toxic and organic solvents. The fabrication of PDMS microchannels is discussed in more detail in 2.7.5.

2.7.3 Basic principals

2.7.3.1 Reynolds number

The fluid mechanics theory is based on the assumption that a fluid is defined as a material continuum, which is able to withstand a static shear stress [140]. Fluid flow can be either laminar or turbulent. This is determined by the ratio of inertia force to viscous forces present within the fluid and is expressed by Reynolds number:

$$R = \frac{\rho VD}{\mu}$$

Where V is the fluid velocity for a fluid flowing in a microfluidic channel, D the diameter or length of the channel, ρ is the density of the fluid and μ is the viscosity of the fluid.

Within microfluidic systems; a low Reynolds number is generally observed (100>Re>0.001) which is due to the dimensions of most devices being relatively small. Fluid flows are laminar for Reynolds numbers up to 2000. Beyond a Reynolds Number of 4000, flow is completely turbulent. Between 2000 and 4000, the flow is in transition between laminar and turbulent, and it is possible to find sub regions of both flow types within a given flow field. Typically, viscous stresses within a fluid tend to stabilize and organize the flow, whereas excessive fluid inertia tends to disrupt organized flow leading to chaotic turbulent behaviour.

2.7.3.2 Laminar flow

Multiple laminar flow occurs when fluid flow in parallel streams occurs with no disruption between each stream [141]. At low velocities fluid flows without lateral mixing, so two or more distinct fluid streams moving in the same direction at low Reynolds number do not develop turbulence at the interface.

Mass transport under laminar flow is characterized by Fickian diffusion and low momentum convection. Diffusion between laminar streams in micro devices has been used in performing immunoassays and in the sorting of particles by size. Brody *et al* [142] fabricated a micro-machined device with channels as small as 20 μM to separate particles and molecules based on their diffusion coefficients. A modelled system was presented which predicted the exponential dependence of the output concentration on diffusion coefficient in certain regiments. Chan *et al* [143] measured the distribution of a labelled probe molecule after it diffused for a short time from one region to another region containing an antigen specific antibody. This was demonstrated using the T-sensor that allowed inter diffusion of the two components. The analyte assayed was phenytoin. The results obtained indicated clinically relevant levels of the analyte measured in blood diluted from 10- to 400 fold in buffer containing the labelled antigen, also could be measured.

2.7.4 Biosensor integrated microfluidic devices

Once a microfluidic device has been fabricated, the area in which the research will progress is in the development of a device that will accommodate biosensor integration. This can be achieved using dual laminar flow microfluidic device in order to allow the detection of metabolites such as glucose and lactate. The microfluidic device developed here is based on a Y- channel design, similar to the

work of Kamholz *et al*. [130]. They developed a T-sensor, which was used for quantitative analysis in a microfluidic channel. The importance of developing a Y-Channel is based upon preliminary studies for the formation of polymeric membranes generated within the microfluidic device. From these experiments it was possible to conclude that the ease with which membranes formed using a simplified dual laminar flow channel such as the Y-Channel was significantly higher than that of other more complex microfluidic shapes.

2.7.5 Applications of microfluidics

Some of the applications of MEMS and microfluidic devices in science are summarised in Table 2.2.

Area	Applications
Genomics / Proteomics	Rapid, high density sequencing DNA fingerprinting, gene expression and DNA assay integration with microfluidics
Chemical / Biological defence	Detection and identification of pathogens and toxins
Clinical diagnostics	Rapid analysis of blood and other bodily fluids
High Throughput Screening	Assay for candidate drug testing Toxicology assays
Biomedical device	*In vivo* monitoring and drug delivery
Sample preparations	Biological sample purification
Amplification of nucleic acids	Polymerase chain reaction (PCR)
Tissue Engineering / Cell biology	*In vitro* monitoring of cellular response to stimuli and cell patterning Cell behaviour

Table 2.2: Applications of Microfluidic devices [144].

2.7.6 Fabrication techniques used in microfluidics

2.7.6.1 Anodic bonding for the formation of microchannels

The oldest bonding technique used in MEMS is anodic bonding. This is done using glass and silicon wafers which are bonded together with a high electrical field (1 kV in voltage) Figure 2.14 outlines the set up required for anodic bonding.

Bonding of the two substrates (glass and silicon) occurs immediately as heat and voltage is applied. The ions in the substrate migrate to the cathode forming a depletion layer at the interface. Electrostatic forces connect the two substrates, which results in contact at the interface.

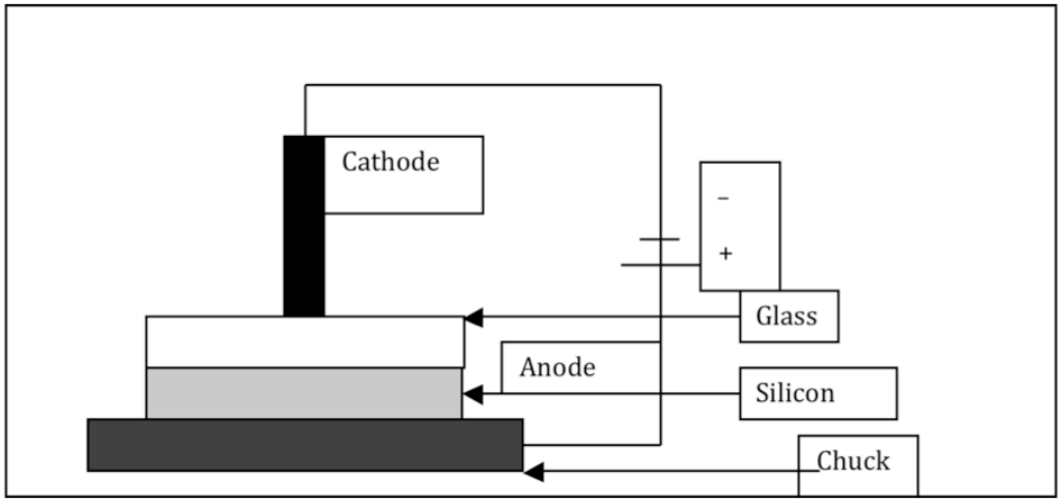

Figure 2.14: Basic set up for anodic bonding.

This bonding process is also known as the 'wafer bonding process'; one of the disadvantages of this method is the high temperature required for the bonding to take place. Satyanarayana *et al*. [145] developed a process whereby the technique involved could be carried out under room temperature for silicon, glass and nitride surfaces using a UV-curable adhesive.

Jia *et al*. [145], also developed a room temperature bonding procedure which enabled microfluidic glass chips to be fabricated resulting in a 95% bond; furthermore this technique did not require the use of clean room facilities, programmed high temperature furnaces, pressurized water sources, adhesives or weights.

2.7.6.2 Photolithography

Photolithography is a form of printing using light. It requires the use of a photosensitive emulsion layer knows as a photoresist; which is used to transfer a pattern using a transparent photo mask on to a substrate (glass, silicon, etc). A mask is produced by creating a design using a computer aided design (CAD) programme. The three main steps involved in the process of photolithography are:

1) Positioning process: the positioning of the mask with the resist coated substrate; here the distance between the mask and the substrate is also adjusted.
2) Exposure process: the resist layer is exposed optically; this transfers the pattern from the mask on to the photo resist layer by changing the initial properties of the area exposed due to curing of the polymer in the exposed area. SU-8 is an example of a commonly used epoxy based negative photo resist. When exposed to U.V light, the molecular chains of SU-8 crosslink and solidify.
3) Development Process: for a negative resist this is done by dissolution and for a positive resist, by etching the resist pattern in a developer solution.

2.7.6.3 Microfabrication using Polydimethylsiloxane (PDMS)

PDMS is an elastomeric material commonly used in the fabrication of microdevices. Typical fabrication procedure in two stages produces a replicated pattern. An elastomeric stamp is imprinted with a patterned structure of the imprinted channel using a computer aided design (CAD) programme. The elastomeric stamp is commonly made of polydimethylsiloxane (PDMS). In a review by Y Xia and G.M Whitesides [146], many different techniques were used to transfer patterns on to elastomeric stamps were evaluated. One such procedure was printing of the design obtained in the CAD programme on to a transparency, which was used as a photomask. This photomask was then used to produce a positive relief on a silicon wafer using a positive photoresist. This is known as the 'master mould' and is then used to generate replicas in PDMS. There are many polymers that can be used to form the elastomeric stamp; however reported studies by Leclerc *et al*. [147] confirm the use of PDMS due to its unique properties suitable to microfluidics.

PDMS consists of an inorganic siloxane backbone; with the methyl groups that attach to a silicon backbone, thus making it more stable. PDMS has low interfacial energy, which means that molecules from other polymers are unable to react with its surface [148]. Studies of the interfacial free energy of PDMS have been carried out indicating possibility for manipulating the surface with plasma treatment. [149]

The main advantage of soft lithography is the reduction of lab cost and the ability of the procedure to save time in long-term use of microfluidic devices, particularly with reference to the cost of producing various designs that can be used. Studies conducted by MacDonald *et al* [150] show that the accuracy of this technique allows

for microfluidic devices with channels of 20-100 μM depending on the resolution of the PDMS device. PDMS is also optically transparent down to 280 nm and can be used alongside UV absorption and fluoresce monitoring. The work of Chiu *et al*. [151] indicated that PDMS is non-toxic, thus allowing mammalian cells to be directly cultured on its surface.

2.7.6.4 Micromachining

This technique works by using a computer aided design (CAD) programme to produce a template design that can be used for the microfluidic device. The template design can then be used to configure and control a production machine, which is linked to the machine by a controlling computer.

Previous studies by Kyriacou *et al* [153] designed and fabricated a Y-shaped flow cell to prevent biosensor fouling. This was fabricated using acrylic plates and consisted of two main sections; a bottom plate where the flow channels were etched using a fast rotating 500 μM diameter round nose borer. A thin strip of PTFE tape was then used to create a seal between the top and bottom plates that were secured together using 3 mm nuts and screws. The Y-shape enabled the entry of separate sample and electrolyte streams with the electrolyte stream serving as a mobile protective layer over the biosensor inserted into the electrolyte microfluidic flow stream.

CHAPTER 3

-

Experimental materials,

instrumentation and methods

3.1 Synthesis of p(HEMA) Enzyme gels

3.1.1 Reagents and materials

p(HEMA) base hydrogel, 2-hydroxyethyl methacrylate (HEMA), tetra-ethyleneglycoldiacrylate (TEGDA) and Poly (ethylene glycol) (400) monomethacrylate (PEGMA) were purchased from Sigma Aldrich (St. Louis, MO USA) and were all of analytical grade. 2-Methacryloyloxyethyl phosphorylcholine (MPC) monomer was synthesised by the University of Tokyo, Japan, as previously described [154], at The University of Tokyo and kindly donated by Professor Ishihara. The remaining chemicals, *N*-[Tris(hydroxymethyl) methyl] acrylamide (HMMA), Polyvinylpyrrolidone (pNVP), 2-(Dimethylamino) ethyl methacrylate (DMAEMA) and 2,2-Dimethoxy-2-phenylacetophenone (DMPA) were purchased from Sigma Aldrich (St. Louis, MO USA). Solvent solution comprising ethylene glycol and Dulbecco's Phosphate buffered saline (D-PBS) in addition to the required enzymes / proteins namely, bovine serum albumin (BSA) (Fraction V-initial fraction by heat shock treatment), fibrinogen from bovine plasma, glucose oxidase (EC 1.1.3.4) from *Aspergillusniger* (GOx), catalase (EC 1.11.1.6) from bovine liver (Cat), and superoxide dismutase (EC 1.15.1.1) from bovine erythrocytes (SOD) were variously purchased from Sigma Aldrich (St. Louis, MO USA) and Sigma (UK).

For cell cultures, human muscle fibroblasts (CRL-2061) were purchased from the American type Culture collection (Manassas, VA). Culture medium, RPMI 1640 supplemented with 10% (v/v) foetal bovine serum (FBS), 20% (v/v) antimycotic/ antibiotic solution, ACLT-PEG (3500)-NHS, HEPES solution (pH 8.5) was obtained from Cellgro, Mediatech, Hendon, VA.

For cell viability analysis a Vybrant MTT cell proliferation assay kit was purchased from Invitrogen (USA) and Trypan Blue solution, 0.4% (w/v), sterile filtered, suitable for cell culture, from Sigma (USA).

3.1.2 Preparation of enzyme and protein stock solutions

Enzyme and protein stock solutions were all prepared using sterile filtered D-PBS. A 9.23 mg/mL GOx stock solution was prepared by dissolving 60 mg of GOx in 650 μL of the solution. By using a 1.53 mg/mL of SOD and 66.6 mg/mL Cat stock solutions, 20 mg of enzyme were dissolved in 300 mL D-PBS. Finally, a 2% (w/v) of fibrinogen stock was prepared by dissolving 100mg of fibrinogen in 500 μL D-PBS and stored at 4^{O}C alongside the enzyme stock solutions.

3.1.3 Preparation of hydrogel monomer solution

For a 3% (w/v) base p(HEMA) gel; 0.05 g DMPA (photoinitiator), 0.05 g Poly(HEMA) and 0.18 g of HMMA were weighed and placed in a 10 mL amber bottle. The methacrylates, namely 2.35 g of 2-(HEMA), 0.04 g PEG(200)MMA and the diacrylate crosslinker, 0.19 g TEGDA, were weighed out and transported into a UV filtered room. Handling of these materials in the UV-filtered room significantly diminished the possibility that ambient UV would lead to premature polymerization of the hydrogel upon removal of the polymerization inhibitors.

The methacrylates and diacrylate listed all contain a polymerization inhibitor (MEHQ), a hydroquinone that must be removed prior to initiation of the polymerization step. Each of the compounds was passed through an inhibitor removal column (product 306312 from Sigma Aldrich Co.). The column contained cream-coloured beads that absorb the MEHQ by the process of column

chromatography. The beads were placed in a burette tip with a piece of cotton wool at the bottom of the column to prevent any of the beads from escaping through the open-ended tip. The cleaned methacrylate and diacrylate compounds were stored in amber coloured vials. The appropriate quantities of each were then added to the amber vial containing the HMMA, DMPA, p(HEMA) 300,000 mixture along with fibrinogen.

3.1.4 Synthesis of enzyme encapsulated p(HEMA) hydrogels

Prior to crosslinking, a 24-well multiwell plate (353847 - BD Primaria™) was surface derivatized by preparing a solution of ACLT-PEG(3500)-NHS dissolved in HEPES solution, pH 8.5, under bioclean conditions. Equal quantities of ACLT-PEG(3500)-NHS solution were aliquoted into each well and incubated for 2 h at room temperature in the dark. Following the incubation period the ACLT-PEG(3500)-NHS solution was removed from each well and washed thrice with deionised water before adding p(HEMA) monomer solution for crosslinking.

Table 3.1 summarizes the concentration and units of activity for each enzyme hydrogel construct.

	Control	GOx (G)	CAT (C)	SOD (S)	GOx-CAT (GC)	GOx-SOD (GS)	GOx-CAT-SOD (GCS)
Concentration (mg/mL)	0	9.23	66.6	1.53	(G) 9.23 (C) 66.6	(G) 9.23 (S) 1.53	(G) 9.23 (C) 66.6 (S) 1.53
Units of Activity (units/mg solid)/ *(units/g solid)	0	*953.4	3809	3619	(G) *953.4 (C) 3809	(G) *953.4 (S) 3619	(G) *953.4 (C) 3809 (S) 3619

Table 3.1: Table of enzyme concentrations and units of activity within each hydrogel construct.

The above enzyme concentration for glucose oxidase was used in accordance to that of implantable glucose biosensors, previously tested *in vivo* [155],[156]. The primary function of catalase and superoxide dismutase in the study was to counteract the effect H_2O_2. Therefore concentrations used were in excess for the amount of H_2O_2 produced from the reaction of glucose oxidase with glucose present in cell culture media.

Previously prepared enzyme stock solutions of glucose oxidase, catalase and superoxide dismutase in pH 7.4 phosphate buffered saline were individually aliquoted into separate Eppendorf tubes consisting of 520 μL of the hydrogel cocktail along with 20 μL of fibrinogen and the required amount of solvent comprising ethylene glycol and D-PBS in 1:1 ratio to reach the final hydrogel volume of 630 μL, allowing for minor pipette error.

Once the enzyme hydrogel cocktails were prepared, the Eppendorf tubes were subsequently degassed and sonicated (sparging through the application of a slow stream of nitrogen gas, which was bubbled through the mixture – one bubble every 5 seconds to remove any oxygen that could inhibit polymerization). Nitrogen was bubbled through the cocktail for about 3-5 min using a burette tip fitted onto the end of the plastic tubing running from the nitrogen gas tank. The amber vial containing the cocktail was placed in a 50 mL beaker approximately half filled with water. The beaker was then placed in the ultrasonic bath. This degassing procedure was performed for about 5 min.

Each of the enzyme hydrogel monomer cocktails were aliquoted in triplicate in the previously surface modified 24-well cell culture dish along with a control monomer hydrogel which comprised a 3% (v/v) base hydrogel monomer cocktail and fibrinogen.

3.1.5 Post synthesis treatment

UV irradiation to crosslink the hydrogels was performed at 1500 (x100) μJ/cm^2 for 5 min [56]. Figure 3.1 shows the p(HEMA) hydrogels after UV crosslinking, following this the remaining unreacted monomers were extracted with sterile filtered D-PBS thrice under bioclean conditions at room temperature. Each hydrogel was later incubated in 20% (v/v) antibiotic/ antimycotic supplemented D-PBS for 30 min under a fume hood four times to sterilize before cell culture (Figure 3.2).

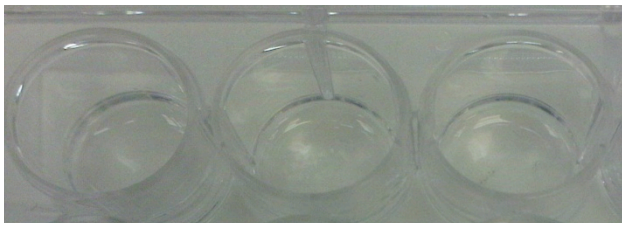

Figure 3.1: p(HEMA) enzyme hydrogels pre-extraction after UV crosslinking.

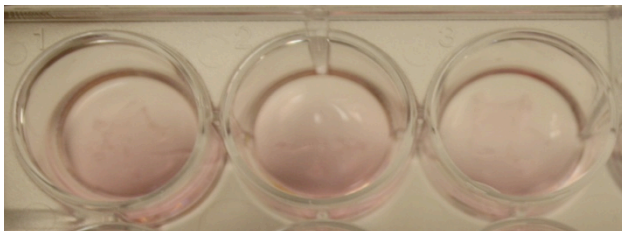

Figure 3.2: p(HEMA) enzyme hydrogels post-extraction in 20% (v/v) antibiotic/ antimycotic supplemented D-PBS with cells seeded.

3.1.6 RMS 13 - cell culture

In vivo Rhabdomyosarcoma (RMS) is the most common soft-tissue sarcoma found in childhood that is able to resist apoptosis and has commonly been used to determine the efficacy of apoptotic inducing agents [157]. RMS 13 cells were used in the current study to investigate the effect of oxidative stress induced by the immobilized bioreceptor (Glucose oxidase), which can also result in apoptotic behavior. However the primary focus in this study uses RMS 13 cells as an *in vitro* model to simulate a biological response of biosensors, which have commonly been implanted in subcutaneous tissues. This also provides an insight into the clinical biocompatibility of synthetic host materials such as p(HEMA). The use of human muscle fibroblast cells (RMS 13) in the study helps to provide an understanding into the extent of biomimicry of cells to p(HEMA) gels as previously studied [56] hence its favourable choice within this application.

For the 6 h study, cells were cultured to either seeding levels of $8.7x10^5$ cells/ml or $1.1x10^6$ cells/ml (24 h study) on the hydrogel surfaces with RPMI 1640 supplemented with 55 mL FBS and 5.5 mL antibiotic-antimycotic solution, thus comprising 10% FBS and 1% antibiotic-antimycotic media.

Gels were incubated for 6 and 24 h respectively at 37^O C in 5% (v/v) CO_2. Cell morphology was analyzed after 24 h of culture by optical microscopy and cell viability was determined after trypsinization to detach cells.

3.1.7 Cell viability

For the purpose of determining cell seeding numbers and establishing the initial viability of cells in suspension and those cultured on the gels cells were stained using Trypan Blue and counted using a haemocytometer.

After performing cell counts for cells trypsinized off the gel surface and those previously remaining in suspension, the remaining cells inside the hydrogels were determined using an MTT assay. The MTT assay was used to determine whether cells were metabolically active and thus, reflected the number of viable cells remaining on the gels. This was achieved by discarding any remaining medium in culture wells and replacing them with 500 μL of fresh RPMI 1640. In addition to this 50 μL of MTT reagent was added to each well and incubated at 37ºC for 6-8 h.

After the 6-8 h incubation period 500 μL of solvent was added into each well and left to incubate for a further 4-5 h. Each well was mixed well by resuspending with a pipette several times before aliquoting 150 μL of the reagent/ solvent mix into 96 well plates and reading at 570 and 670 nm on a UV spectrophotometer. Figure 3.3 demonstrates the MTT calibration standard for RMS13 cells cultured on p(HEMA) hydrogels.

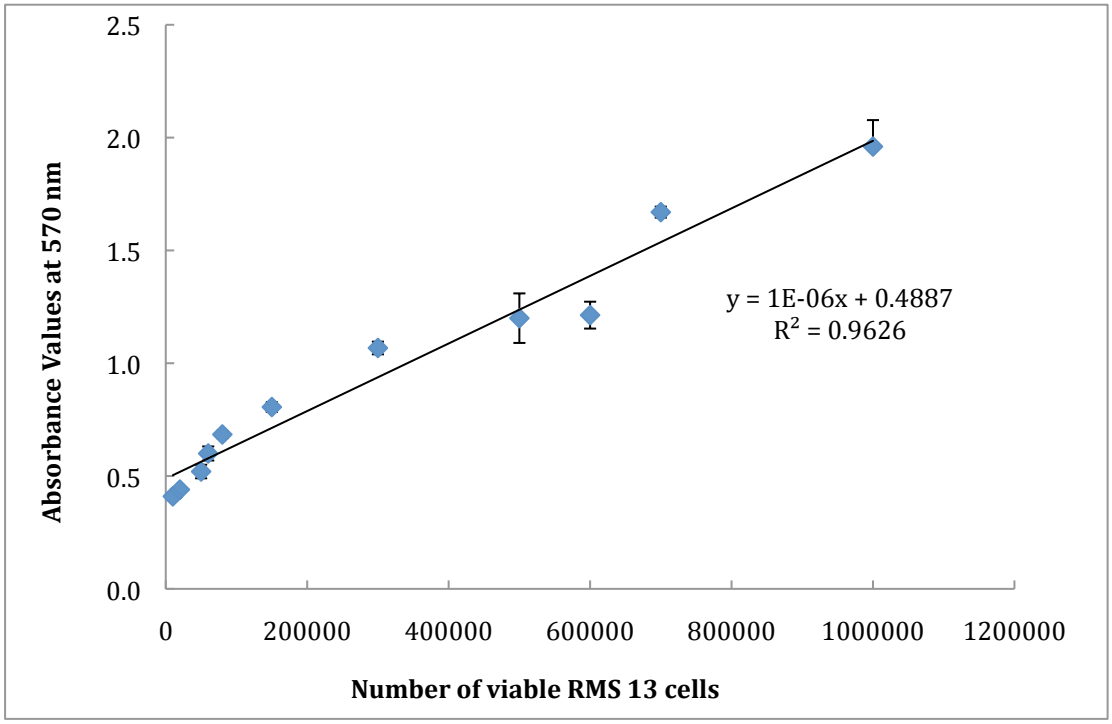

Figure 3.3: Calibration plot of the MTT assay with different RMS 13 cell densities.

3.2 Agarose enzyme gels

3.2.1 Reagents and materials

For the 1% (w/v) agarose gel, agarose (low gelling temperature, BioReagent, suitable for cell culture) along with sterile, filtered Dulbecco's Phosphate buffered saline (D-PBS) was purchased from Sigma Aldrich (UK). Origins of protein and enzyme solutions used were same as those in section 3.11.

Cell culture: Rat neuronal cells (B50 Cells) were purchased from Health Protection Agency Culture Collections (UK). Dulbecco's Modified Eagle's Medium (DMEM), Penicillin/Streptomycin solution, L-Glutamine (200 mM solution), Dulbecco's Phosphate Buffered Saline (D-PBS), Trypsin 10X solution, all purchased from Sigma Aldrich (UK).

Cell viability was carried out using PrestoBlue cell viability reagent obtained from Invitrogen (US). PrestoBlue was used to establish whether cells present on the samples were metabolically active. Viable cells maintain a reducing environment within the cytosol. Therefore the PrestoBlue reagent functioned as a cell viability indicator to quantitatively measure the proliferation of cells.

Viability studies on 90ºC heat-treated enzyme entrapped agarose gels were carried using Trypan Blue solution, 0.4% liquid sterile filtered, suitable for cell culture purchased from Sigma (UK). Prior to staining cells, were fixed in 4% (w/v) paraformaldehyde solution, (Sigma 158127). Stains used were 3,3′-Dioctadecyloxacarbocyanine perchlorate (dioc 18 (3)), hematoxlylin (H3136), eosin Y solution 5% (w/t) in H_2O (318906) purchased from Sigma Aldrich & Co. (UK).

3.2.2 Synthesis of agarose gel entrapped enzyme

The synthesis procedures for the enzyme-loaded gels are illustrated in Figure 3.3. One percent agarose gel was prepared by weighing 1% (w/v) of agarose in D-PBS at a temperature of 70^{O}C and continuously stirring until fully dissolved. The agarose solution was then cooled to around 40 ^{O}C before being transferred into an Eppendorf tube containing the specified concentration of enzyme stock solution as shown in Table 3.1. Along with the enzyme, 20 μL of 2% (w/v) of fibrinogen stock solution was added and the enzyme gel solution was gently mixed by resuspending the contents of the Eppendorf in a pipette. Finally 200 μL of the enzyme gel solution was pipetted into three sections of a 24 well plate, until a uniformed thin gel layer was formed in each well. The gels were then allowed to cool for 10-15 min before being kept hydrated in D-PBS supplemented with 10% antibiotic/ antimycotic solution.

3.2.3 Denatured enzyme loaded agarose gels

For studies investigating the effect of heat control agarose enzyme loaded gels, one percent gels were synthesised as described in section 3.2.2, however, once fully dissolved the specified concentration of enzyme stock Table 3.1 was added to the molten agarose solution and heated for 5 min at a temperature ranging between 80 ^{O}C and 90 ^{O}C to ensure that the enzyme was denatured by heat. Following this, the agarose enzyme solution was allowed to cool to around 40 ^{O}C before the addition of 2% (w/v) fibrinogen stock solution and gently mixed as in section 3.2.2 before casting in 24 well plates.

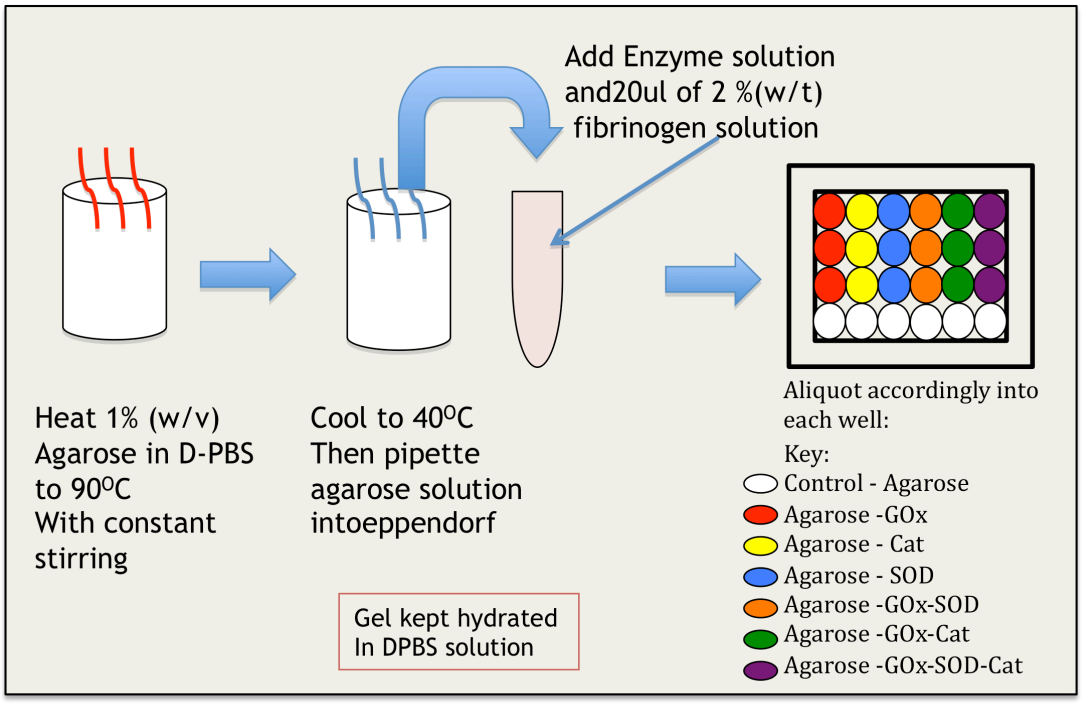

Figure 3.4: Schematic diagram summarizing the fabrication of agarose enzyme gels.

3.2.4 B50 - cell culture and viability

Due to the low cell adhesion and proliferation properties of agarose, it was favourable to culture cells of a highly adhesive nature hence the use of B50 cells that

have been known to grow and proliferate on most surfaces [27]. In addition to this B50 cells expresses integrins that allow their attachment to motifs found in fibrinogen. The current study investigates the effect of oxidative stress on cells for which in clinical settings occurs in most neurodegenerative conditions [158][159], hence the use of neuroblastoma cells. Prior to clinical research, the majority of biosensors tested *in vivo* are primarily carried out in rats. Therefore the use of B50 cells in this study served as a simulated model for studies conducted *in vitro*.

For heat control studies with enzyme loaded agarose gels, 0.5 mL of $1x10^6$ cells/mL B50 neuronal cells were seeded on the surface of the gels and incubated for 6 and 24 h intervals. Cell viability was determined by trypsinzing and enumerating cells stained with 0.4% Trypan Blue solution in a 1:2 dilution.

A haemocytometer was used to count non-viable cells (stained blue), against viable cells (unstained). Percentage viability of cells was calculated using the following formula:

$$\frac{\text{No. of viable cells}}{\text{Total no. of cells}} \times 100$$

3.2.5 Calculation of viable cells present on gels using PrestoBlue viability assay

Cells were cultured to seeding levels of 0.05 $x10^6$ cells/ml on the hydrogel surfaces with DMEM supplemented with 55 mL FBS comprising 10% FBS media. A calibration standard for the PrestoBlue cell viability reagent was used to predetermine the seeding level that was suitable for use with the agarose gels as

shown in Figure 3.5. This was achieved by incubating cells with a range of cell seeding densities: $0.01x10^6$, $0.02x10^6$, $0.03x10^6$, $0.04x10^6$, $0.05x10^6$ cells/ml on 1% (w/v) agarose supplemented with 2% (w/v) fibrinogen. The cells were incubated in accordance with study times of 3,6,12,24 h before the addition of the PrestoBlue viability reagent. Following this, the calibration gels were further incubated at 37^{O} C in 5% CO_2 for 2 h along with a media blank reference before a fluorescence reading was taken using the Fluostar galaxy fluorometer between 544 nm and 590 nm and normalized against a media blank.

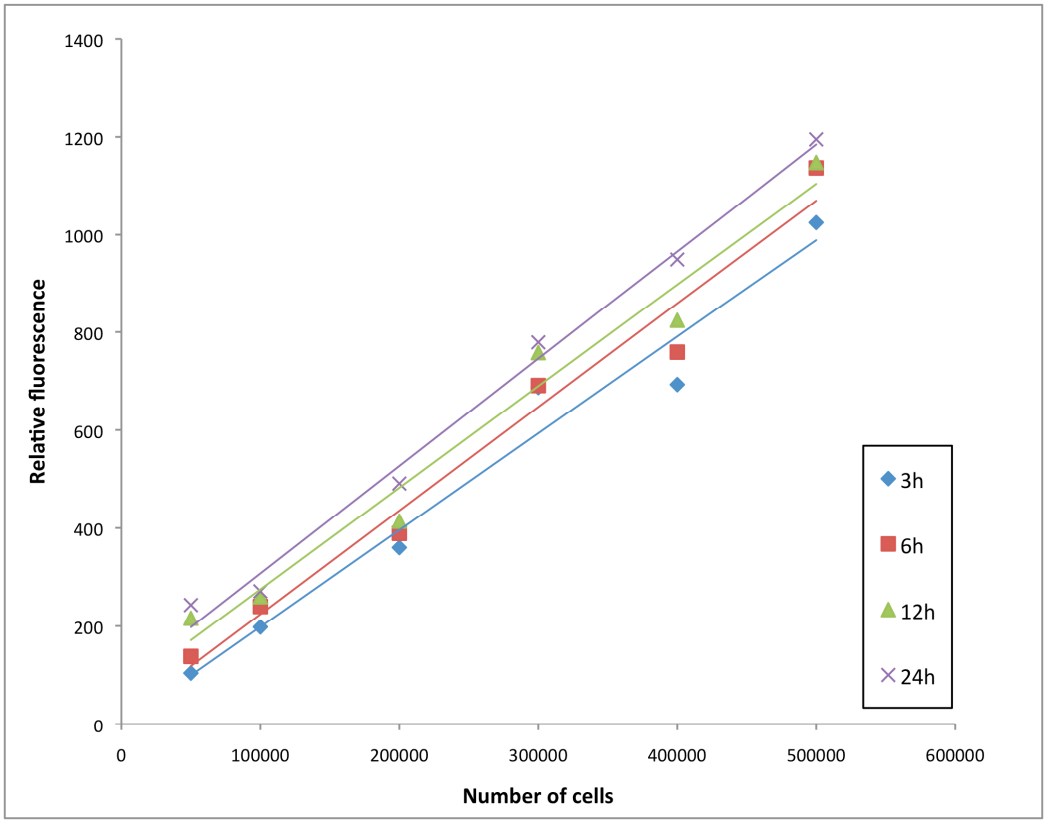

Figure 3.5: demonstrates the calibration standard of relative fluorescence values for agarose gels incubated with a range of seeding densities over 3,6,12, and 24 h.

3.2.5.1 Calibrated standard for PrestoBlue cell viability assay on agarose gels

The active reagent, resazurin present in PrestoBlue functions as a cell viability reagent by quantitatively measuring the intracellular reduction of resazurin to resorufin [160] through fluorometric detection, facilitated by mitochondrial, microsomal and cytosolic oxidoreductases [161]. Resazurin has been reported as a electron acceptor in GOx catalyzed oxidation of glucose under anaerobic conditions through electrochemical analysis [162], to date there has been no research to suggest such interaction between resazurin and oxidorectase enzymes in *in vitro* cell viability studies. However, the encorporation of redox enzymes such as GOx as used in the present study could potentially result in a biochemical interaction, resulting in positive fluorescence readings. Therefore an additional control experiment was carried out to determine the fluorescence values of the enzyme gels (if any) in the absence of cells.

The enzyme gels were incubated at 3,6,12, and 24 h intervals at 37^{O} C in 5% $CO_{2.}$ Cell morphology was analyzed after each time interval of culture by light optical microscopy and cell viability determined by the PrestoBlue cell viability assay. This was achieved by adding the 10X PrestoBlue reagent directly into each well and incubating for 2 h at 37^{O}C. After the incubation period the fluorescence was read between 544 nm and 590 nm and normalised against a reference reading containing DMEM and PrestoBlue along with fluorescence values obtained for the enzyme gels with no cells present to eliminate any background fluorescence.

The number of viable cells at a defined time point was calculated by obtaining a ratio using the following approach:

As an example:

In the case of 500,000 cells/mL: fluorescence at t_0 = X: fluorescence t_1

Fluorescence at t_0 = 1035 relative fluorescence units

Fluorescence at t_1 = 1354 relative fluorescence units

t_0 = number of cells at 3 h (500,000 cells/mL)

t_1 = (X) number of viable cells at 6 h

The number of cells at t_1 =

Number of cells seeded at t_0 (500,000) : Fluorescence at t_0 (1035) = X : Fluorescence at t_1 (1354)

Therefore $X = \frac{(500{,}000 \times 1354)}{1035}$

Number of cells at t_1 = 654,106 cells/mL

Percentage increase and decrease between each interval was also calculated by comparison of cell numbers at the time of culture to the number of viable cells calculated after each period of time.

3.2.6 Fixation and staining of cells

3.2.6.1 Paraformaldehyde fixation

Prior to staining, cells were fixed in a 4% (w/v) paraformaldehyde. For a 50 mL stock of 4% (w/v) paraformaldehyde solution, 2 g of paraformaldehyde was added to

25 mL of Deionised water (dH_20) and heated to 57-60ºC. The solution was then removed from the heat and a few drops of 10 M NaOH was added before being placed back on a hot plate and stirred until completely dissolved. The solution was then filtered to remove any precipitate and allowed to cool before the addition of 25 mL of 0.2 M Phosphate buffer. Cells were fixed by aspirating media from each sample well with the addition of cold 4% (w/v) paraformaldehyde solution for 5 min. Each sample was then washed thrice with PBS and transferred to microscope slides.

3.2.6.2 3,3′-Dioctadecyloxacarbocyanine perchlorate (Dioc 18 (3)

Dioc 18 (3) was prepared to a 1 mg/mL solution in ethanol, this was added to the fixed samples for approximately 10 min and washed with 100% (v/v) ethanol to remove any excess dye present before viewing under fluorescence microscopy.

3. 3 Stabilization of biosensors with the use of needle-based recess electrodes

3.3.1 Reagents and materials

Phosphate buffered saline tablets (pH7.4), Sulfuric acid (95%), glucose oxidase (from *Aspergillus niger*, lyophilized powder, glutaraldehyde 25% (v/v) aqueous solution), bovine serum albumin, glucose, hydrogen peroxide 30% (v/v), ascorbic acid were all obtained from Sigma-Aldrich (UK). Solutions were prepared in deionised water. UV superglue LOCTITE 3211 was purchased from Loctite, Herts, UK. Conductive Epoxy was obtained from RS Components (UK). Stainless steel tubing with inner diameter of 0.38 mm and outer diameter of 0.50 mm were

purchased from Goodfellow, Cambridge (UK) and aluminium oxide polishing films of 1, 3, 5 μM were purchased from Thorlabs Ltd. (UK).

3.3.2 Fabrication of non-recessed gold electrodes

The main structural components of both non-recessed and recessed electrodes comprised gold-filled silica capillaries, which were surrounded by a protective stainless steel tube connected with a low noise coaxial cable. The gold filled capillaries were prepared by the Max Planck Group by pumping molten gold through the hollow fused silica capillaries until they were completely filled.

The tip of the gold capillary was then polished sequentially using 5, 3 and 1μM aluminium oxide films before insertion into stainless steel tubes. Around 2 mm of the tip was left visible outside of the stainless steel tubing, with the gap between the gold filled capillary and stainless steel tube insulated with a small amount of UV epoxy glue to ensure that the capillary was isolated from aqueous samples.

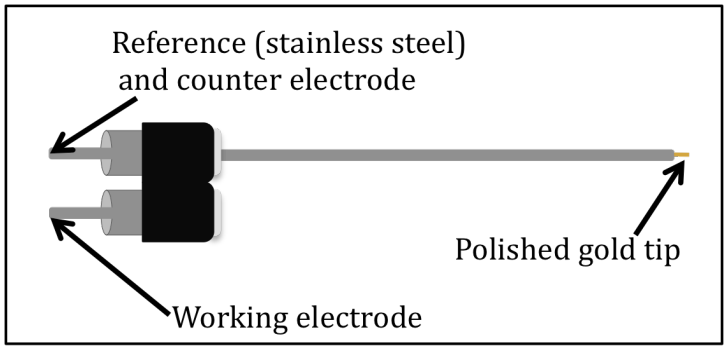

Figure 3.6: Schematic of a non-recessed tip electrode.

The sensing surface of the electrode was cleaned by immersing the tip for 2 min in acetone, ethanol, water in sequentially in an ultrasonic bath. The electrodes were then dried at 40°C for 30 min before platinization. This was achieved by depositing Pt on the polished gold (Au) electrode by electroplating in 5% hexachloroplatanic

acid at an applied potential of -1.0 V (vs. Pt electrode). This was run for 200 s before the Au-Pt was placed in stirred deionized water for 1 h. A final electrochemical clean in 50 mM of Sulfuric acid sweeping potential of 100 mV/s with 20 cycles between -0.4 and +1.5V vs. an Ag/AgCl reference electrode and using a Pt counter electrode.

3.3.3 Formation of agarose gel protective cross-linked enzyme sensing layer

After electrochemical cleaning the non-recessed electrode was washed by placing the electrode tip in deionised water for 2 min intervals, repeated three times and then the sensing layer was prepared by crosslinking glucose oxidase (GOx) and bovine serum albumin (BSA) with glutaraldehyde. This was achieved by mixing 6 mg of GOx and 40 mg of BSA in 200 μL of phosphate buffered saline solution. The prepared enzyme stock solution was stored at 4^{o}C.

The electrodes were then dip coated in a mixture of 8 μL of GOx stock solution and 4 μL of 1.2% (v/v) glutaraldehyde, which was allowed to crosslink for 10 min. The enzyme-coated electrodes were then washed in buffer solution to ensure any excess glutaraldehyde was removed, and left to dry overnight. Finally the enzyme-coated electrodes were dipped in 1% (w/v) agarose that was prepared by dissolving 50 mg of agarose in 5 mL of phosphate buffer solution and heating to 60^{o}C and then allowed to cool to room temperature in order to ensure that the enzyme layer was not denatured by heat. The agarose coated enzyme layer was then left to gel at room temperature for 30 min before any measurements were carried out.

3.3.4 Fabrication of recessed gold electrodes

The recessed electrodes were fabricated by etching the gold within the silica capillary using KI/I_2 solution. The electrodes were fabricated as described in section 3.3.2 above and fixed vertically into place using clamps with the tip of electrode immersed in KI/I_2 solution for approximately 10 -15 min before washing in deionised water several times to stop further etching. The recess depth was measured using optical microscopy. The depth of the recess is dependant on the length of time the electrodes were immersed in the etch solution as previously described in the work of Anastasova *et al*. It was reported that etching speeds of ~2.5 μM/min can be observed for wires of 80 μM in diameter with the etching solution used [115].

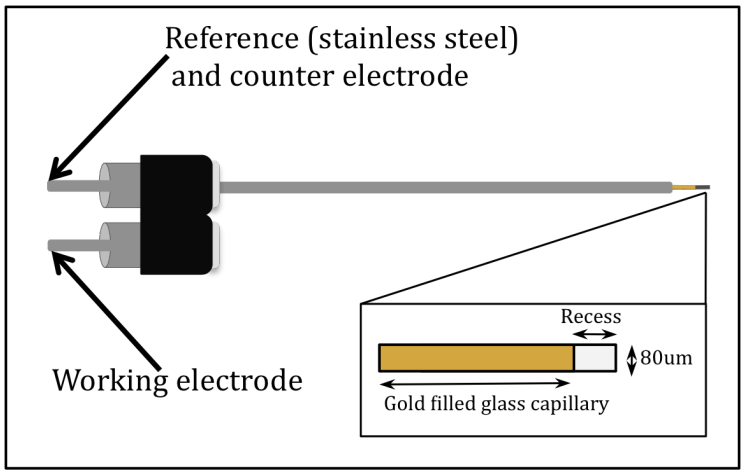

Figure 3.7: Schematic diagram of a recessed tip electrode.

The recessed tip electrodes were cleaned in a similar fashion to the non-recessed electrodes in section 3.3.2, through sequentially cleaning using ultra-sonication for 2 min in acetone, ethanol and water. Due to the fragility of the recessed tip, every effort was made to ensure the tip of the silica capillary did not come into contact with the edge of glass vials containing the cleaning solutions to ensure the tip was not easily broken. The recessed electrodes were dried by gently blotting the tip of the

electrode on lint free paper to absorb any of the excess water from the electrodes tip, before electrochemically cleaning in 50 mM of sulphuric acid, again using a sweeping potential of 100 mV/s with 20 cycles between -0.4 and +1.5V vs. an Ag/AgCl reference electrode and using a Pt counter electrode.

3.3.5 Formation of recess filled agarose gel protective cross-linked enzyme sensing layer

The recessed electrodes were filled with a crosslinked enzyme layer by mixing the GOx stock solution as stated in section 3.3.3 with 1.2% (v/v) glutaraldehyde in a 2:1 ratio on a microscope slide. The recess part of the electrode was carefully passed through the mixture and immediately held vertically in position to crosslink for 10-15 min. Immersing the electrode in water for a period of 5 min washed the excess glutaraldehyde away; this process was repeated thrice before drying the electrode by blotting the recessed tip on lint free tissue paper at an angle. The final agarose layer consisting of approximately 4 μL of 1% (w/v) agarose as outlined in section 3.3.3, used to fill the recess by passing the tip of the electrode through the agarose solution and immediately holding the electrode tip upwards for 30 min until completely gelated.

3.3.6 Agarose gel coated non-recessed electrode for hydrogen peroxide, acetaminophen and glucose sensing

Amperometric detection of hydrogen peroxide, acetaminophen and glucose was carried out in two-electrode mode, which used the stainless steel tubing as the reference and counter electrode. Prior to any measurements being taken the

electrodes were conditioned in the phosphate buffer solution to allow stabilization for approximately 30 min- 1 h. All measurements were carried out in a 20 mL sample volume of phosphate buffer solution, with continuous stirring using magnetic stirrer and carried out using a potential of +650 mVvs stainless steel.

Initial measurements were taken to determine electrode response to hydrogen peroxide (100 mM), using three previously fabricated bare electrodes. Following this, each of the three bare electrodes was tested individually for interference using ascorbic acid (50 mM), uric acid (5 mM) and acetaminophen. With each electrode being washed in between using phosphate buffer solution. Following this, the same non-recessed bare electrodes were washed in phosphate buffer solution before being dip coated with a cross linked enzyme layer as outlined in 3.3.3 and amperometric detection of acetaminophen, ascorbic acid and glucose were subsequently carried out through the addition of glucose, ascorbic acid and acetaminophen, respectively, in the sample volume. In between detection of each analyte, the electrodes were again washed using phosphate buffer solution. After the final measurement was taken on each electrode, a final wash in buffer and deionised water was carried out before the electrodes were covered and allowed to dry at room temperature for 1 h.

Once the membrane coated non recessed electrodes were fully dried and dip coated in 1% Agarose as outlined earlier in 3.3.5, each electrode was again used to detect if there was a change in the response for glucose, and also to interfering substances such as ascorbic acid and acetaminophen.

3.3.7 Agarose gel filled recess electrodes for Hydrogen peroxide, Acetaminophen and Glucose detection

The recess depths tested for each electrode were measured by light microscopy.

As with non-recessed electrodes, each recess electrode was first tested for the detection of hydrogen peroxide before being filled with a cross-linked enzyme layer to measure glucose before subsequently testing for interference of acetaminophen and ascorbic acid. Concluding this, the recess electrodes were then washed in phosphate buffer and water before drying using lint free paper. The recesses of the electrode were then filled with 1% (w/v) agarose as outlined in and the further response to glucose was determined to establish if there was any difference in signal due to the presence of the gel layer. Interferences to acetaminophen and ascorbic acid were also compared.

3.3.8 Fabrication of platinised needle electrodes for H_2O_2 detection on agarose enzyme gels.

Materials: Membranes coating the electrode surface were sulphonated polyesther ether sulphone – polyether sulphone (SPEES/PES) copolymer (ICI Colloids and Polymer Group, Runcorn, UK) and polyurethane membrane was based on the prepolymer Trixene SC7602 (Baxenden Chemicals Ltd, Accrington, UK).

The fabricated sensors were about 3 cm in length, with the sensing tip about 1 mm edge from the surrounding stainless steel tubing. The electrodes were cleaned in 50 mM of sulphuric acid, again using a sweeping potential of 100 mV/s with 20 cycles between -0.4 and +1.5V vs. an Ag/AgCl reference electrode and using a Pt counter electrode. Following this the cleaned electrode tip was dip coated with SPEES/PES membrane 10% (w/v) in dimethylsulphoxide, and dried overnight at ambient room

temperature. Finally, external 20% and 30% (w/v) polyurethane coatings prepared in tetra-hydrofuran were applied before any measurements were taken. The sensors were treated in 70% (v/v) ethanol for 1 h with a final wash in DI water before measurements with cells.

Amperometric measurements were performed in a two-electrode system at room temperature (23±1°C), using stainless steel tube as both counter and reference electrode and platinum wire as a sensing electrode. Electrochemical measurements were done using a PalmSens potentiostat, controlled by a PC with associated electrochemistry software (PS Trace). Temperature was maintained to 37ºC to maintain cell culture conditions. This was achieved by a water bath in which the sample vial was clamped to. Figure 3.8 illustrates the experimental set up for the detection of H_2O_2. Prior to any measurements with cells or enzyme gels, a calibration of H_2O_2 was carried out by stepwise additions of 100 mM H_2O_2 into DMEM to achieve known concentrations.

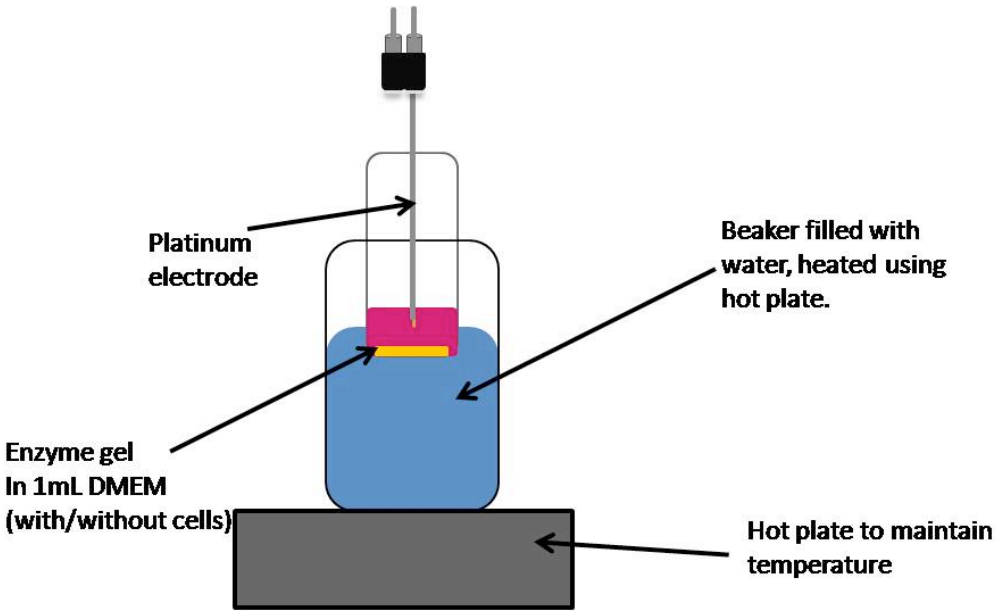

Figure 3.8: Experimental set up for the detection of H_2O_2 in agarose GOx and GOx-CAT gels using Pt electrode.

3.4 Cell viability and morphology of B50 cells cultured on crosslinked protein membranes

3.4.1 Reagents

For the preparation of pH 7.4 phosphate buffered saline (PBS);di-sodium hydrogen phosphate (Na_2HPO_4) and sodium di-hydrogen phosphate (NaH_2PO_4) were purchased from BDH, (Dorset, UK). Sodium chloride (5 mM, NaCl) along with 5 M sodium hydroxide (NaOH) was purchased from Sigma Aldrich & Co. (UK). Protein solutions comprising bovine serum albumin (BSA), from heat shock treatment and fibrinogen from bovine plasma (Type I-S, 65-85% protein) were also purchased from Sigma Aldrich (UK) along with crosslinking agent's glutaraldehyde, Terephthaloyl chloride (TCL) and distilled xylene.

For cell viability studies, 0.4% (w/v) Trypan Blue and PrestoBlue cell viability reagent was purchased from Life Technologies (Invitrogen, UK).

3.4.2 Solution preparation

3.4.2.1 Phosphate buffered Saline

All protein solutions were prepared in pH 7.4 phosphate buffered saline. This was prepared by weighing 7.50 g L^{-1} of Na_2HPO_4 (52.8 mM), 1.87 g L^{-1} of NaH_2PO_4 (15.6 mM), 2.98 g L^{-1} of NaCl and dissolving in 1 L of distilled water with the aid of a magnetic stirrer. The pH was adjusted to 7.4 by adding 5 M NaOH drop wise. The prepared buffer solution was stored at room temperature.

3.4.2.2 Protein solutions

The 20% (w/t) of BSA solution was prepared by dissolving 1.25 g of BSA in 5 mL of 7.4 pH PBS as previously described. The solution was covered and left to dissolve fully at room temperature (23^0C) for approximately 4 h. Fibrinogen solution 3.8% (w/t) was prepared similarly by dissolving 0.2 g of fibrinogen in 5 mL PBS and left once again at room temperature until fully dissolved. Once dissolved, the solutions were kept at 4^OC.

3.4.2.3 Crosslinking solutions

For the formation of crosslinked protein membranes, a 1% (w/t) solution of Terephthaloyl chloride (TCL) was prepared by dissolving 0.1 g TCL in 10 ml of xylene in a sealed bottle, with continuous stirring for 2 h at room temperature. For protein membranes containing glucose oxidase (GOx), the crosslinking solution used was 1.2% (v/v) glutaraldehyde by diluting 25 μL in 475 μL PBS.

3.4.3 Protein membrane formation

3.4.3.1 Large surface area protein membranes

Membranes were formed by aliquoting 2 mL of protein solution (4.2.2) into a glass vial. Following this 1 ml of crosslinking solution (4.2.3) was carefully layered on top of the protein solution forming an instantaneous immiscible layer at the interface of both solutions. The vial was covered and was stored at 4^0C over two days to allow a membrane to form of a reasonable thickness for handing. Figure 3.9 demonstrates the procedure followed to form large surface area crosslinked protein membranes.

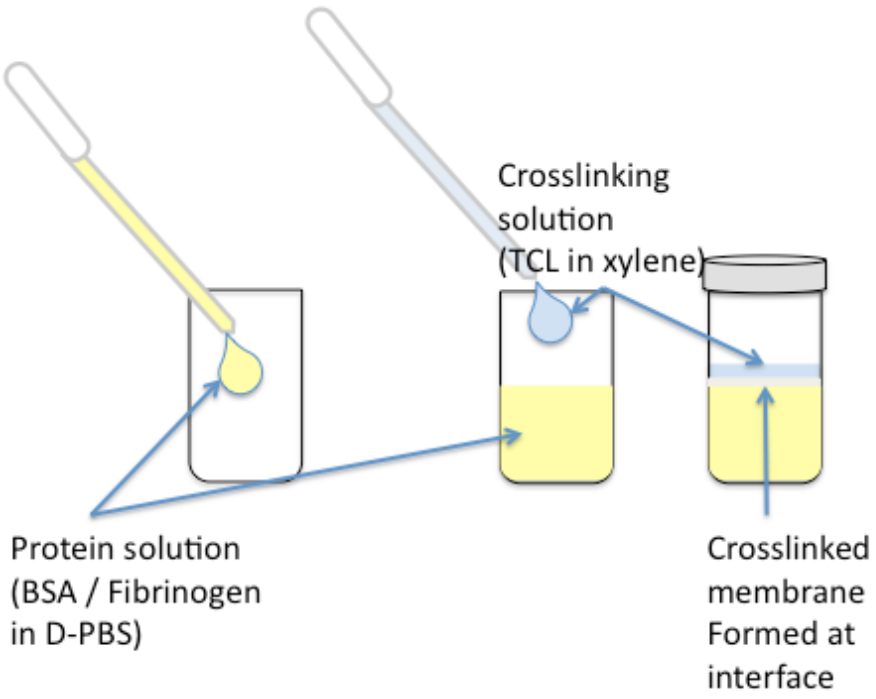

Figure 3.9: Schematic diagram of the fabrication process of crosslinked protein membranes.

The membrane was detached from the vial by slowly removing the excess crosslinking solution above the membrane, and then using a 0.5 mm spatula to gently loosen the membrane from the edge of the vial. Once the membrane was lifted from the vial it was washed by immersing in distilled water at five-minute intervals several times to ensure any excess crosslinker was removed with a final wash in ethanolamine.

Following mounting of the membrane between glass cover slips, and measuring the space between the cover slip edges using light microscopy the thickness of the membrane was determined. Prior to any cell work being undertaken, the membranes were stored in 10% (v/v) antibiotic/ antimycoctic solutions prepared in D-PBS.

3.4.3.2 Spin coating method for protein membrane formation

Albumin and Fibrinogen protein solutions were added drop-wise on a glass cover slip and spin coated at a low speed of 500 rpm for 10 seconds to allow an even distribution of the protein on the cover slip. Following this, one drop of the cross linking agent (TCL) was added to the middle of the protein coated cover slip and spin coated for a further 10 seconds at 500 rpm. The membranes formed were allowed to dry at room temperature for 30 min before washing with PBS.

3.4.4 Cell morphology and viability studies

B50 rat neuronal cells were cultured for 3-4 days at 37^0C in 5% CO_2 until they reached approximately 70% confluence. Following this, cells were detached using trypisin and cell density was established using hemocytometer. Approximately 0.25 mL of $1.5X10^6$ cell/ml cell suspension was dispensed into 24 well plates consisting of the different crosslinked protein membranes. Protein membranes present were triplicates to ensure reproducible results. All membranes were fixed in 4% paraformaldhyde (PFA) solution for 10-20 min. The samples were washed in PBS thrice before cell morphology was determined by light microscopy with the aid of stains such as haematoxylin and eosin. For large surface area membranes, cell morphology was determined after a period of 6, 18, 24 and 48 h for both fibrinogen and albumin membranes. After fixation in 4% PFA the samples were washed thoroughly in deionised water to remove any salts present before viewing using scanning electron microscopy (SEM).

Initial viability studies on crosslinked protein membranes formed from spin coating were carried out using the Trypan Blue exclusion method [163]. After incubation

periods of 24 and 48 h, cells were trypsinized and stained using Trypan Blue in a 1:2 dilution. A hemocytometer as shown in Figure 3.10, was used to count the cells and non-viable cells (stained blue) resolved from viable cells (unstained). The percentage viability of cells was calculated using the following formula:

$$\frac{\text{No. of viable cells}}{\text{Total no. of cells}} \times 100$$

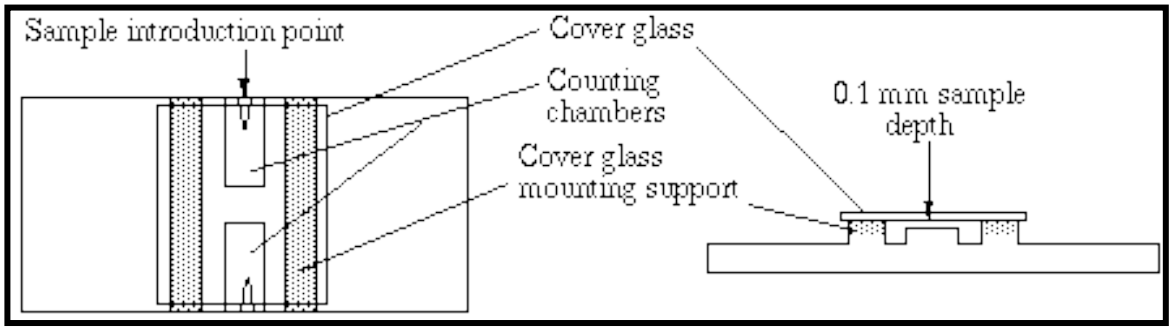

Figure 3.10: Cross section of Hemocytometer (Cascade Biologics) [164].

Viability studies on protein and enzyme membranes incubated for 3, 6, 12, and 24 h was determined using PrestoBlue cell viability reagent as outlined in section 3.2.5.

3.5 Development and fabrication of microfluidic devices

3.5.1 Design and fabrication of microfluidic flow cell

For the fabrication of a microfluidic channels, different methods and materials were used in order to produce a working microfluidic system. The initial design for the channel was based on previous studies within the research group by Chang et al [165] of Y shaped channels, which were fabricated using glass cover slips. The diagram below demonstrates the basic design used and outlines the dimensions of the

channels. The width of the main channel was 2 mm with a depth of 100 μM. Two smaller channels of 1 mm in width and 100 μM in depth were used as inputs for the transportation of various solutions to the main channel.

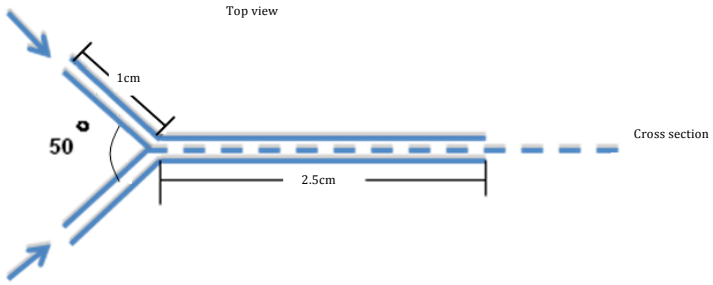

Figure 3.11: Schematic diagram of Y-shaped flow cell, two inputs each 1cm in length with a main channel length of 2.5 cm [165].

3.5.2 Fabrication of Perspex flow cell

Following the above design, the channels for the flow cell were micro-machined by Mr. Tony Willis (School of Engineering and Materials Science workshop) onto a Perspex block and secured against another plain block using eight 2 cm screws. An O-ring was placed in between the two Perspex blocks to prevent leakage. Holes were drilled through the Perspex block as input fluid connectors for the two smaller channels and one at the end of the main channel as an output. Figure 3.12 is an image of the fabricated device.

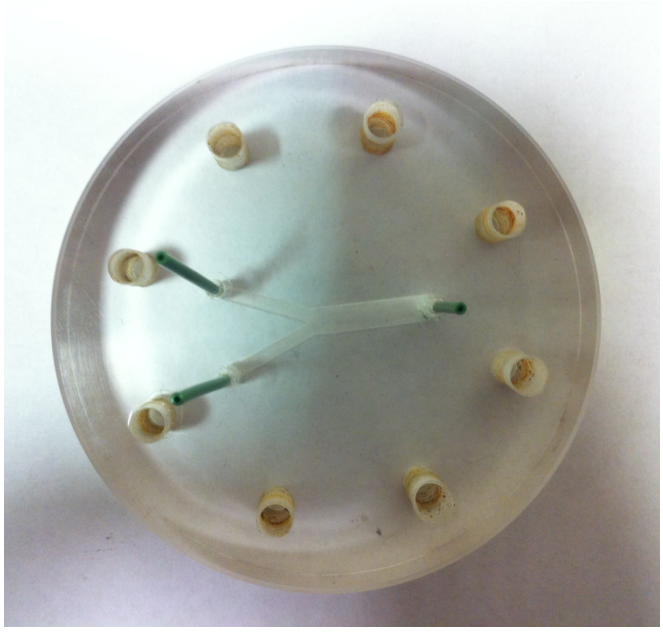

Figure 3.12: Image of Perspex flow cell.

3.5.3 Fabrication of PDMS microfluidic channel

The fabrication of PDMS microfluidic channels involved four stages:

- Fabrication of a mould
- PDMS Casting
- Fluidic port connections
- Channel sealing

The first stage required a mould to be fabricated. Two different substrates were used to fabricate the mould, a brass substrate and single sided copper coated PCB board.

Materials:

For the brass mould, a 6 mm thick brass plate was purchased from Clickmetal (UK). A fibreglass pre-sensitized single sided copper clad PCB board (# JP55K) along with Ferric chloride etchant (# XX12N) and Universal PCB (# AP01B) developer was purchased from Maplin electronics (UK).

PDMS was supplied in two parts Slygard -184 (A) and Slygard – 184 (B), these contained 30-60 and 10-30% (w/t) of dimethylvinylated and trimethylated silica fillers.

Fabrication of moulds

The brass substrate used to fabricate the Y channel, as designed in Figure 3.11 was carried out by a member of the research group (Mr. Hussein Ershadi-Oskoi). This was achieved by spin coating a thin layer of photo resist on the brass plate and then exposing the Y channel design using UV. The substrate was then developed using the developing solution containing sodium hydroxide and finally etched using ferric chloride. Any remaining photoresist was cleaned using ethanol and finally acetone before drying.

A similar procedure was used to fabricate the fibreglass mould. The copper coated PCB board contained a thin film of positive photoresist protected by a plastic sheet, the designed microchannel was printed on to a transparency and layered directly on the top of the photoresist layer and exposed using a UV box. The exposed design was then placed into the developing solution heated at approximately $40^{O}C$ for around 20 seconds. The PCB board was then transferred to a heated solution of ferric chloride ($40^{O}C$) until the solution become a blue due to the copper coating being etched away from the fibre glass. The mould was then cleaned using ethanol and acetone before drying at room temperature.

PDMS Casting

PDMS was mixed in a 10:1 of Slygard-184 (A) / Slygard-184 (B). The two parts were weighed and mixed in a plastic cup using a glass rod to vigorously mix the two

components. The air bubbles produced at the mixing stage were removed by placing the cup containing the mixture into a desiccator and applying a gentle vacuum for approximately 10 min repeating several times until all the bubbles were removed. Once the PDMS was degassed it was then poured over the substrate and cured in an oven at 65^{O}C for a minimum of 4 h.

The PDMS cast was then peeled away from the mould and then covered to prevent dust from settling on the surface.

Fluidic port connections

The PDMS was pierced using a flat tipped 20-gauge syringe needle. This made the connections for the fluidic ports. This was done at the two inputs and the single output at the end of the Y channel. The edges of the ports were then sealed with UV curable glue to prevent any leakages.

Sealing of the channel

This was achieved by firstly cleaning a glass microscope slide thrice with water, ethanol and acetone. Both the PDMS cast and the glass slide were washed again in isopropyl alcohol and dried using nitrogen gas before treatment with oxygen plasma for 10-15 seconds. The two substrates were then pressed together which immediately sealed the channel and left for 48 h at room temperature before use.

3.5.4 Sensor integrated microfluidic channel

A microfluidic channel was fabricated as outlined in Section 3.5.3, however the initial design incorporating a secondary channel along the side of the main Y channel was not produced as this prevented the flow from being laminar. Polyester insulated

platinum wire of 0.014 mm thickness, with a conducting diameter of 0.125 mm was integrated within the side of the channel before bonding.

3.6 Instrumentation

3.6.1 Electrochemical measurements

Electrochemical measurements were taken using a PalmSens potentiostat /galvanostat (Palm Instruments BV, Netherlands), which was supported with the PalmSens PC software (Ivium Technologies). Cyclic voltametry was carried out at room temperature (23 ^{O}C) using a programme on the Palmsens with a three-electrode cell with a Ag/AgCl reference (MF 2052), and a Pt counter electrode (MW 1032) both from Bioanalytical systems Inc.(UK). Solutions were constantly stirred with a magnetic stirrer (IKA Werke GmbH & Co. , KG Germany).

3.6.2 Microscopy

3.6.2.1 Light microscopy

Images of cells stained with H&E were taken using a Leica DM IRB inverted microscope with integrated digital camera and software from Leica Microsystems (UK) Ltd. A Nikon Eclipse E600 microscope also with digital camera and software from Nikon UK (Ltd) was used to image gel and membranes samples and to measure the depth of the recess electrodes.

3.6.2.2 Scanning electron microscopy (SEM)

A Jeol JSM 6300 high field scanning electron microscope (SEM) from Jeol (UK) was used to image the surface of protein membranes and B50 cells cultured on the

surface of the membrane. SEM provides images with micron scale resolution with a magnitude ranging from x10 – 500,000. SEM samples were coated with a thin layer of gold by a sputter coater before placing into a vacuum column.

3.6.3 Fluorescence measurements for cell viability assays

Fluorescence measurements associated with the PrestoBlue cell viability assay were obtained by using the FLUOstar galaxy fluorescence micro plate reader from BMG Labtech. The spectra range used for the viability assay was excitation at 544 nm and emission at 590 nm with a gain adjustment of 90 %.

CHAPTER 4

-

Cell viability on enzyme encapsulated hydrogels

4.1 Introduction

Implantable biosensors have had little success for long-term implantation. The material and biotransducer elements of these biosensors elicit an inflammatory response initiated by cell death as a result of poor biocompatibility. Injured cells *in vivo* release danger signals known as damage associated molecular pattern molecules (DAMPs), which alert the host to cell death. The majority of DAMPs exist as nuclear or cytosolic proteins. On exposure at the cells surface following tissue injury, they migrate from a reducing to an oxidizing environment, resulting in denaturation [166]. These molecules are recognised by cellular receptors that stimulate and generate pro-inflammatory mediators from either intracellular or extracellular sources. This interaction then orchestrates the inflammatory response, which in some chronic cases causes the development of granulation, foreign body reaction and eventually resulting in the fibrous encapsulation of implantable devices [11][167]. Despite development of novel, biocompatible, host compatible bio-membranes such as biologically derived and biomemetic structures and hydrogels, this problem persists. In this study I aimed to investigate whether the immobilized enzyme bioreceptor, usually an oxidoreductase enzyme, in this case glucose oxidase, is also responsible for cell death.

Glucose oxidase catalyses the oxidation of β-d-glucose to d-glucono-β-lactone and hydrogen peroxide, with molecular oxygen as an electron acceptor. Hydrogen peroxide can be potentially harmful to cells; hence in this study catalase was used to remove the effect of peroxide. However, this may not be fully effective because some peroxide form superoxide and peroxide radicals, so the need for GOx, CAT and SOD used together was investigated. The reaction process is summarised in

Figure 4.1. The enzymes were incorporated by physical immobilization; no covalent conjugation was carried out.

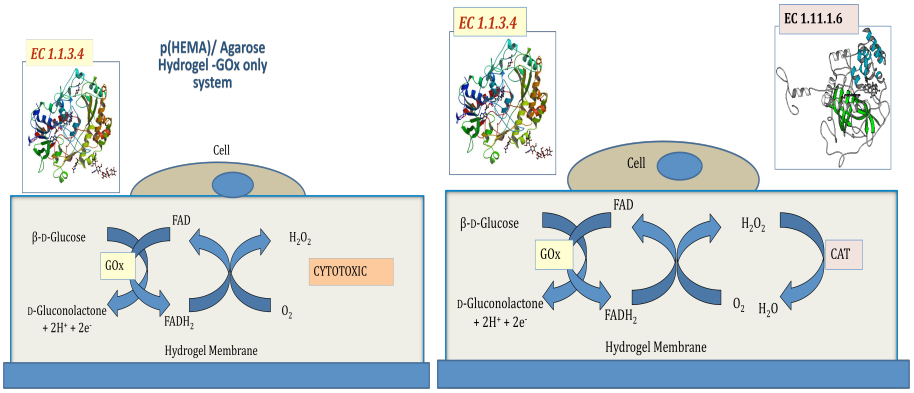

(A) (B)

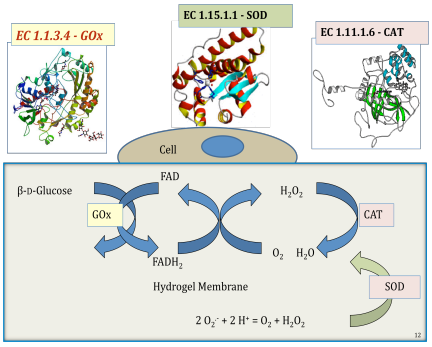

(C)

Figure 4.1: Reaction of immobilized enzymes system (A) Glucose oxidase only system, (B) Glucose oxidase and Catalase system, (C) Glucose oxidase, Catalase and Superoxide dismutase system.

Two types of hydrogels were used in this study, 1% (w/v) concentration agarose gels and 3 mol% concentration of TEGDA p(HEMA) gels. The effect of the enzymes on cell growth and viability on agarose and p(HEMA) hydrogels was studied. Two cell lines were used, human muscle fibroblasts (RMS 13) cells were cultured on p(HEMA) gels and rat neuroblastoma cells (B50) were cultured on 1% (w/v) agarose gels.

4.2 Cell viability on enzyme hydrogels

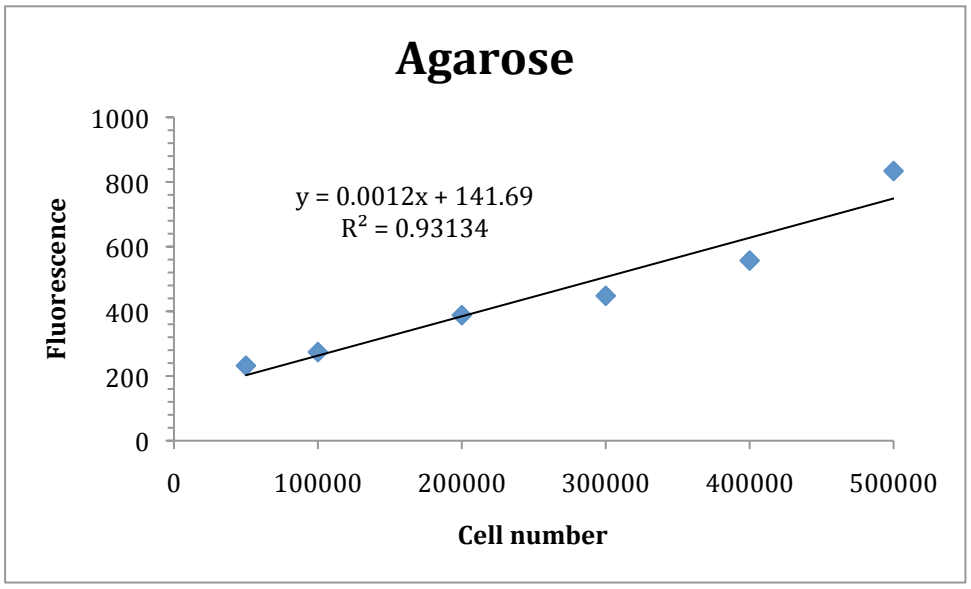

Figure 4.2: Relative fluorescence values measuring the metabolic activity of B50 cells grown on 1% (w/v) agarose gels.

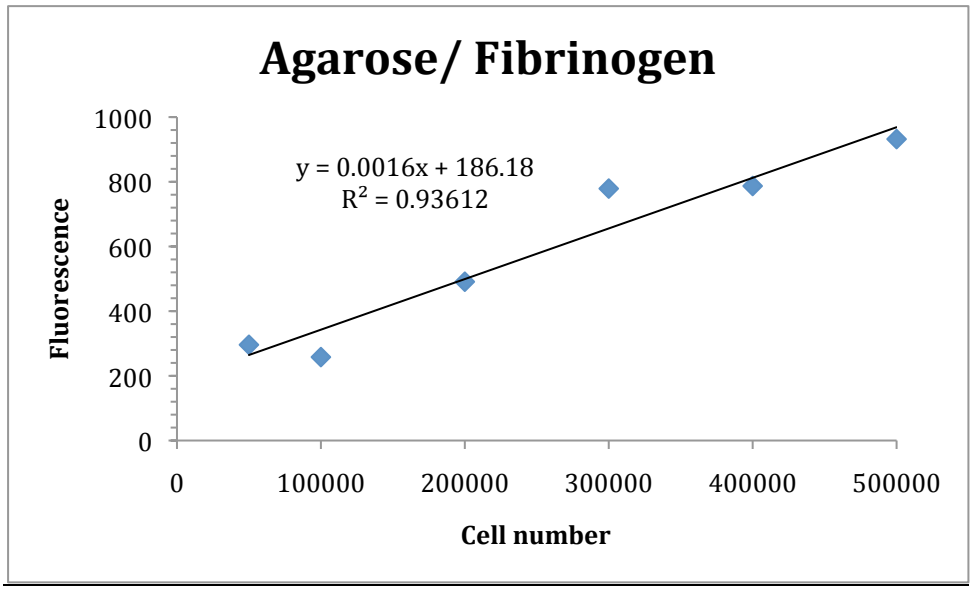

Figure 4.3: Relative fluorescence values measuring the metabolic activity of B50 cells grown on 1% (w/v) agarose gels supplemented with 2% (w/v) fibrinogen.

Viability data was collect through the use of the vital stain Trypan blue in a dye exclusion method to determine viable and non viable cells on p(HEMA) and agarose gels. This was used in conjunction with the MTT assay as an end point measurement of cell toxicity to determine the metabolic activity of cells.

The PrestoBlue reagent is a cell permeable resazurin-based solution that functions as a cell viability indicator by using the reducing power of living cells to quantitatively measure the metabolic activity of cells. When added to cells, the PrestoBlue reagent is modified by the reducing environment of the viable cell and turns red in color, becoming highly fluorescent. The color change can be detected by fluorescence or absorbance measurements. PrestoBlue was preferred to the MTT assay as it is non-toxic to cells [168][169], and does not require cell lysis thus enabling a live cell assay of up to 24 h it is also highly sensitive and can detect as little as 12 cells per well on 384 well plate. In the current study the use of PrestoBlue helped to determine whether the cells present were metabolically active and indicated cell proliferation after incubated time frames.

Preliminary studies into the culture of B50 cells cultured on agarose hydrogels revealed poor adhesion properties of B50 cells to the agarose surfaces. This was likely to be due to the mechanical stiffness of agarose being high. This was easily overcome by reducing the concentration of agarose to a 1% (w/v) gel along with the addition of fibrinogen, which further increased the ability of cells to adhere to the gel surface over a longer period of time. A series of B50 cells were incubated for 24 h on 1% (w/v) agarose gels and 1% (w/v) agarose gels supplemented with 2% (w/v) of fibrinogen. The PrestoBlue viability assay was then carried out Figure 4.2 and 4.3

which revealed an overall higher metabolic activity of cells cultured on agarose gels supplemented with fibrinogen over plain 1% (w/v) agarose gels, though even here adhesion was better than the stiffer, more concentrated agarose.

4.3 Cell viability on heat control enzyme loaded agarose gels after 6 & 24 h

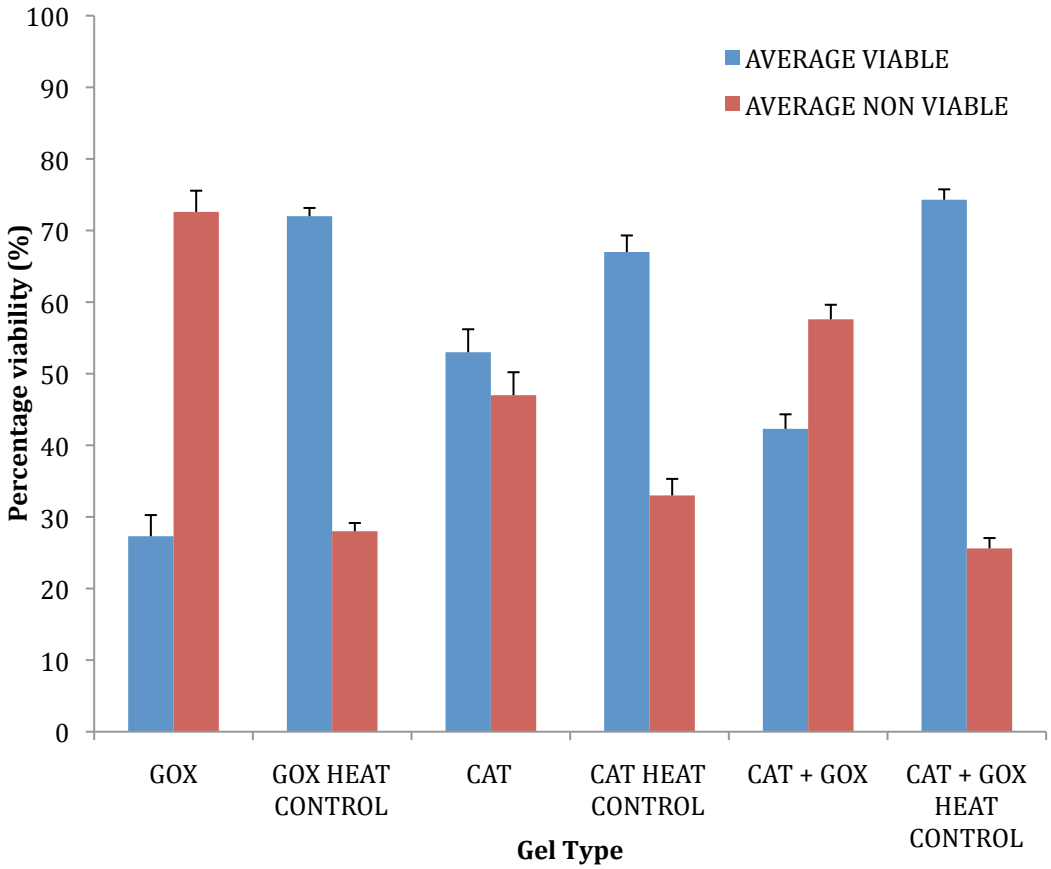

Figure 4.4: Cell viability of enzyme loaded agarose gels with and without heat treatment and after 6 h of cell culture (± SE, n=3).

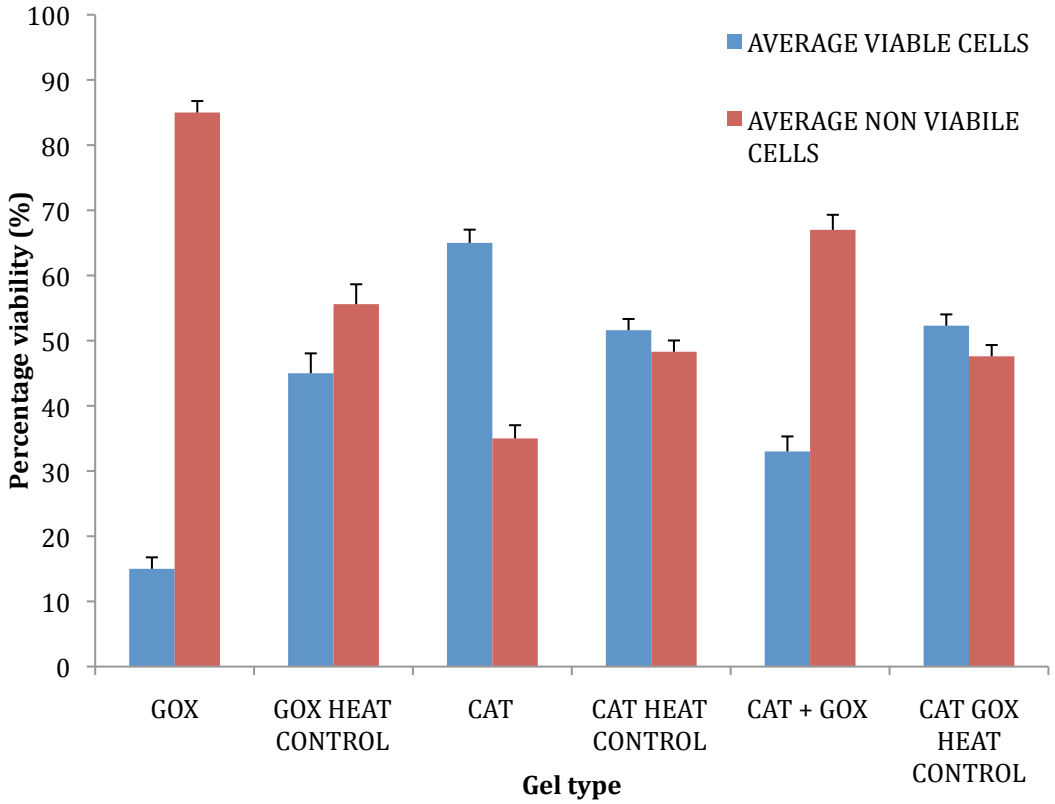

Figure 4.5: Cell viability on enzyme loaded agarose gels with and without heat treatment after 24 h of cell culture (± SE, n=3).

Studies revealed that after 24 h of cell culture, cells proliferated best with no enzyme present; with most cells appearing to be fully developed. The presence of GOx affected the viability and growth of B50 cells. It was noted that the number of viable cells present was considerably lower than that of cells cultured on agarose gels consisting solely of fibrinogen. It is presumed that this is due to competition for glucose along with oxygen, by the enzyme and also the resulting accumulation of H_2O_2. To overcome this, the addition of catalase to the GOx enzyme gels, was investigated thus degrading H_2O_2 produced.

Two control experiments were carried out in order to test the hypothesis of whether enzyme based agarose gels affected cell growth and proliferation. The first control

used simply agarose with fibrinogen to enhance cell adhesion. Following this, control gels for studies after 6 and 24 h of cell culture consisted of gels which contained enzyme that was treated at temperatures exceeding 130^0 C to denature the GOx present and to eliminate any possible enzyme activity. After 6 h, viability studies revealed 42.3 ± 2.03 % cell viability of B50 cells cultured on agarose gels with GOx and CAT both present, in comparison to gels containing solely GOx which indicated only 27.3 ± 2.96 % of cells present were viable. Gels with only CAT present showed 53 ± 3.21 % of viable cells present.

Heat controls of GOx produced a 72 ± 1.15 % viability with similar results seen when GOx was used in conjunction catalase and exposed to heat, resulting in a 74.3 ± 1.45 % viability. Thus, denatured enzyme present in the heat controls allowed for significantly more viable cells than those present on active enzymes.

As the incubation period of cells increased from 6 to 24 h; it was also noted that cell viability in most enzyme gels dropped considerably but not for the gel with catalase which showed an increase in viability from 53 ± 1.15 % to 65 ± 2.03 %.

4.4 Cell morphology on heat-treated agarose enzyme gels

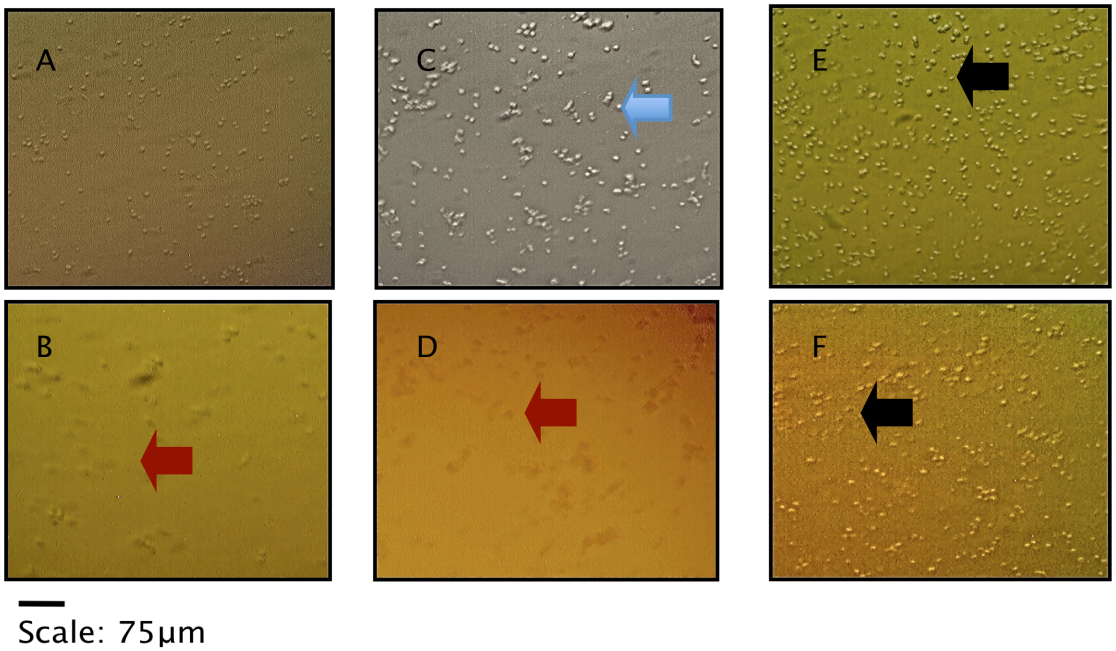

Figure 4.6: B50 cells on heat control enzyme gels after 6 h of culture
A: CAT heat control, B: GOx, C: CAT D: CAT + GOx, E: CAT + GOx heat control, F: GOx heat control.
Blue arrow show sickle shaped cells with signs of neurite formation; red arrows show poor adhesion of cells with aggregation, black arrows indicate majority of spherical shaped cells present.

Cell structural development in all cases was poor with most cells present appearing to be spherical with very little or no neurite formation (Figure 4.6); the exception was gels containing catalase (Figure 4.6 (C)). Here it is noted that some cells appear more sickle shaped, and over time there was no change in cell morphology. It can therefore be concluded that the presence of enzymes can be a limiting factor in cell growth and proliferation, however in the presence of denatured enzyme (Figure 4.6 (F)) cells appear attached to the gel and are spherical in shape and are generally more densely arranged, though with no signs of elongation at even 24 h to indicate proper cell compatibility of even the denatured GOx.

4.5 Cell viability on enzyme encapsulated p(HEMA) hydrogels

4.51 Cell viability on p(HEMA) enzyme gels after 6 h

GEL TYPE	CELLS SEEDED	TOTAL VIABLE	TOTAL NON VIABLE	CELLS REMAINING IN GEL
GOx	1125000	27897	253219	843884
CAT	1125000	12876	254292	857833
SOD	1125000	3219	324435	797746
GOx-SOD	1125000	6438	244635	873927
GOx-CAT	1125000	2146	111588	1011266
GOx-CAT-SOD	1125000	6438	233906	884656
CONTROL	1125000	116952	196352	811696

Table 4.1: Normalized cell viability of RMS 13 cells after 6 h of culture, sample repeat *(n=3)*.

RMS 13 cells were counted on enzyme encapsulated using 3 mol % TEGDA p(HEMA) hydrogels as outlined in Chapter 3 Section 3.1.7.

After an initial cell incubation period of 6 h, enumeration of cells from the p(HEMA) gels indicated that control gels with no enzyme contained the highest number of viable cells present as summarized in Table 4.1. Gels consisting solely of GOx or CAT indicated similar viability with, however, GOx gels producing double the number of viable cells compared with CAT only cells when enumerated. Combined GOx and CAT produced the least number of viable cells.

SOD used in combination with GOx and CAT resulted in similar cell viability as that of GOx and SOD, however SOD alone produced the highest number of non-viable cells.

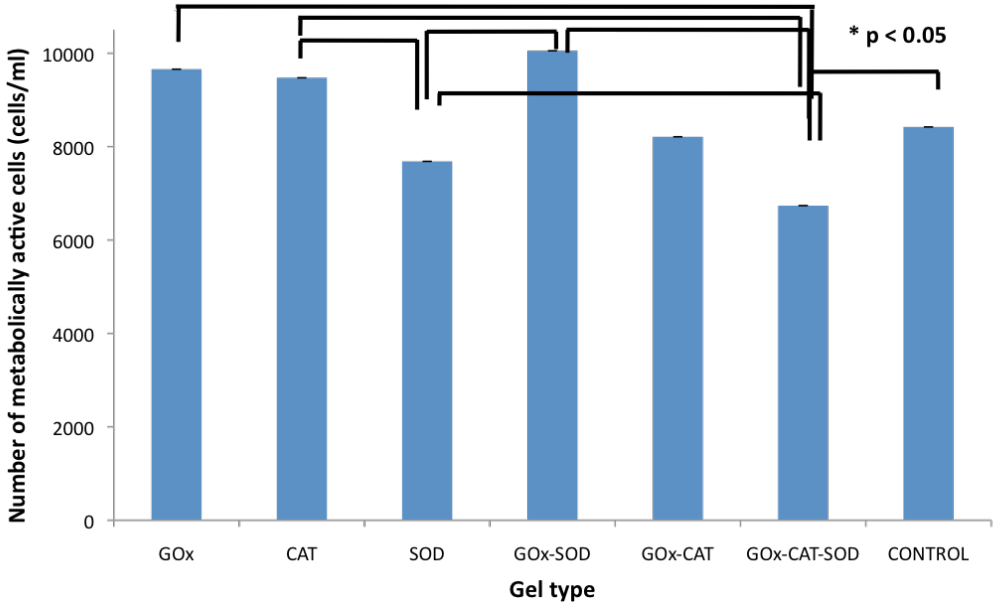

Figure 4.7: Normalized number of metabolically active RMS 13 cells derived from MTT assay on p(HEMA) enzyme gels after cell enumeration post 6 h. (± SE, n=9) * $p < 0.05$ indicating a significant statistical difference between sample types.

After the enumeration of cells from the p(HEMA) enzyme gels, an MTT assay was performed to account for any cells remaining on gels that were unable to be trypsinized. The assay also indicated that gels of GOx-SOD alone produced most number of metabolically active cells remaining on the gels with GOx a close second. MTT data also confirmed that GOx-CAT-SOD gels produced the least number of active cells.

Statistical analysis of MTT assay data as indicated in Figure 4.7 revealed there to be a significant difference between GOx-CAT-SOD gels compared to all other gel types. SOD only gels also indicated a significant difference when compared with CAT only and GOx-SOD gels.

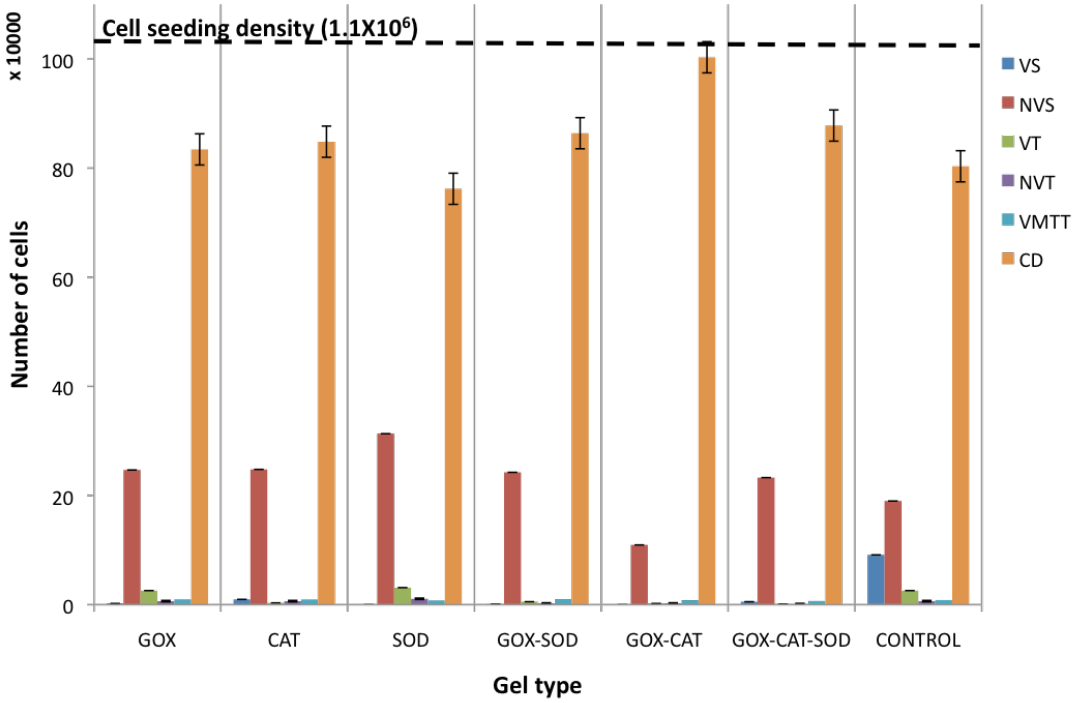

Figure 4.8 Viability of RMS 13 cells on p(HEMA) enzyme gels after 6 h (± SE, n=3) VS = Viable cells in suspension, NVS= Non-viable cells in suspension, VT= Viable cells trypsinized, NVT= Non-viable cells trypsinized, VMTT= Viable cells from MTT assay, CD= Calculated difference.

** CD = Cells seeded –(VS+NVS+VT+NVT+VMTT)*

Figure 4.8 indicates the distribution of viable and non-viable cells within each sample. In comparison to cells present in suspension, cells trypsinized accounted for the majority of viable cells with the exception of control samples, indicating cellular

attachment occurred by 6 h in most samples. There were also fewer non-viable cells present that were trypsinized compared to that of non-viable cells in suspension. From the calculated total number of cells remaining on gels at 6 h from Table 4.1, very few of the cells remaining were calculated to be metabolically active from MTT assay results in Figure 4.7 therefore resulting in a large calculated difference as shown in Figure 4.8. These results indicate that the effect of the enzyme in the gels could be different from those on the surface or in suspension. The high calculated difference could also be a result of poor enumeration.

4.52 Cell viability on p(HEMA) enzyme gels after 12 h

GEL TYPE	CELLS SEEDED	TOTAL VIABLE	TOTAL NON VIABLE	CELLS REMAINING IN GEL
GOx	1125000	33930	114027	-18333
CAT	1125000	848	1010464	113688
SOD	1125000	848	112667	-2545
GOx-SOD	1125000	5090	727093	392816
GOx-CAT	1125000	4242	1068156	52602
GOx-CAT-SOD	1125000	1697	845871	277432
CONTROL	1125000	22907	855204	246889

Table 4.2: Cell viability of RMS 13 cells after 12 h of culture, sample repeat *(n=3)*.

After 12 h, control gels consisting solely of fibrinogen and no enzyme indicated high cell viability as with control gels at 6 h. The least viable cells present were on gels containing only SOD or CAT.

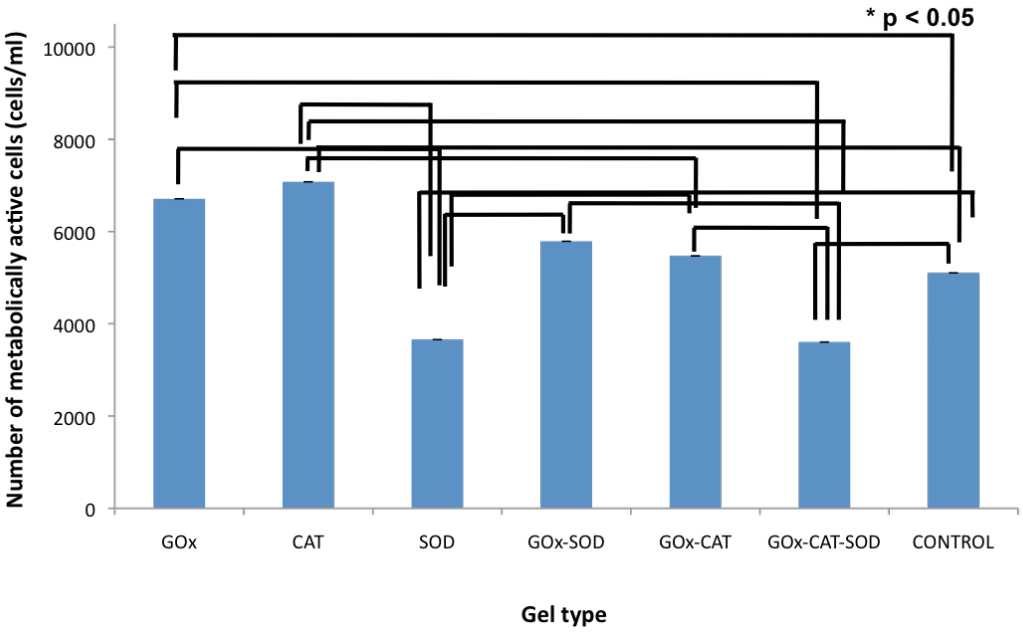

Figure 4.9: Normalized number of metabolically active RMS 13 cells on p(HEMA) enzyme gels derived from MTT assay after cell enumeration post 12 h. (± SE, n=9), *p <0.05 indicating a significant statistical difference between sample types.

Gels containing GOx and SOD produced the most number of viable cells enumerated in comparison to the other enzyme gels however this was not confirmed in the MTT assay as the absorbance readings revealed that CAT gels produced the most number of metabolically active cells within gels with similar results from GOx gels.

Figure 4.9 indicates statistical significance between gel types. SOD only and GOx-CAT-SOD gels were calculated to be statistically different compared with other gel types.

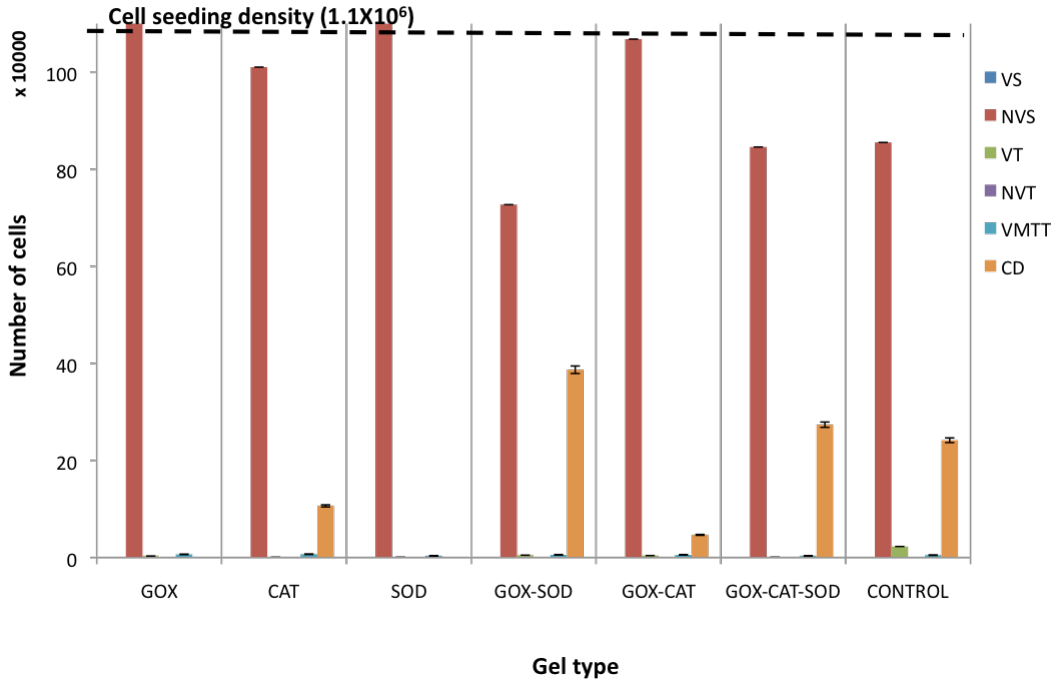

Figure 4.10: Viability of RMS 13 cells on p(HEMA) enzyme gels after 12 h (± SE, n=3) VS = Viable cells in suspension, NVS= Non-viable cells in suspension, VT= Viable cells trypsinized, NVT= Non-viable cells trypsinized, VMTT= Viable cells from MTT assay, CD= Calculated difference.

** CD = Cells seeded –(VS+NVS+VT+NVT+VMTT)*

Figure 4.10 indicated a lower calculated difference in most gel types after 12 h in comparison to that observed at 6 h. Gels consisting of only GOx or SOD resulted in a higher number of non-viable cells being counted than that seeded, thus accounting for a negative calculated difference as noted in Table 4.2. Figure 4.9 concluded there to be some metabolically active cells present, which confirms that there may have been miscalculation of enumerated cells in these two sample types.

4.53 Cell viability on p(HEMA) enzyme gels after 24 h

GEL TYPE	CELLS SEEDED	TOTAL VIABLE	TOTAL NON VIABLE	CELLS REMAINING IN GEL
GOx	1125000	0	337500	787500
CAT	1125000	4167	440833	680000
SOD	1125000	833	350000	774167
GOx-SOD	1125000	833	325833	798333
GOx-CAT	1125000	833	417500	706667
GOx-CAT-SOD	1125000	0	296667	828333
CONTROL	1125000	25000	418333	681667

Table 4.3: Cell viability of RMS 13 cells after 24 h of culture, sample repeat *(n=3)*.

After 24 h, GOx gels and GOx-CAT-SOD gels showed zero cell viability (Table 4.3) indicating that the enzyme induced damaged was cumulative with maintained high enzyme activity resulting in degradation and excess hydrogen peroxide increasing the cytotoxic effect on cells. Viability on control samples demonstrated a consistent increase over time, indicating the proliferation of cells. There was also an increase in viability of CAT only gels between 12-24 h, this indicated that some of the cells noted to be non-viable at 12 h may have been able to recover and proliferate by 24 h.

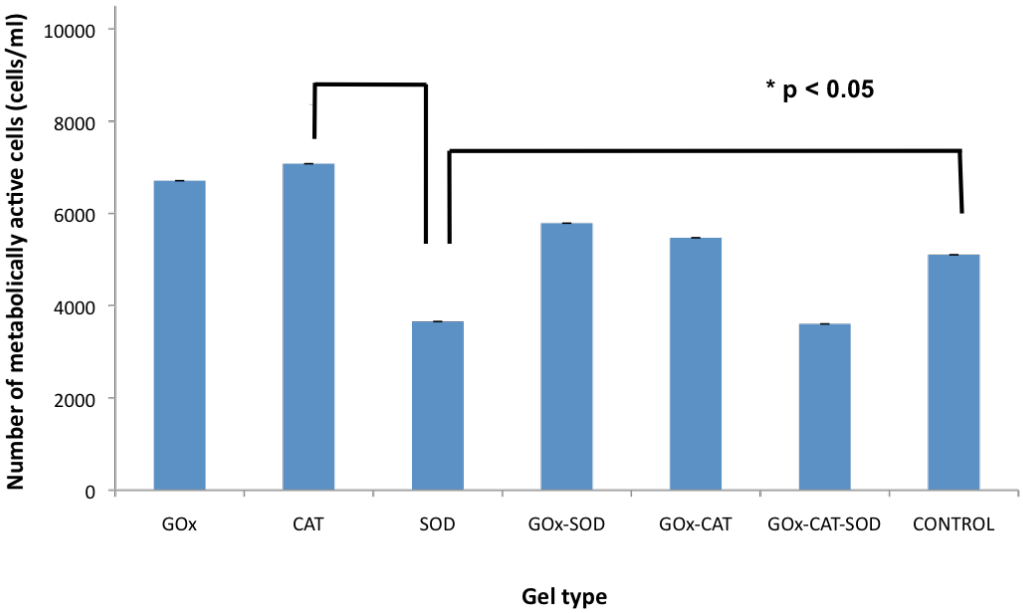

Figure 4.11: Normalized number of metabolically active RMS 13 cells on p(HEMA) enzyme gels derived from MTT assay after cell enumeration post 24 h. (± SE, n=9), * p value < 0.05 indicating a significant statistical difference between sample types.

MTT data conducted on gels after enumeration revealed GOx gels to have a similar number of metabolising cells remaining on gels to that of CAT gels. CAT gels produced the most number of metabolically active cells after 24 h in an enzyme gel system, which indicated that in long-term studies catalase could be beneficial in the proliferation of cells. CAT gels were also shown to be statistically different when compared with SOD. GOx-SOD and GOx-CAT gels produced a similar number of viable cells after 24 h.

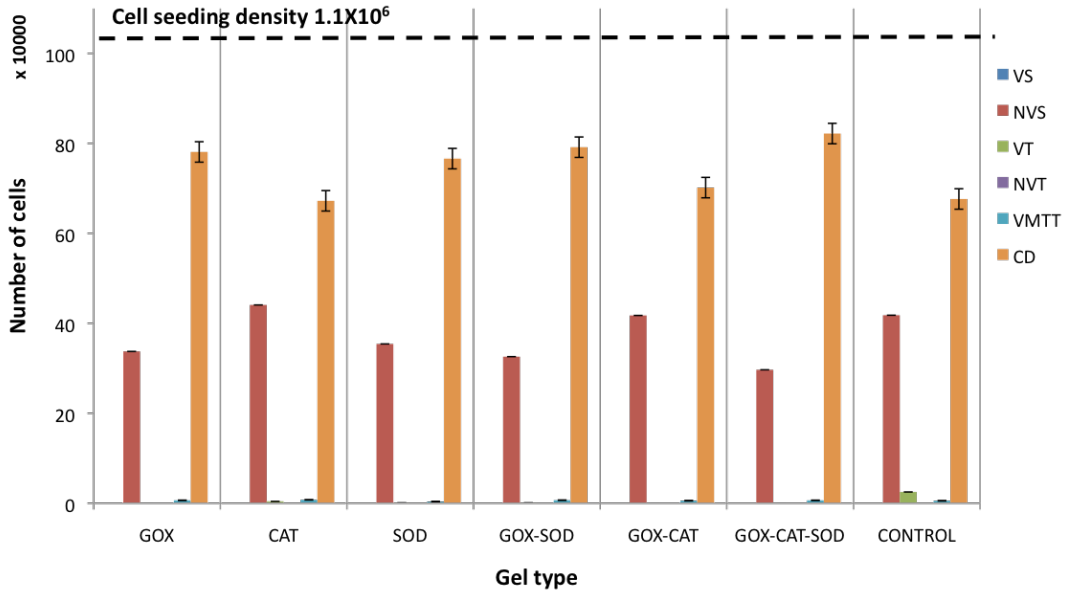

Figure 4.12: Viability of RMS 13 cells on p(HEMA) enzyme gels after 24 h (± SE, n=3) VS = Viable cells in suspension, NVS= Non-viable cells in suspension, VT= Viable cells trypsinized, NVT= Non-viable cells trypsinized, VMTT= Viable cells from MTT assay, CD= Calculated difference.

** CD = Cells seeded –(VS+NVS+VT+NVT+VMTT)*

Calculated difference values in Figure 4.12 demonstrate an increase when compared with 12 h studies in Figure 4.10. The CD values obtained are similar to that obtained at 6 h. It would be expected that at this time period the majority of cells present in all GOx containing gels to be non-viable with very few viable cells present. The statistical significance of each sample between time intervals is indicated in Figure 4.13.

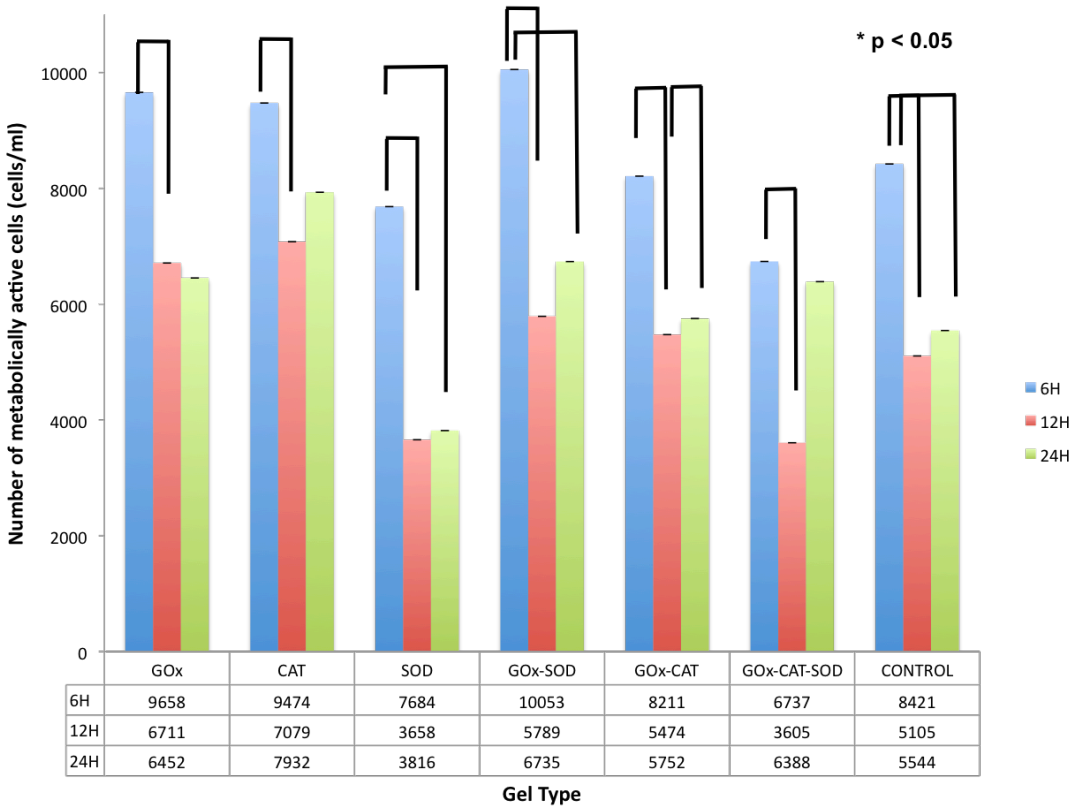

	GOx	CAT	SOD	GOx-SOD	GOx-CAT	GOx-CAT-SOD	CONTROL
6H	9658	9474	7684	10053	8211	6737	8421
12H	6711	7079	3658	5789	5474	3605	5105
24H	6452	7932	3816	6735	5752	6388	5544

Figure 4.13: Statistical difference between normalized number of metabolically active RMS 13 cells on p(HEMA) enzyme gels derived from MTT assay after cell enumeration. (± SE, n=9), * p value < 0.05 indicating a significant statistical difference in samples between time intervals.

4.6 Cell viability of B50 cells on enzyme encapsulated agarose hydrogels

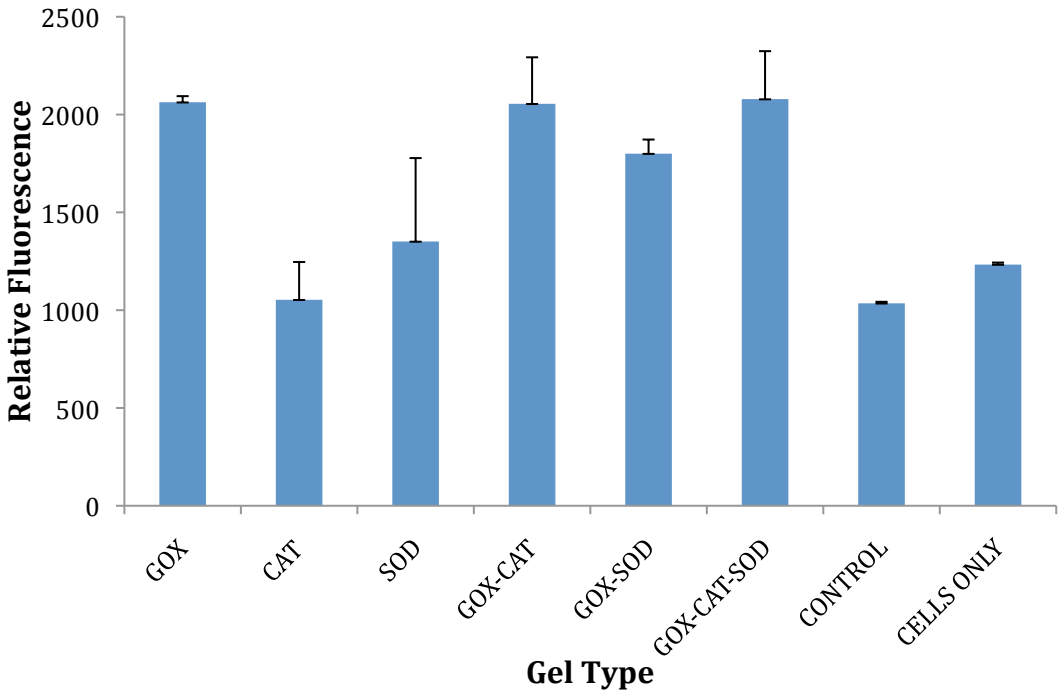

Figure 4.14: Relative fluorescence of B50 cells on agarose enzyme gels at 3 h. (± SE, n=9)

Figure 4.14 shows the relative fluorescence values of the enzyme gels after 3 h of cell seeding indicating the highest level of cellular metabolic activity on cells cultured on GOx-CAT-SOD agarose gels, which displayed a fluorescence reading averaging at 2079 nm. GOx only agarose and GOx-CAT agarose gels closely followed with readings of 2063 and 2055 nm, which further indicated that gels containing GOx somehow promoted the metabolism of cells in comparison to cells seeded on SOD and cell only control samples which indicated similar levels of activity. Cells in the presence of GOx compete for glucose present in the cell culture

medium, and the reaction of GOx with the glucose occurs rapidly producing hydrogen peroxide, which over time is accountable for cell death [170].

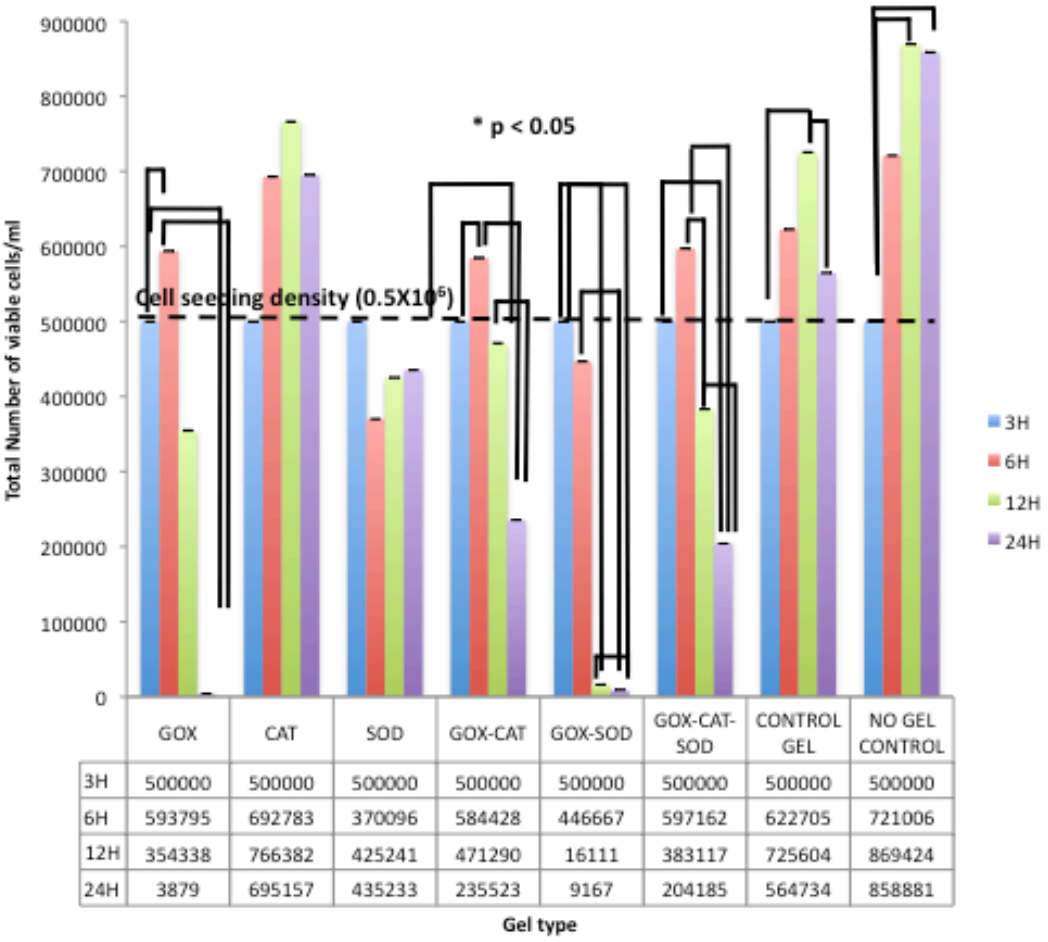

	GOX	CAT	SOD	GOX-CAT	GOX-SOD	GOX-CAT-SOD	CONTROL GEL	NO GEL CONTROL
3H	500000	500000	500000	500000	500000	500000	500000	500000
6H	593795	692783	370096	584428	446667	597162	622705	721006
12H	354338	766382	425241	471290	16111	383117	725604	869424
24H	3879	695157	435233	235523	9167	204185	564734	858881

Figure 4.15: Number of viable B50 cells present on agarose enzyme gels
(± SE, n=9) * p value < 0.05 indicating a significant statistical difference in samples between time intervals.

Percentage change (%)	3-6 h	6-12 h	12-24 h
Gel Type			
GOX	+ 18.7	- 40.3	- 98.9
CAT	+ 38.6	+ 10.6	- 9.3
SOD	- 26.0	+ 14.9	+ 2.4
GOX-CAT	+ 16.9	- 19.4	- 50.1
GOX-SOD	- 10.7	- 96.4	- 43.1
GOX-CAT-SOD	+ 19.4	- 36.8	- 46.7
CONTROL GEL	+ 24.5	+ 16.5	- 22.1
NO GEL CONTROL	+ 44.2	+ 20.6	- 1.2

Table 4.4: Percentage change in cell number in agarose enzyme gels.

From Figure 4.15 analysis of B50 cell growth on agarose, it was concluded that cells seeded at t_0 (3 h study) were seen to be viable, at t_1 (6 h study) indicated an all round increase in viability with cells proliferating in most cases with the exception of SOD gels and GOx-SOD gels. At 6 h there was a statistically significant difference between cell viability in GOx only gels compared with CAT only, SOD and both control types. GOx-CAT and GOx-CAT-SOD and SOD alone also proved to be statistically different when compared to controls. In general GOx-CAT and GOx-CAT-SOD proved to be dissimilar in viability compared with all of the other gel types. This was also the case for GOx-SOD and GOx only gels at 12 and 24 h.

Catalase gels showed a 38.6% increase in cell number between the 3 h and 6 h study (Table 4.4) this increased further by 10.6% between 6 and 12 h before decreasing at 24 h by at least 9% relative to gel only controls. B50 cells on SOD gels proliferated after 6 h. Gels containing GOx solely or in combination with SOD or CAT resulted in a decrease in cell numbers post 6 h. Cells on GOx alone gels decreased in number by 40.3% between 6-12 h and by a further 98.9% between 12-24 h. Control samples consisting of cell only controls and agarose with added fibrinogen were essential in providing a relative comparison between enzyme effects *vs*. the effect of the gel alone on cell proliferation. In general the control gel increased cell number over time, however, the majority of enzyme gel samples saw a decrease in cell number between 12-24 h.

4.7 B50 cell morphology after 24 h on enzyme gels encapsulated gels

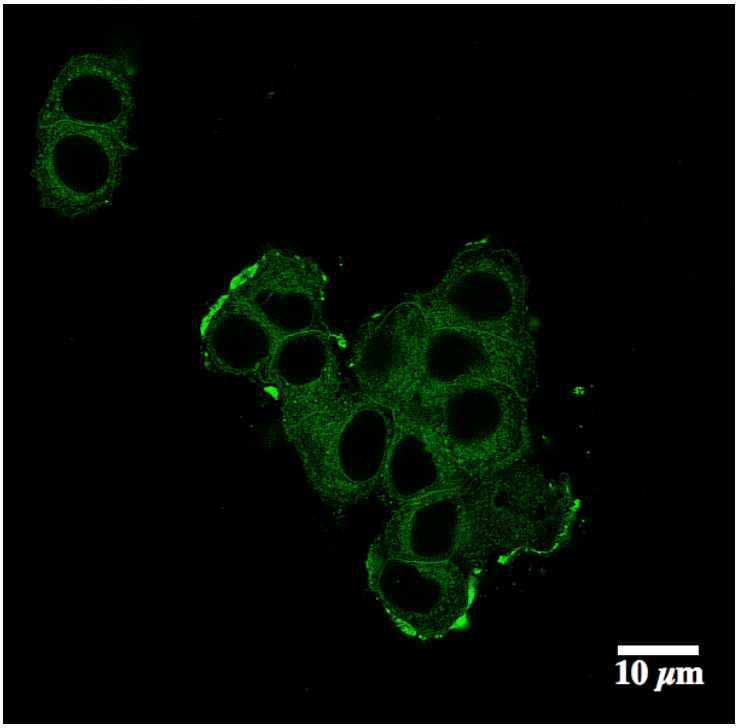

(A)

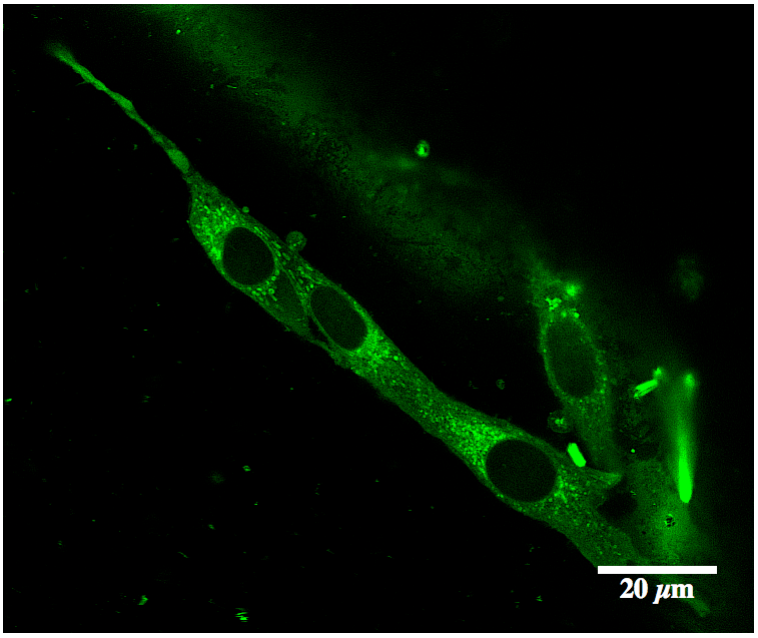

(B)

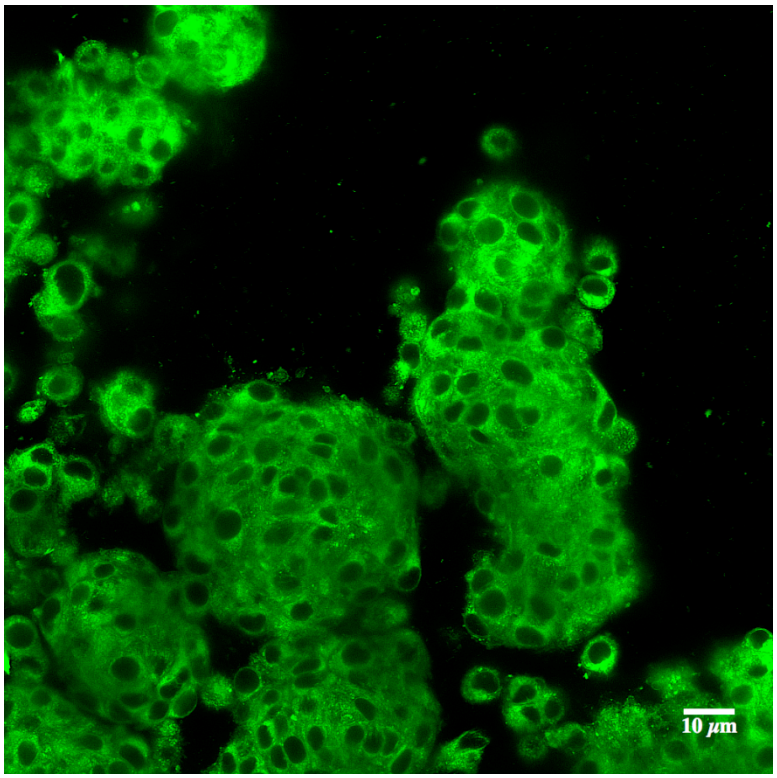

(C)

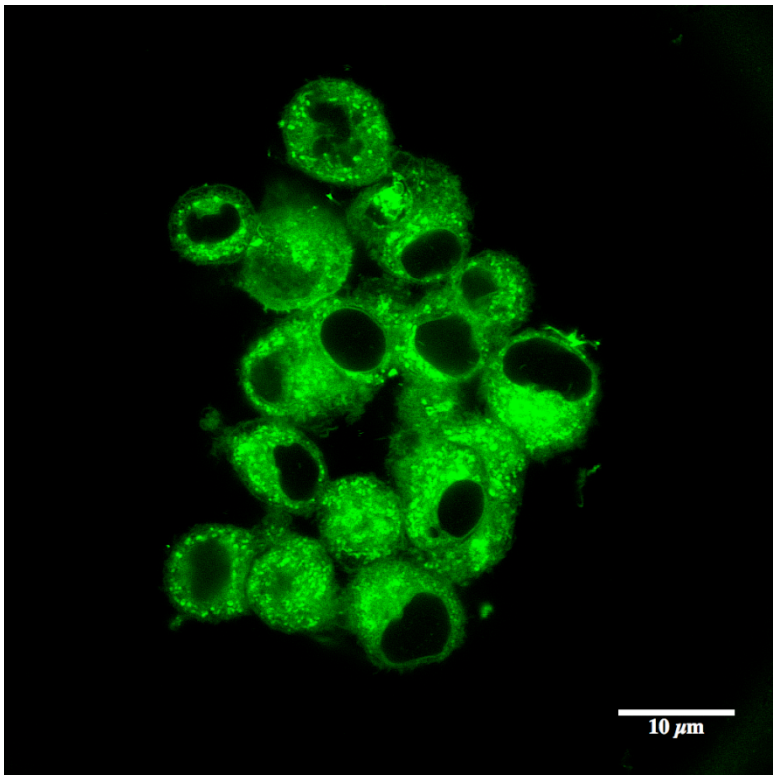

(D)

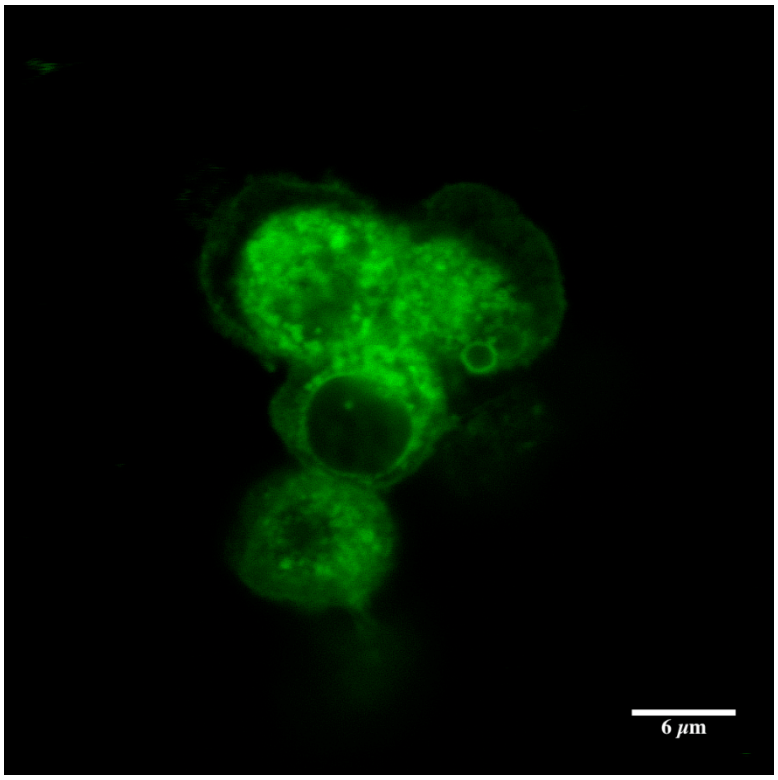

(E)

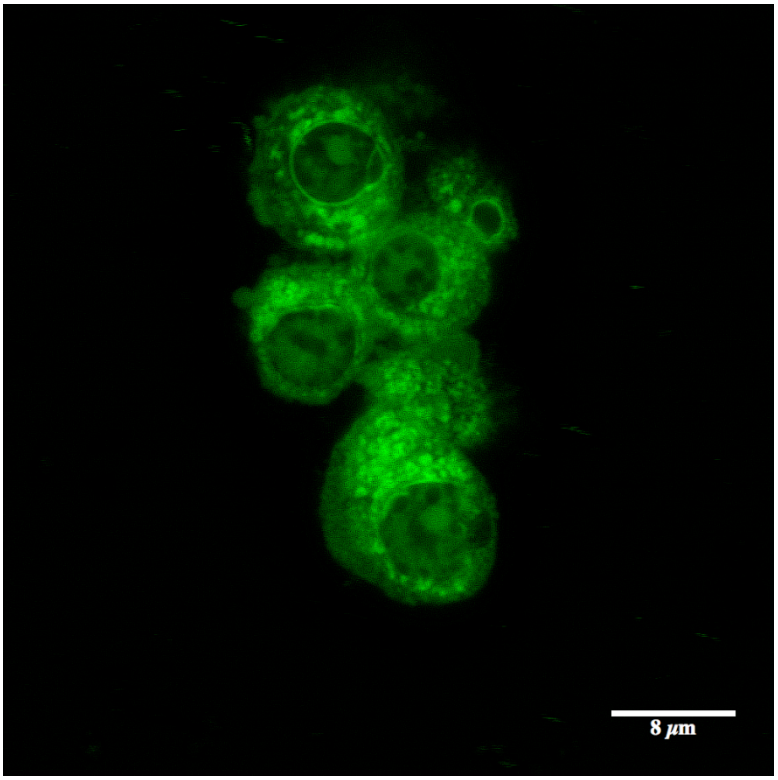

(F)

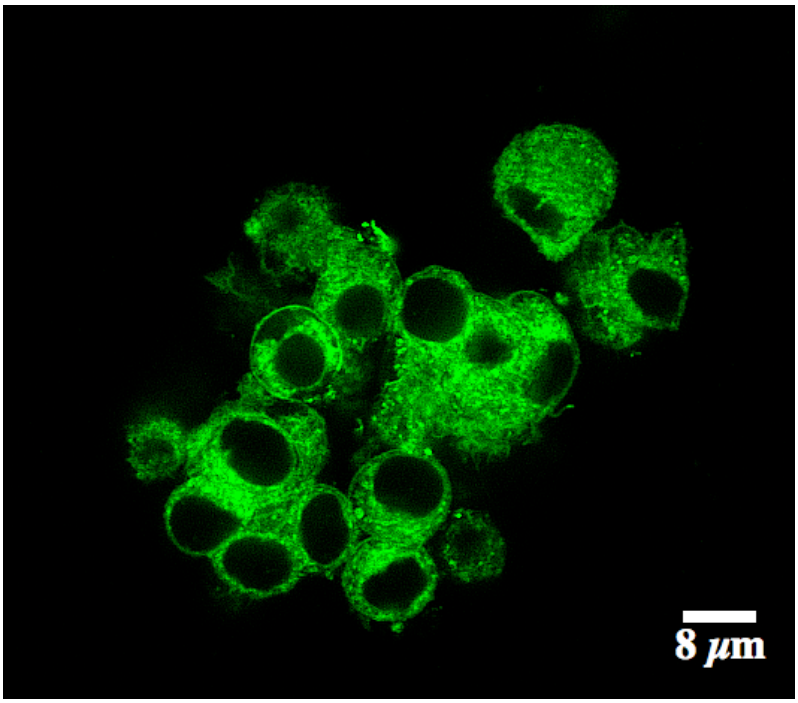

(G)

Figure 4.16: Confocal micrographs of fluorescently labelled B50 cells using Dioc 18 (3) on enzyme encapsulated 1% (w/v) agarose gels. (A) Control gel consisting of solely agarose supplemented with 5% (w/v) fibrinogen, (B) CAT only agarose gel, (C) GOx only agarose gel, (D) SOD agarose gel, (E) GOx-CAT agarose gel, (F) GOx-SOD agarose gel, (G) GOx-CAT-SOD. *Cells were incubated for 24 h prior to fixation in 4% PFA overnight.*

After an incubation period of 24 h, B50 cell morphology was assessed on the enzyme agarose gels. Figure 4.16 (A) shows the control gel; despite viability data confirming the presence of viable cells on control samples the cells control samples appeared to grow in small clusters. Catalase samples (B) did confirm the presence of viable cells, which grew to spindle like neuronal morphology. GOx cells shown in (C) appeared as large clusters of aggregated cells that could suggest apoptotic behavior of the cells. SOD samples (D) resulted in similar morphology to control samples where

cells present were spherical in shape and poorly developed. Both GOx-CAT (E) and GOx-SOD (F) samples indicated enlarged spherical cell bodies and nuclei. Gels containing all three enzymes (G) also produced a large number of spherical shaped cells in clusters, particularly noticeable was the enlarged nuclei.

4.8 Summary

After 6 h of cell culture, GOx and catalase gels indicated similar viability in p(HEMA) gels. However when combined, GOx-CAT gels produced the least number of viable cells. SOD used in combination with GOx and catalase resulted in similar viability to that of GOx and SOD used separately. MTT assays revealed that GOx-SOD p(HEMA) gels produced the most viable cells remaining on the gel. After 12 h, control gels showed high viability with SOD and CAT producing the least number of cells enumerated. In contrast to this, MTT values revealed that CAT gels produced the most number of viable cells with similar viability noted on GOx gels. After 24 h GOx and GOx-CAT-SOD gels indicated zero viability with catalase maintaining a high level of viability, also confirmed by the MTT values.

In agarose gels, catalase accounted for a consistent increase in cell viability relative to control samples. GOx initially produced viable cells at 6 h, however post 6 h viability dramatically decreased with the least number of viable cells produced within any gel system at 24 h. When combined with GOx, GOx-CAT-SOD did not appear to have any beneficial effect on cell viability. Cell morphology on agarose enzyme gels suggested the presence of GOx to induce apoptotic behaviour. It was also noted that catalase promoted cell growth on gels.

CHAPTER 5

-

Comparison of recess and non-recess disc electrodes for glucose measurement - stabilisation effect of agarose gels

5.1 Introduction

Biosensors are analytical devices that combine specific biological component with physicochemical measurement. Biological component can be enzyme, DNA, microorganism, antibody or other biologically derived material reacting specifically with analyte. Detection principle of a biosensor can be optical, piezoresistive, electrochemical, gravimetric etc. Enzyme based biosensors are the most widely used biosensors in biomedical applications; one of the first biosensors to be designed targeted the measurement of glucose using an enzyme based membrane which was located on an oxygen probe [109].

Most widely studied biosensors are those for glucose measurement. This is not only due to high occurrence of diabetes across the world but also due to extraordinary stability of glucose oxidase enzyme. Glucose biosensors are commonly used by healthcare professionals to measure the glucose concentration in the blood of diabetic patients [12].

Electrochemical biosensors are the most popular due to the low cost, possibility of miniaturisation, high sensitivity and the fact that the output comes out as an electrical signal, which makes need for signal conversion unnecessary. The concept of biosensing has evolved from traditional electrochemistry for the fabrication of robust, reliable and invasive probes [9]. These electrochemical measurement protocols have proved to be advantageous in recent micro and nano device fabrication [108]. The two main types of amperometric electrodes used are invariably planar or needle shaped [112] that are exposed to the analytical sample by directly or through permeable membranes.

A common drawback of these electrodes is the deposition of biological components during implantation, which results in the encapsulation [11], which can be detrimental to the performance of the device.

Recessed interfaced needle electrodes have been fabricated to potentially overcome the problem of signal drift [156]. First described by Shneiderman and Godlstick [171], recessed O_2 electrodes were designed for use *in vivo*. These electrodes provided fast responses, which were independent of sample stirring. Further studies reporting the use of recessed tip electrodes for use in biological samples proved to reduce bio fouling caused by protein deposition [116]. The majority of adverse reactions take place at the interface of the electrode and tissue. Figure 5.1 demonstrates the possible failure mechanisms that can cause biosensors to lose functionality.

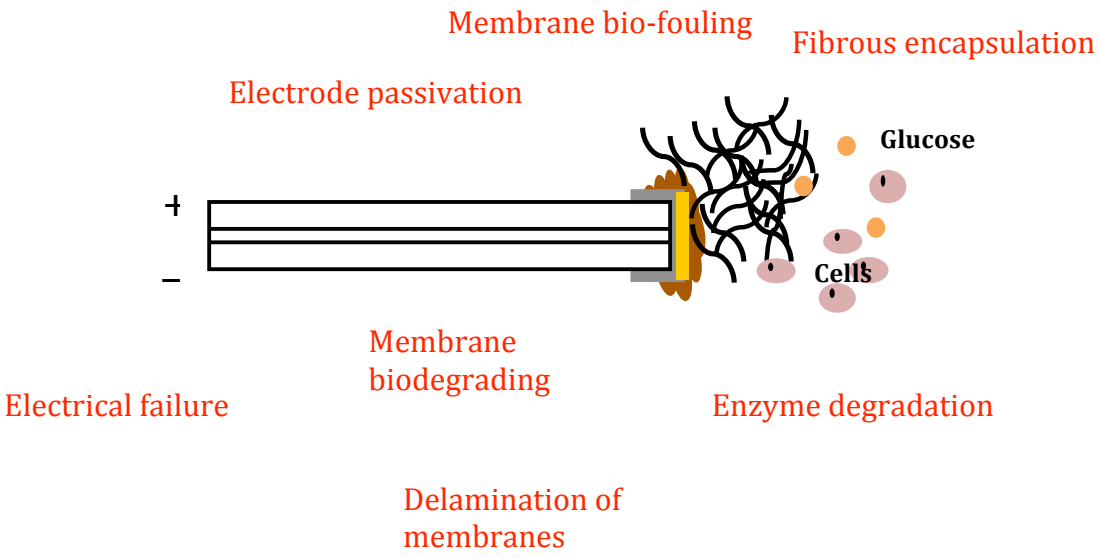

Figure 5.1: Schematic diagram of possible biosensor failure mechanisms (adaptation of Richert *et al* [116]).

Recessed electrodes are said to create an additional buffer zone between the sensing surface and the bio-interface, which can complement protection and further enhanced by the use of traditional membranes and encapsulating agents such as gels.

In this study the fabrication and use of miniaturised gold-filled silica recess and non-recess disc electrodes is described. Agarose gels were investigated as possible stabilisation media. An additional study using platinized needle electrodes were also used to investigate the amount of H_2O_2 produced by enzyme gels in the presence of cells as described in Chapter 4.

5.2 Characterisation of electrodes using cyclic voltammetry

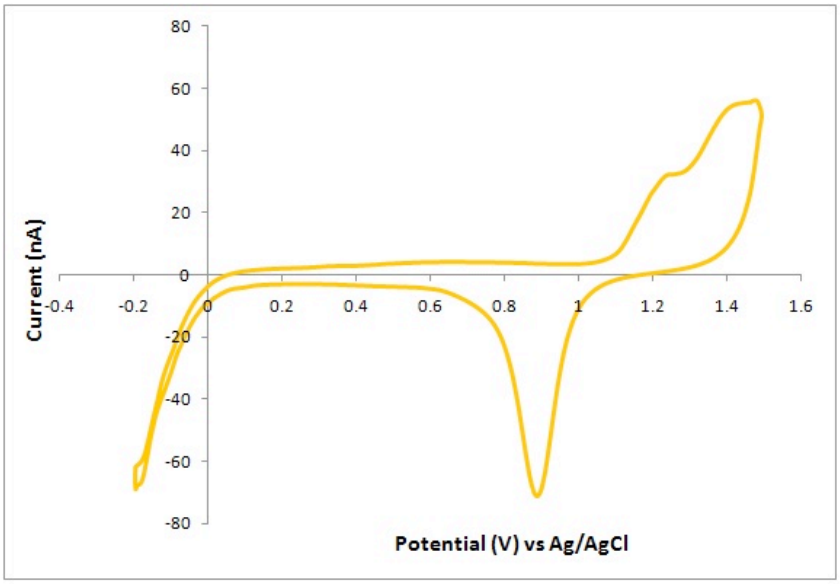

(A)

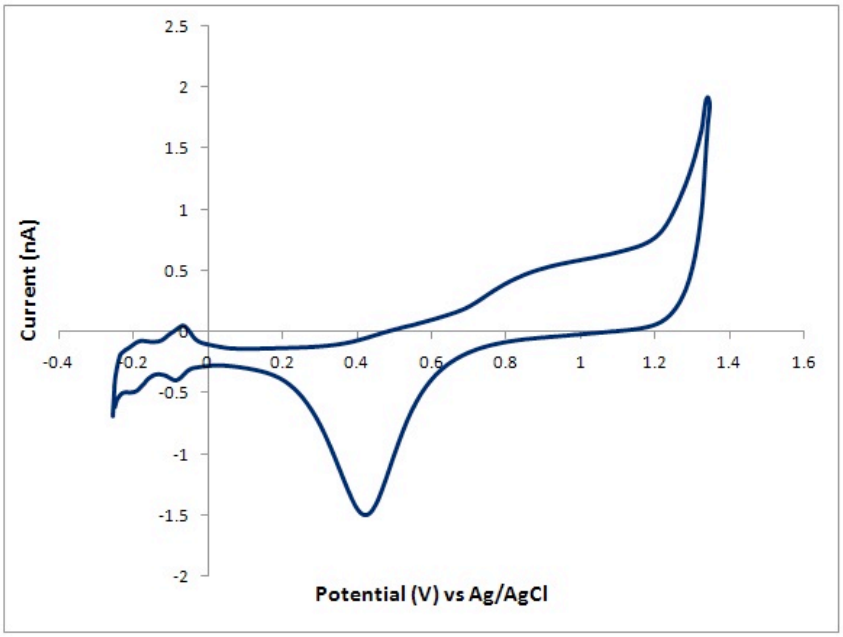

(B)

Figure 5.2 : Cyclic voltammograms (A) Non-recess electrode Au (B) Non-recess platinised Au electrode, both electrodes 80 μM in diameter), in 50 mM sulphuric acid between -0.4 and +1.5 V vs Ag/Cl reference electrode and standard Pt counter electrode (scan rate of 100mVs^{-1}).

Prior to any electrochemical measurements being carried out, the electrodes were cleaned electrochemically in 50 mM sulphuric acid for 20 cycles between -0.4 and +1.5 V vs Ag/Cl reference electrode and standard Pt counter electrode (scan rate of 100mVs^{-1}). The voltammograms of the electrodes was an indication of the performance of the electrodes. Figure 5.2 demonstrates the cyclic voltammograms of non-recessed gold disk electrodes (A) and non-recessed Au electrode after platinization (B). In platinization increase the surface area and is generally better in the detection of H_2O_2 due to the slightly more extended hydrogen region seen on the left of the voltammogram. Both electrodes demonstrate the reduction of Au oxide within the cathodic region of the voltammogram, however this peak is located more towards the right in Au electrodes.

5.3 Measurement of recess depths

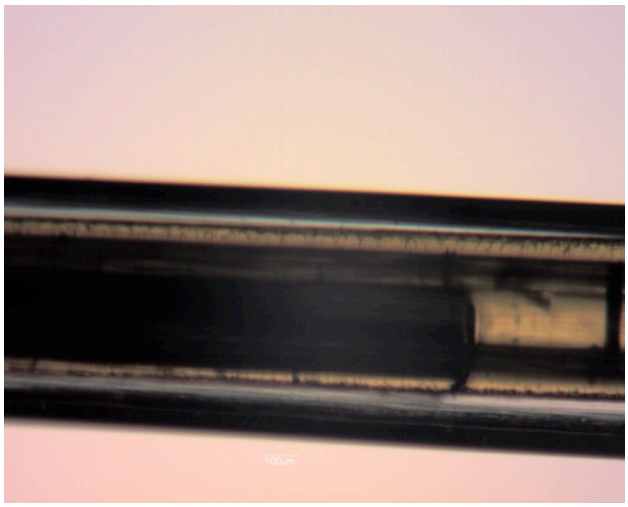

(A)

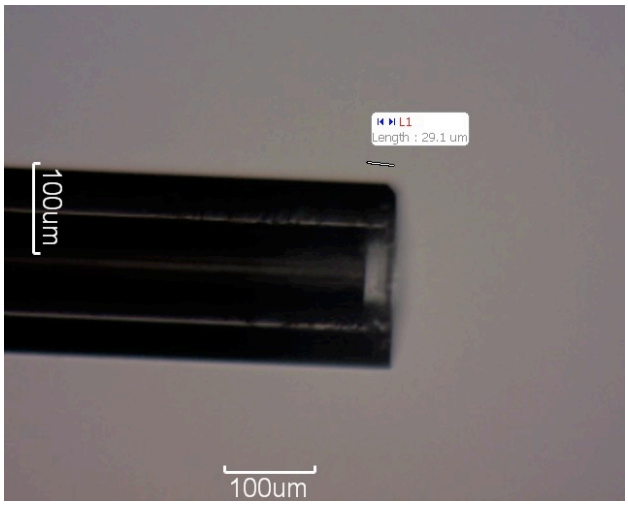

(B)

Figure 5.3: Microscope image of recess electrodes (A) 850 μM depth (B) 29.1 μM depth.

Prior to any electrochemical measurements taking place, the depths of the recess electrodes were measured using light microscopy as illustrated in Figure 5.3 (A) recess depth was measured at 850 μM and (B) at 29.1 μM.

5.4 Amperometric measurements

5.4.1 Detection of Hydrogen peroxide (H_2O_2)

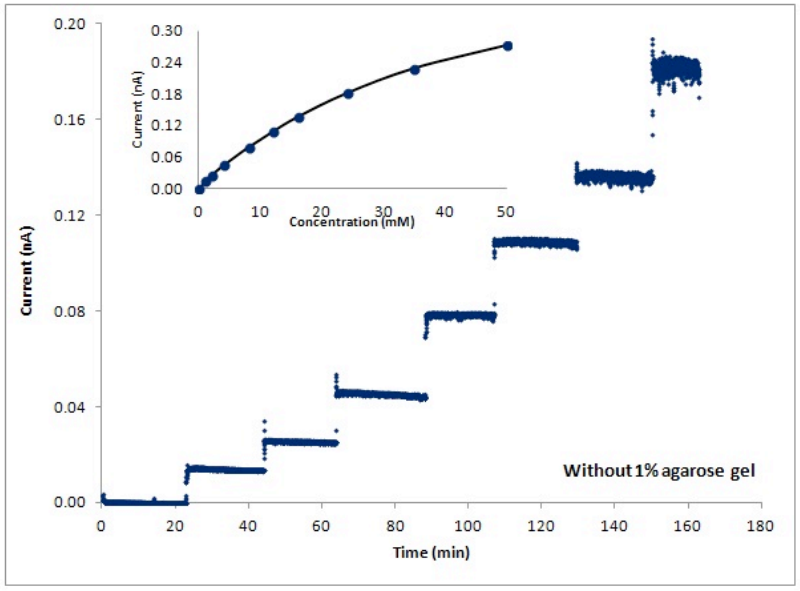

(A)

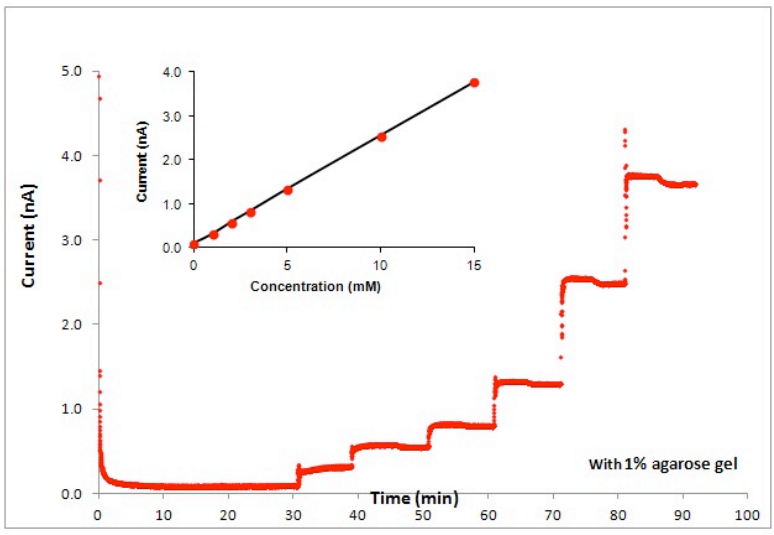

(B)

Figure 5.4: Detection of H_2O_2 using non-recess electrodes (A) with 1% (w/v) agarose gel (B) without 1% (w/v) agarose gel layer.

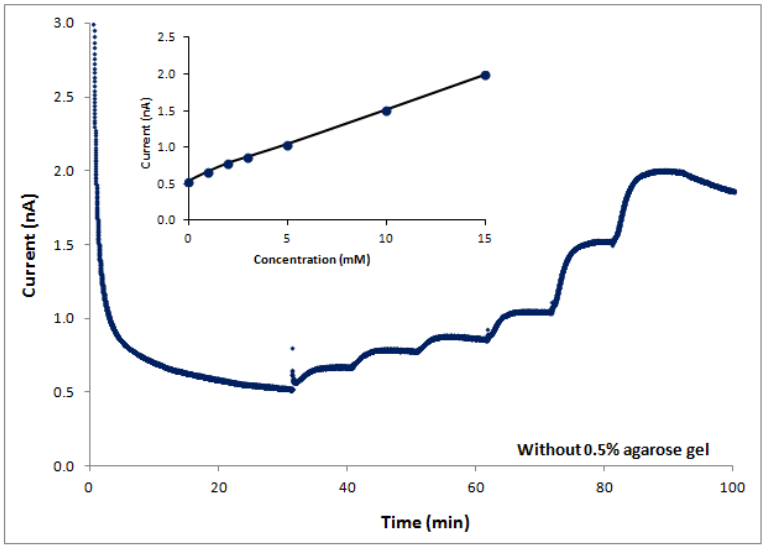

(A)

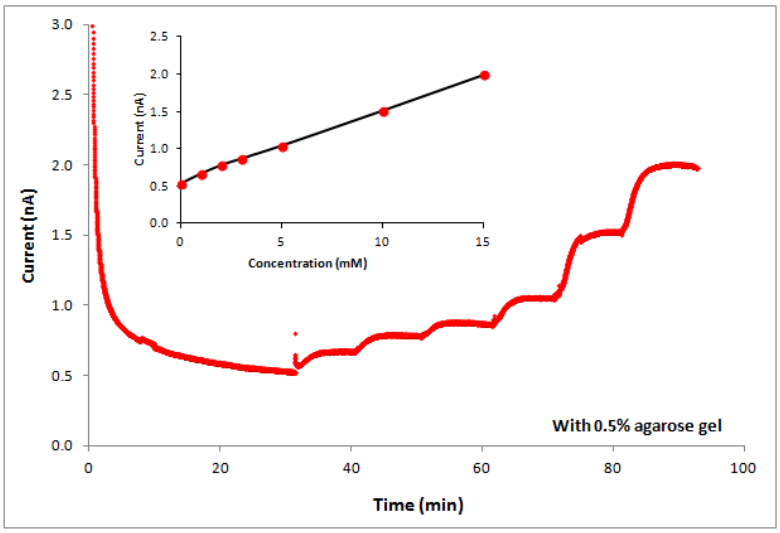

(B)

Figure 5.5: Detection of H_2O_2 using recess electrode (recess depth 29.1 μM), with (A) and without (B) recess filled 0.5% (w/v) agarose gel.

The applicability of both recess and non-recess electrodes as H_2O_2 were established by carrying out amperometric measurements of H_2O_2. This involved the calibration of the electrodes by means of a gradual increase in H_2O_2 concentration through a series of step wise additions of H_2O_2 at 1,2,4,8,12 mM added directly to the Phosphate buffered saline conditioning the electrode. The solutions were constantly stirred throughout the measurements.

There was a notable difference in the sensitivity of H_2O_2 detection in non-recess *vs*. recess electrodes, with the non-recess electrodes higher in sensitivity than recess electrodes. The results for both electrodes also confirm a linear dependence on H_2O_2 within the range of 1-12 mM and in the case of non-recess electrodes (Figure. 5.4) linearity can be achieved for concentrations of up to 50 mM, however also present is the increase of noise.

Non-recess electrodes coated with a 1% (w/v) agarose gel layer were also calibrated for H_2O_2 as demonstrated in Figure 5.4 along with recess electrodes filled with 0.5% (w/v) agarose gel. A lower concentration of agarose was used to fill recesses as 1% (w/v) agarose proved too viscous to be taken up by capillary action of the recess electrodes. Figure 5.5 indicates the detection of H_2O_2 in recessed electrodes with and without a 0.5% (w/v) agarose gel. There was no difference noted in the measurements obtained.

5.4.2 Detection of glucose

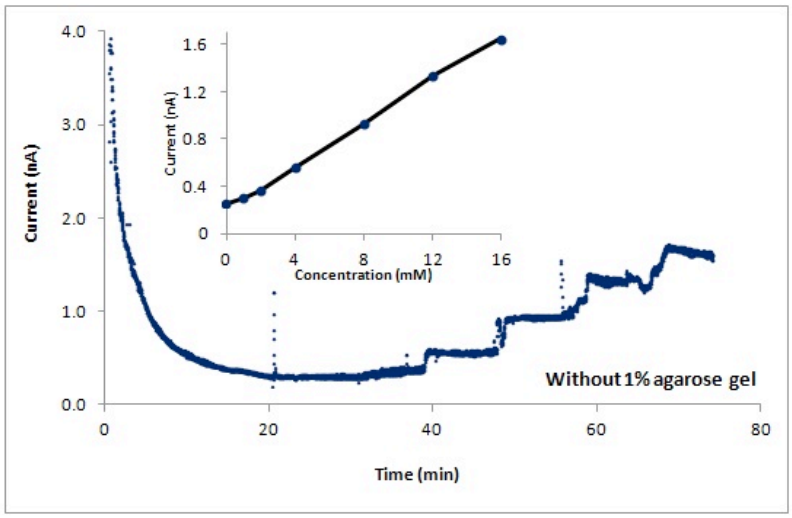

(A)

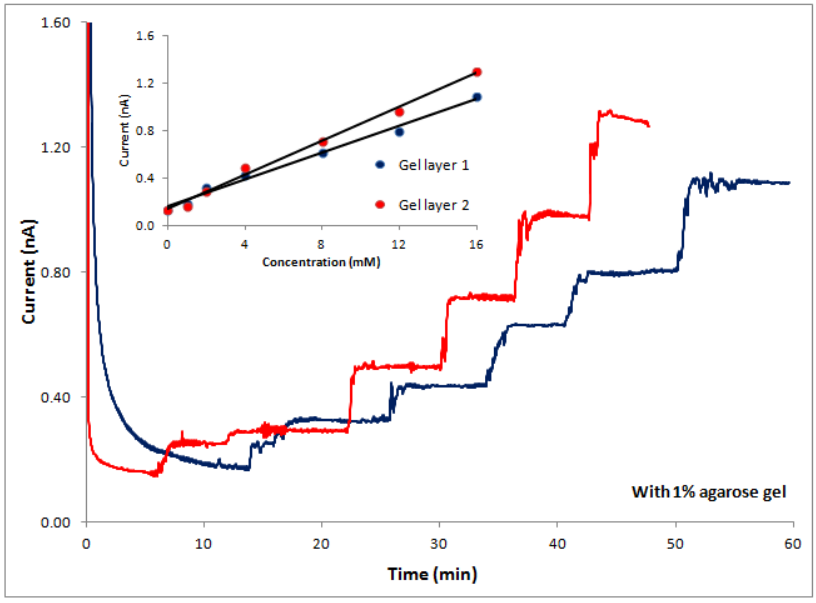

(B)

Figure 5.6: Measurement of glucose using non-recessed electrodes (A) without gel layer (B) with two layers of 1% (w/v) agarose.

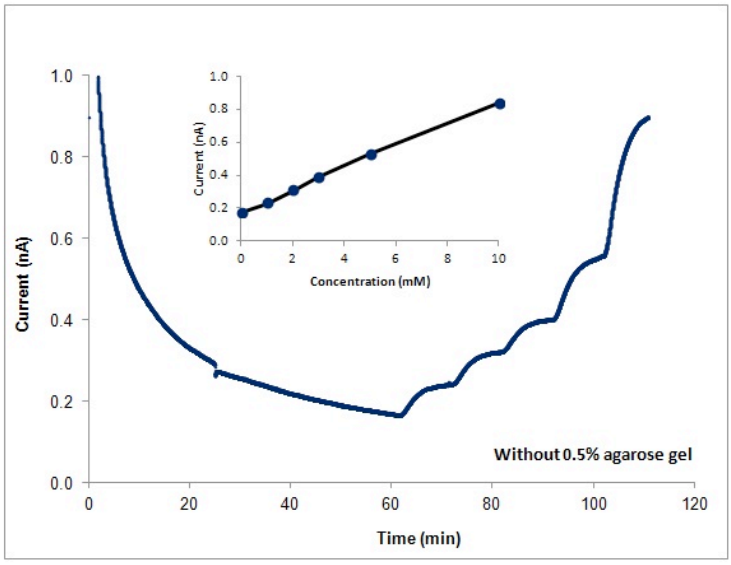

(A)

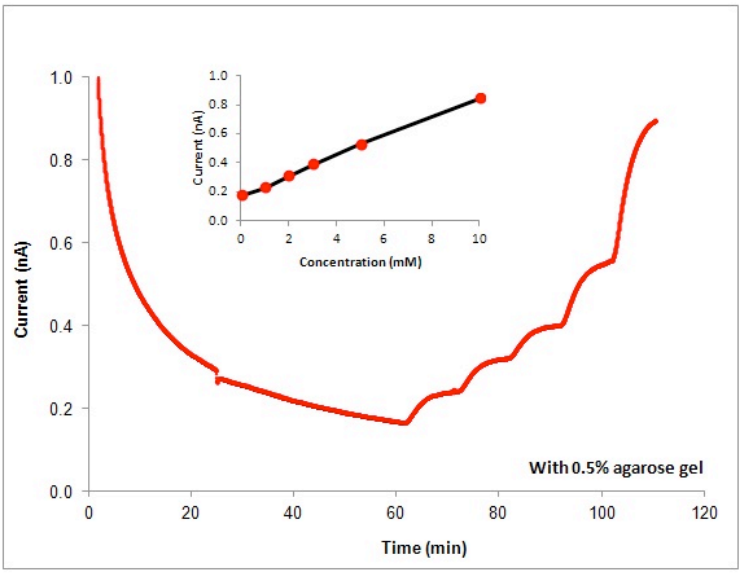

(B)

Figure 5.7: Detection of glucose using recess electrode (45 μM recess depth) (A) without gel, (B) with 0.5% (w/v) agarose gel.

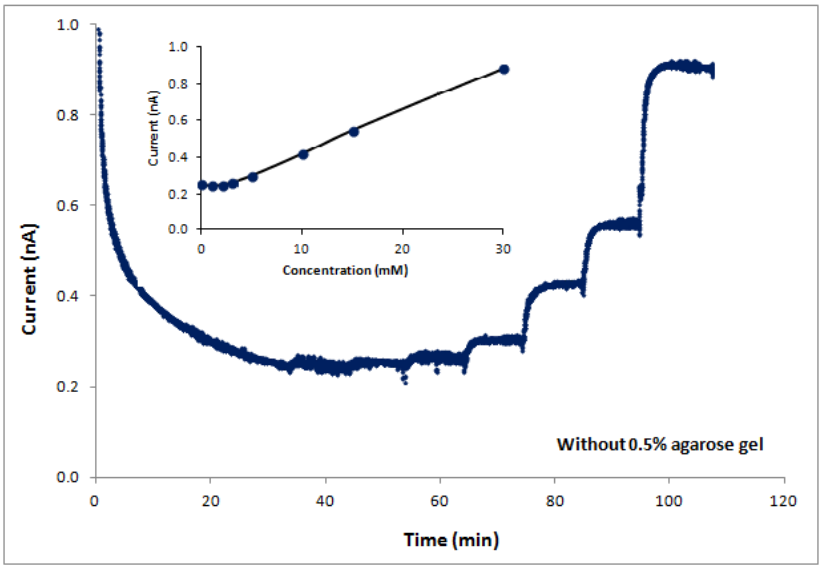

(A)

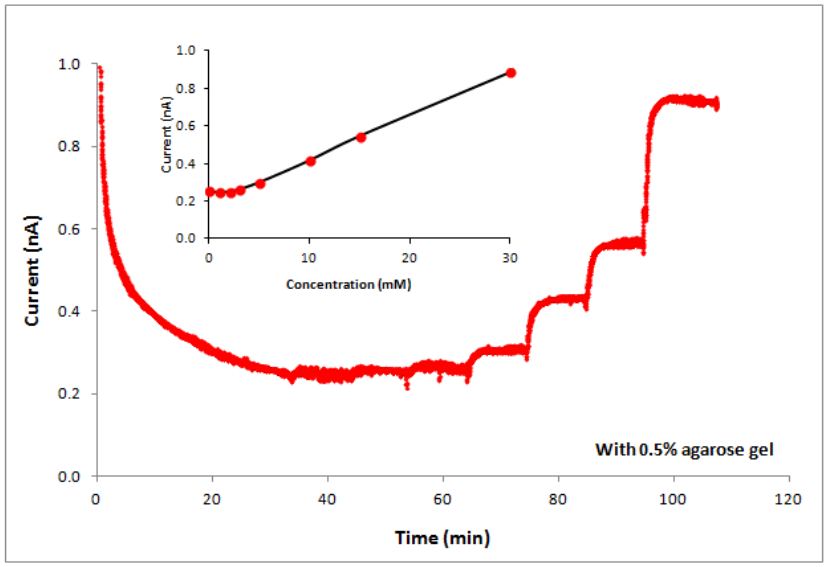

(B)

Figure 5.8: Detection of glucose (850 μm recess depth) (A) without gel, (B) with 0.5% (w/v) agarose gel.

The use of glucose oxidase (GOx) in clinical monitoring enables long term monitoring and investigations due to the stability of the enzyme. The need for continuous monitoring of glucose is particularly desirable is a fundamental part of diabetes care [10] hence the need for an improvement in physiological control.

On comparison of non-recess *vs* recessed electrodes (Figure 5.6. & 5.7) it is noted that non-recess electrodes exhibit a faster response time in comparison to recess electrodes. Figure 5.6 shows a linear range of 0-16 mM being achieved for glucose on non-recess electrodes and Figure. 5.8 demonstrated a linear range between

0-30 mM for glucose concentrations. The increase in recess depth allowed for a higher-level measurement of glucose to be obtained. The presence of 0.5% (w/v) agarose within the recess electrode resulted in no difference in response to the detection of glucose (Figure 5.8), with or without gel. However a faster response time was observed between recess and non-recess electrodes (Figure. 5.7). Figure 5.8 (A) and (B) also indicated that an increase in the thickness of the agarose gel layer can result in a slower response.

5.4.3 Selectivity measurements using recess and non-recess electrodes

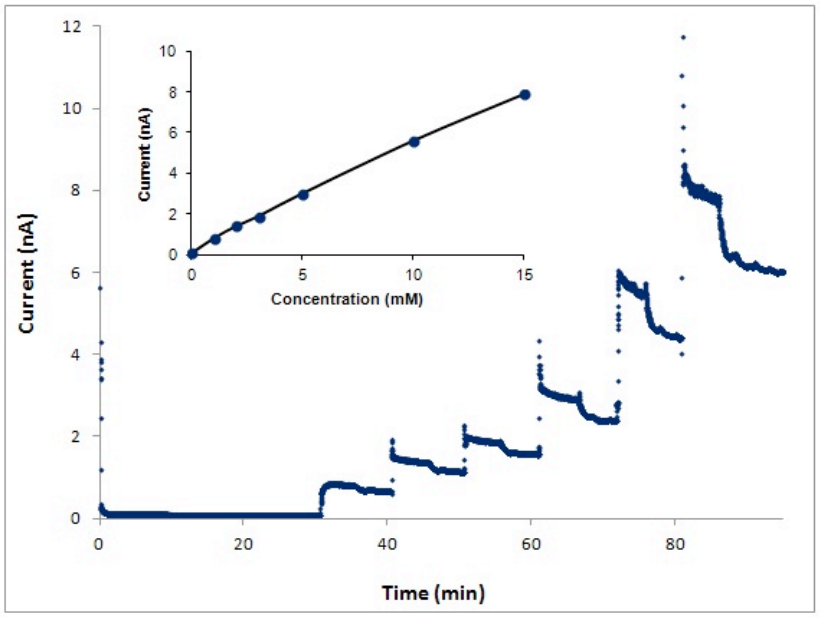

(A)

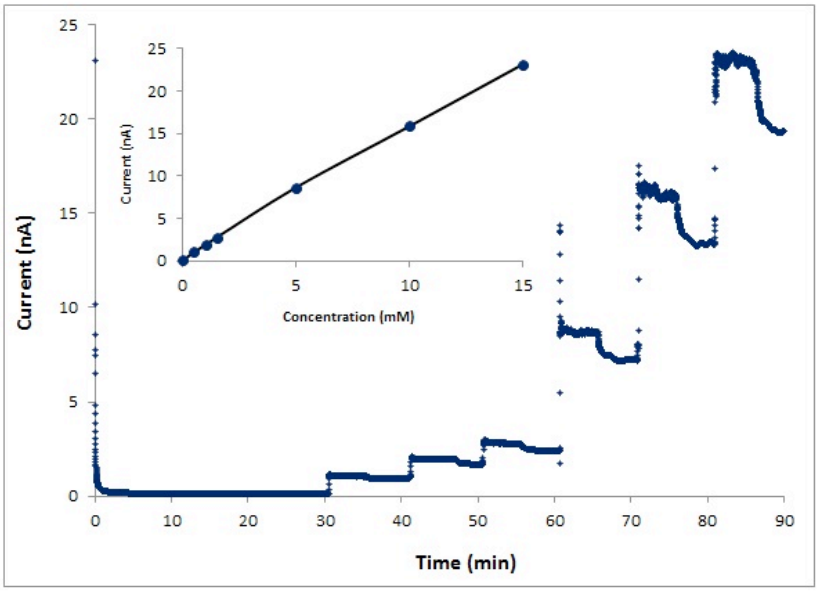

(B)

Figure 5.9: Response to of non-recess electrode to interfering species (A) Ascorbic acid (B) Acetaminophen.

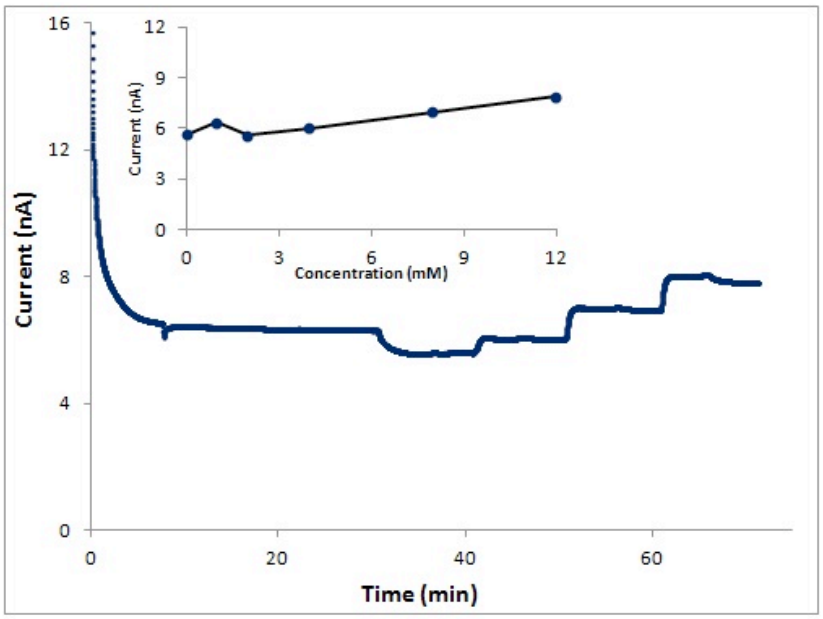

(A)

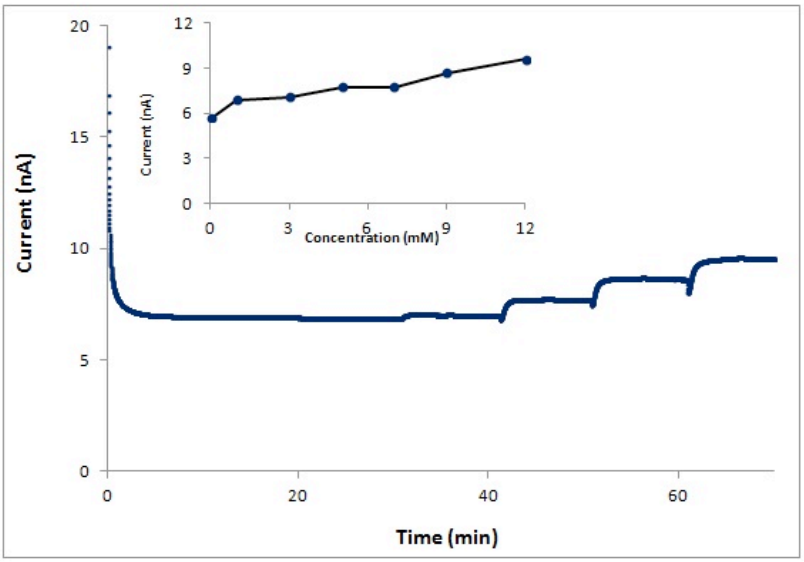

(B)

Figure 5.10: Response to of recess electrode to interfering species (A) Ascorbic acid (B) Acetaminophen.

Figures 5.9 and 5.10 show the response of both recess and non-recess electrodes to the addition of interferants such as ascorbic acid and acetaminophen. It is demonstrated that in recess electrodes a decrease in the level of interference can be observed in Figure 5.10 compared with Figure 5.9.

5.5 Additional Study: Detection of H_2O_2 from enzyme encapsulated agarose gels using platinised electrodes

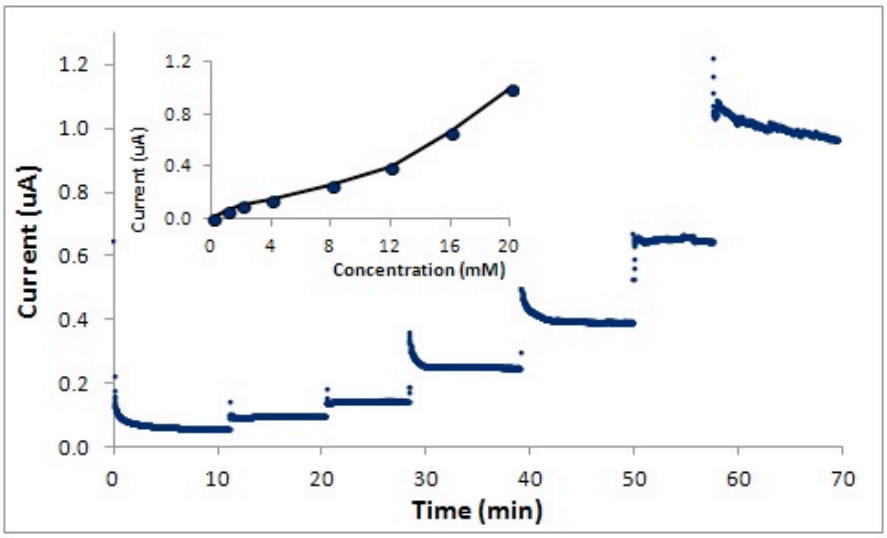

Figure 5.11: Calibration curve of H_2O_2 in 10% (v/v) FBS supplemented DMEM by stepwise addition of 100 mM Hydrogen peroxide solution.

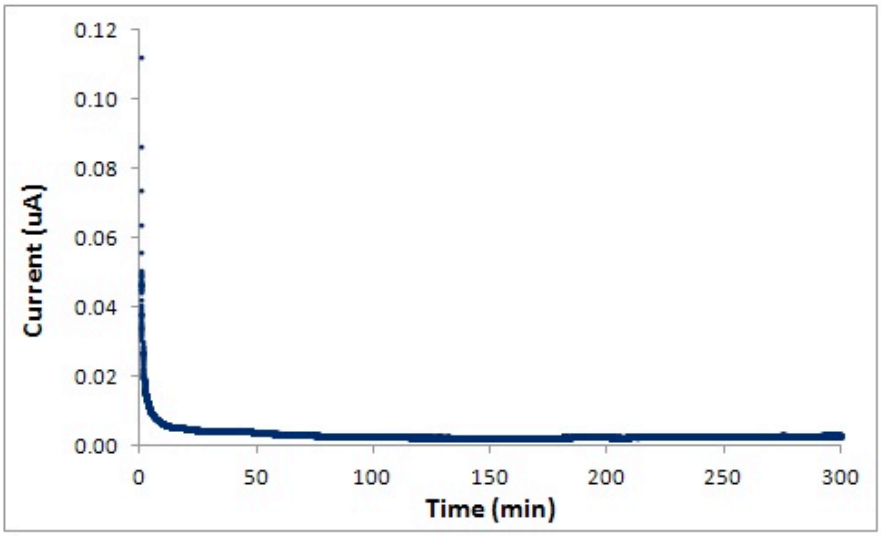

Figure 5.12: Detection of H_2O_2 in 10% (v/v) FBS supplemented DMEM with cells.

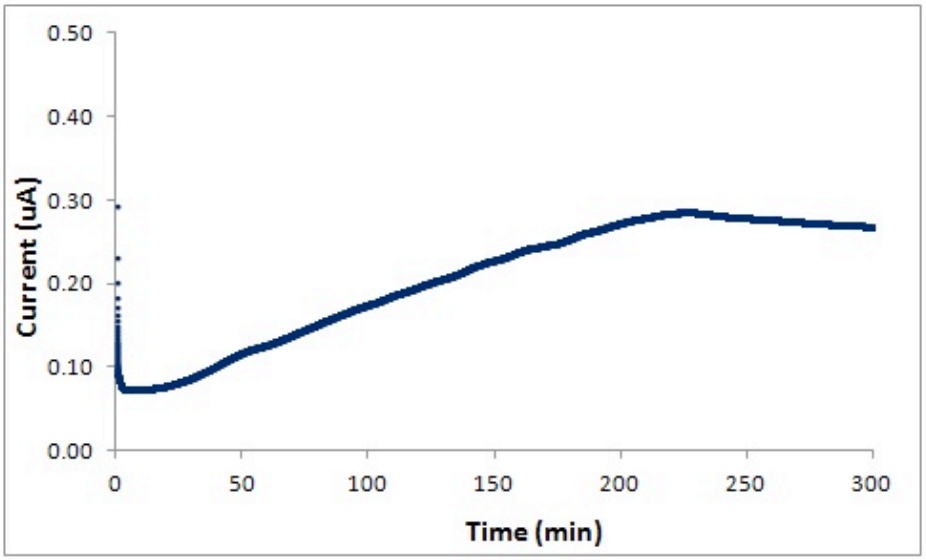

(A)

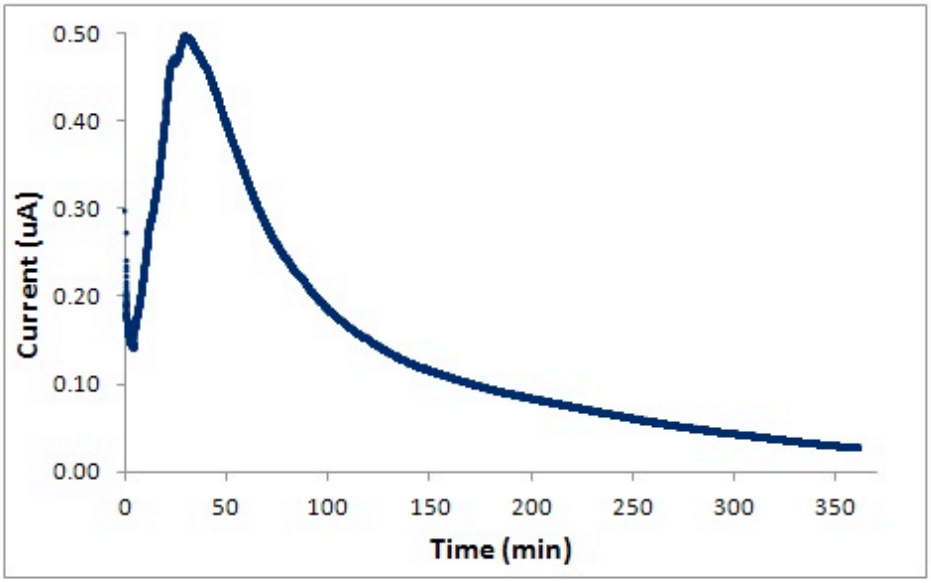

(B)

Figure 5.13: Detection of H_2O_2 produced by leeching of GOx from agarose gels in DMEM (A) without cells, (B) with cells.

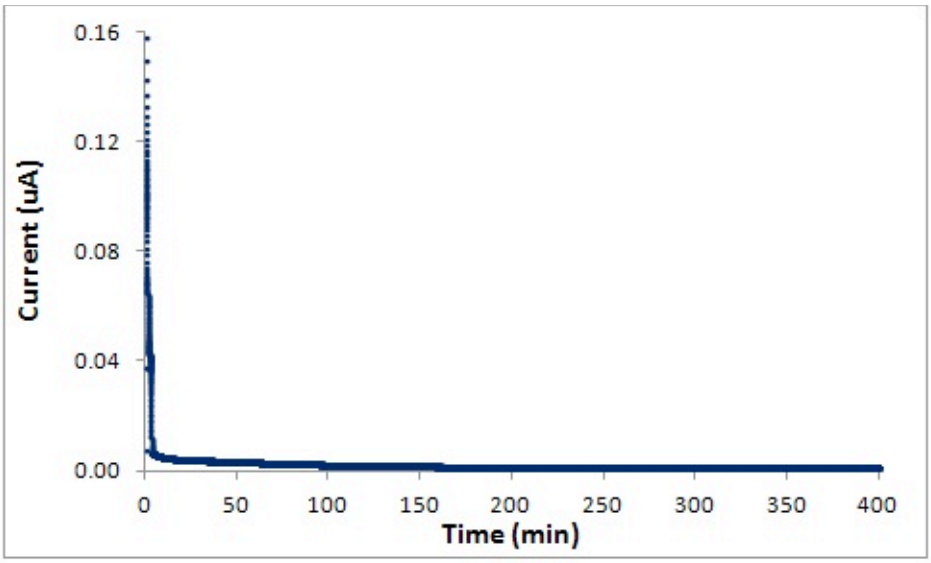

(A)

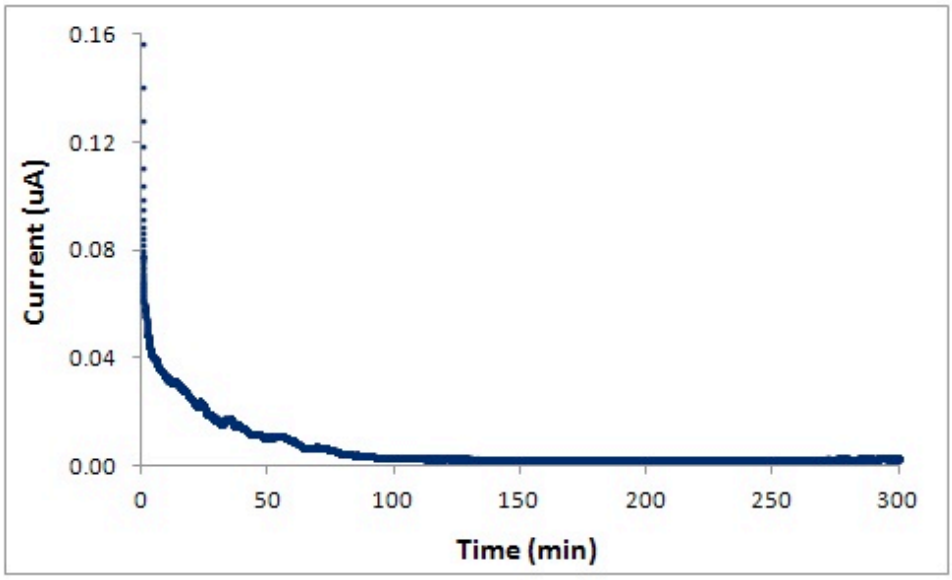

(B)

Figure 5.14: Detection of H_2O_2 produced by leeching of GOx/ Catalase from agarose gels with DMEM (A) without cells, (B) with cells.

To investigate the amount of H_2O_2 produced from the reaction of GOx with glucose present in Dulbecco's modified eagles medium (DMEM), and to confirm the enzyme leeching effect of GOx from agarose gels; platinised electrodes were used.

Figure 5.11 shows the calibration of the electrode by means of a gradual increase in H_2O_2 concentration through a series of step-wise additions of H_2O_2 at 1,2,4,8,12,16,20 mM added to a stirred solution of 1 mL of DMEM. Linearity was achieved for concentrations of up to 20 mM. In addition to determine the calibration of H_2O_2 in DMEM, an investigation to rule out the presence of H_2O_2 produced by cells in media in the absence of enzymes was also carried out. Figure 5.12 confirmed that cell suspension of 5000 cells/ml in DMEM did not produce any H_2O_2.

In the absence of cells, the highest concentration of H_2O_2 achieved as a result of enzyme leeching in GOx only agarose gels was 8 mM until the enzyme reached saturation past 200 min (Figure 5.13 A). However in the presence of cells an increase in H_2O_2 concentration of 14 mM was observed, with a rapid decrease in H_2O_2 production noted from 50 min onwards until the enzyme saturated (Figure 5.13 B). This suggests that any changes in cell viability and growth of cells cultured on GOx agarose gels as described in Chapter 4 past 2½ h is attributed by an increase in H_2O_2 present in DMEM as a by product of the reaction between GOx and glucose present in the culture media. In gels containing both GOx and catalase (Figure 5.14), there was no H_2O_2 detected in samples with and without cells. This confirms the active presence of catalase, which reduces H_2O_2 to H_2 and O_2.

5.6 Summary

In this Chapter inlaid and recessed type electrodes were compared for glucose measurement. Agarose gels were tested for stabilisation effect. Recessed electrodes had slower response than inlaid electrodes due to the longer diffusion times needed for the analytes to reach the sensor surface. Notably, recessed electrodes had lower interference responses to anionic interferents, such as ascorbate, compared with non-recessed electrodes. Thus, silica disc of recessed electrodes appears to behave as an anionic membrane. Agarose gels did not have any measurable effect on the response of the sensors, but eased sensor handling by preventing air entrapment. The production of H_2O_2 as a result of GOx leeching from agarose gels was quantified from 3.75 h in GOx only gels. The presence of catalase activity was confirmed by the reduction of H_2O_2. Larger recess depths accounted for longer response times than that of shorter depths.

CHAPTER 6

-

Cell viability on crosslinked protein membranes

&

The development of sensor-integrated microdevice for amperometric detection of H_2O_2

6.1 Introduction

Since the 1960's the use of polymer membranes within biotechnology, pharmaceutical and healthcare industries have been invaluable in biomedical applications. Membranes serve as thin barriers that enable selective mass transport between separated components [172]. A variety of organic and inorganic polymers and materials have been used to fabricate membranes in which the structure and function is defined. Common commercial membranes include regenerated cellulose for use in dialysis and ultra filtration, Polypropylene for microfiltration and Polyether sulfone commonly used as a protective membrane layer in biosensors. Recently membranes have been used in micro-reactor systems. They can be engineered to be biocompatible or biodegradable for use in tissue engineering [173] or as use in scaffolds [174]. These membranes exist as porous or dense structures.

Lipid bilayer membranes supported on solid substrates have been reported to connect biological and artificial materials by mimicking the ECM. It has been possible to couple various biomolecules to support membranes, resulting in an interface that can control and organise the properties and function of membranes and membrane associated proteins [175]. Also reported is the fabrication of biofunctional surfaces for cell proliferation and tissue growth [176].

The most common method used to form polymeric membranes is through crosslinking. This is achieved by the formation of chemical bonds between two polymers, forming an infinite network [107]. In particular many proteins such as enzymes have been crosslinked to improve stability.

In this study, the crosslinking agent Terephthaloyl chloride (TCL) was used to create solid protein membranes formed by interfacial crosslinking. TCL exists as a crystalline solid that is soluble in organic solvents. It has been used in the crosslinking of polymers to provide chemical resistance and structural stability [177]. Figure 6.1 demonstrates the reaction scheme for the protein crosslinking with TCL. The reaction involves the nucleophiliic substitution between the amino groups of the protein with carbon deficient electron on the acid chloride. A C=O double bond is formed with the removal of the chloride ion and the production of HCL.

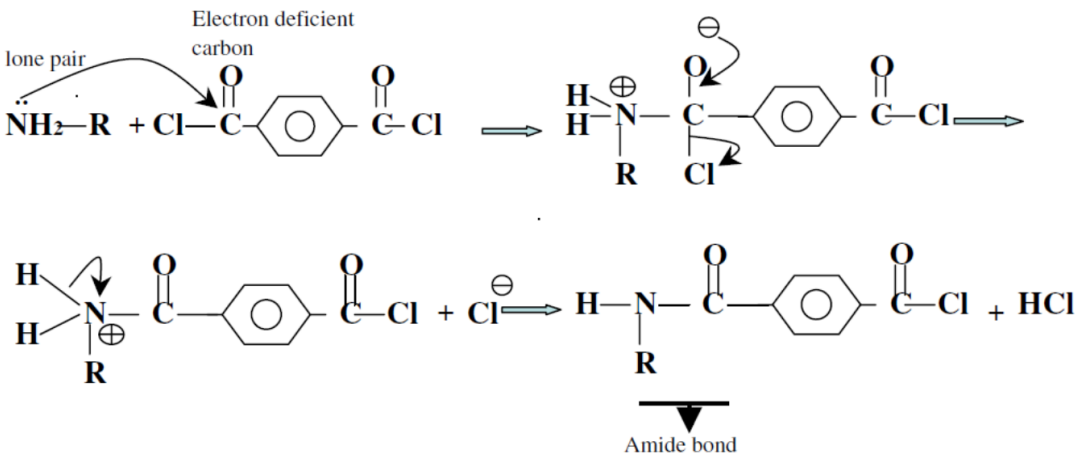

Figure 6.1: Amino based protein crosslinking reaction with Terephthaloyl chloride [165].

6.2 Cell attachment on crosslinked protein membranes formed by spin coating.

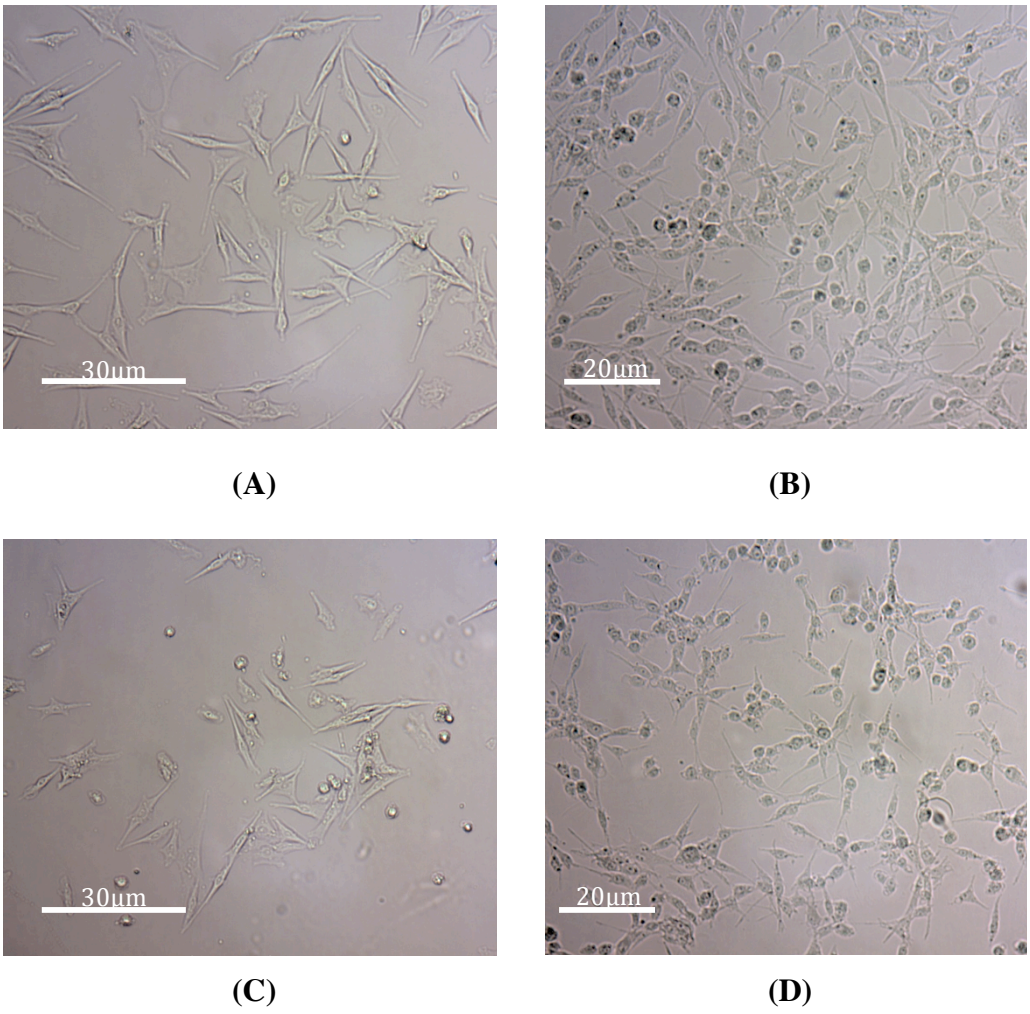

Figure 6.2: B50 cells on (A) crosslinked albumin 20% (w/t) with fibronectin 0.05% (w/t), (B) crosslinked fibrinogen 3.8% (w/t) (C) cross linked albumin 20% (w/t), (D) crosslinked fibrinogen 3.8% (w/t) with fibronectin 0.05% (w/t), *fixed using 4% PFA.*

To date there is nothing reported on the toxicity of the crosslinking agent Terephthaloyl chloride (TCL) on cells. Therefore, it was necessary to establish the effect of protein membranes formed by spin coating as described using TCL on cell attachment and growth. B50 neuron hippocampal cells cultured on different planar membranes were proved viable for up to 72 h.

Figure 6.2 compares the growth of cells on membranes at 24 h after seeding. It was found that cell adhesion and growth was enhanced on all membranes relative to cells seeded on glass cover slips (image not shown). BSA membranes (Figure. 6.2 (C)) showed the least number of fully developed viable cells, along with the presence of a few undeveloped cells spherical in morphology.

Cells on fibrinogen membranes grew to approximately 70% confluence, with the majority of cells adopting a typical B50 neuronal structure. Membranes made with crosslinked fibronectin, despite its specific cell-binding RGD motif, had no added effect on cell density or morphology when compared with fibrinogen. However, there was a significant effect noted on the morphology of cells on crosslinked albumin with added fibronectin, where cells adopted a more spindle like morphology of normal B50 cells.

6.3 Cell viability on large surface area membranes

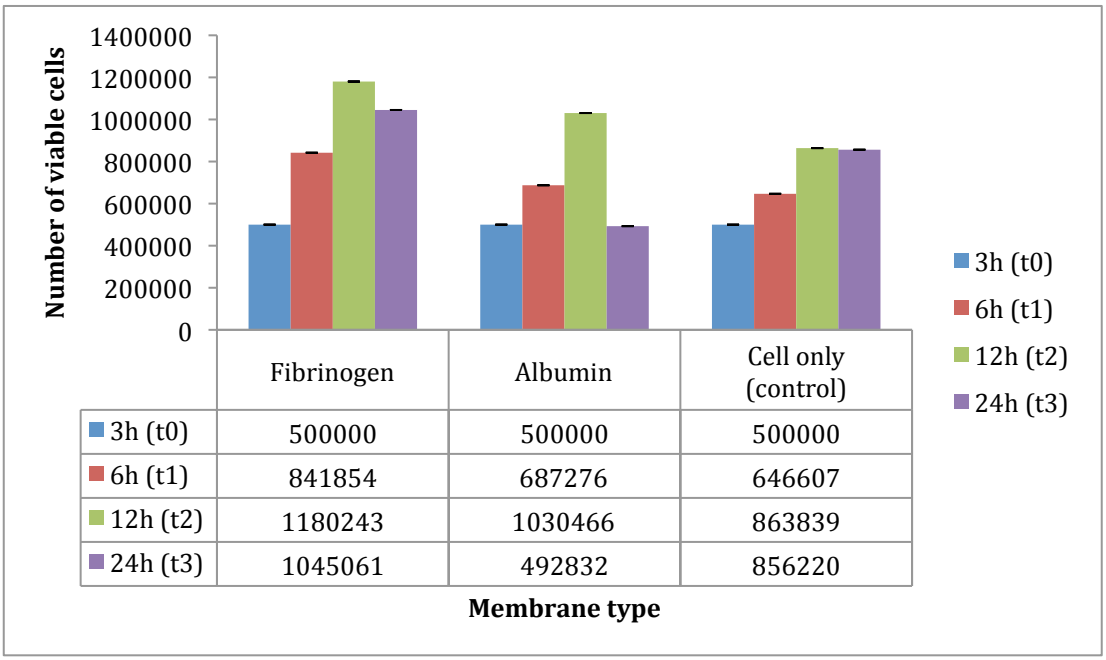

Figure 6.3: Cell viability on albumin and fibrinogen membranes using PrestoBlue (*Sample n= 4 ± S.E*).

Percentage change (%)	3-6 h	6-12 h	12-24 h
Fibrinogen	68	40	-11
Albumin	37	50	-52
Cell only	29	34	-1

Table 6.1: Percentage change in cell viability on crosslinked protein membranes.

The width of each membrane was measured at approximately 20 mm, with the thickness of the membranes measuring between 300-350 μM for fibrinogen and 70-80 μM for albumin. Cell viability and proliferation was determined on the crosslinked membranes at 3,6,12 and 24 h using the PrestoBlue cell viability reagent

to establish the number of metabolically active cells present, thus indicating viability. Figure 6.3 shows the number of viable cells present after each incubated time period compared with cell only controls of cells seeded directly on uncoated polystyrene tissue culture wells in the absence of a crosslinked membrane layer. Cells on control wells were seen to grow to confluence at 24 h. At 6 h, cell numbers increased by 70% between 3 and 6 h on fibrinogen membranes (Table 6.1), with a ~40% increase in cell numbers noted on albumin membranes.

Cells on fibrinogen membranes reach a rapid growth phase quicker than that of albumin membranes, which were not dividing between these time periods. Between 6 and 12 h there was a 50% increase in cell number on albumin membranes as cells entered the rapid growth phase and a 40% increase on fibrinogen membranes as cells here reached confluence. This changed between 12 and 24 h as cell numbers started to decrease by -11% in fibrinogen and -52%, presumably due to the lack of space required to facilitate the expansion of cells and cells exceeding the capacity of medium to support further growth.

6.4 Cell morphology on large surface area crosslinked protein membranes

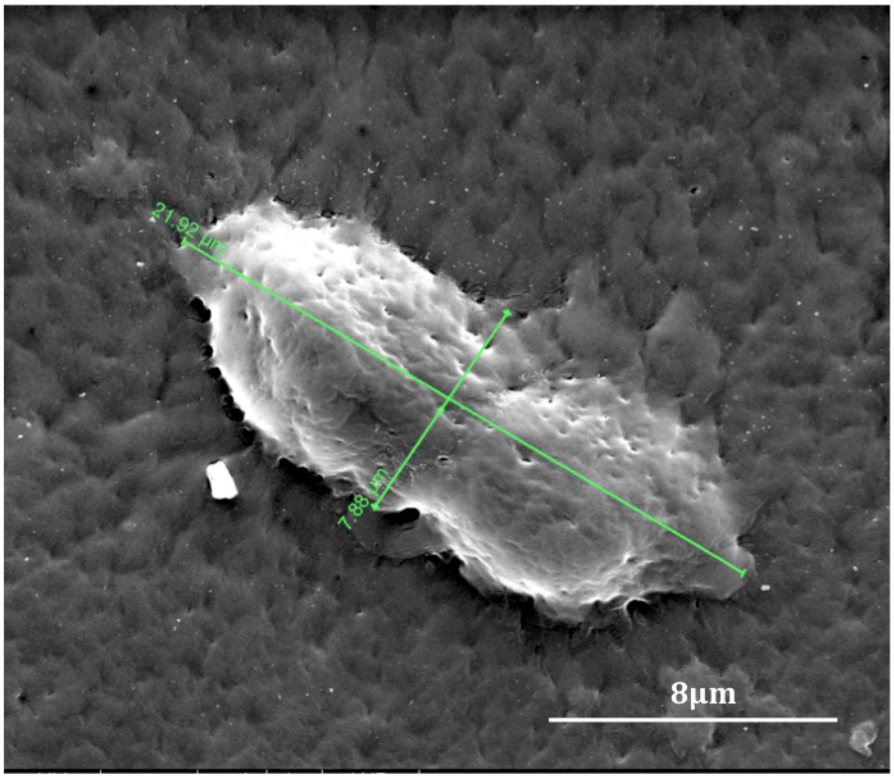

(A)

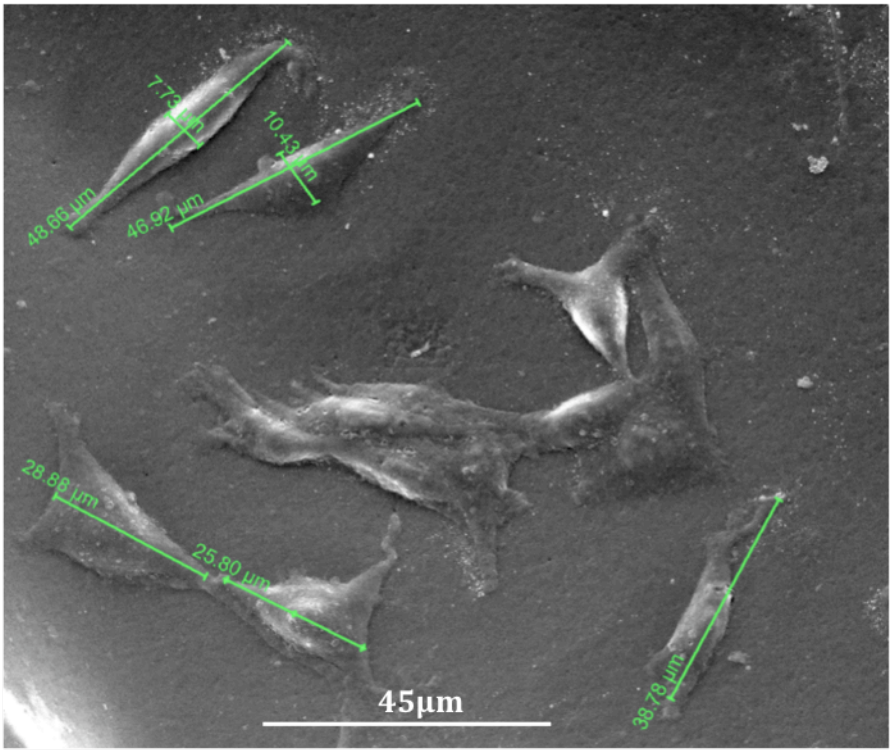

(B)

Figure 6.4: Morphology of B50 cells cultured on crosslinked fibrinogen membranes at 6 h of incubation (A) parent cell begins to divide (B) cells begin to elongate.

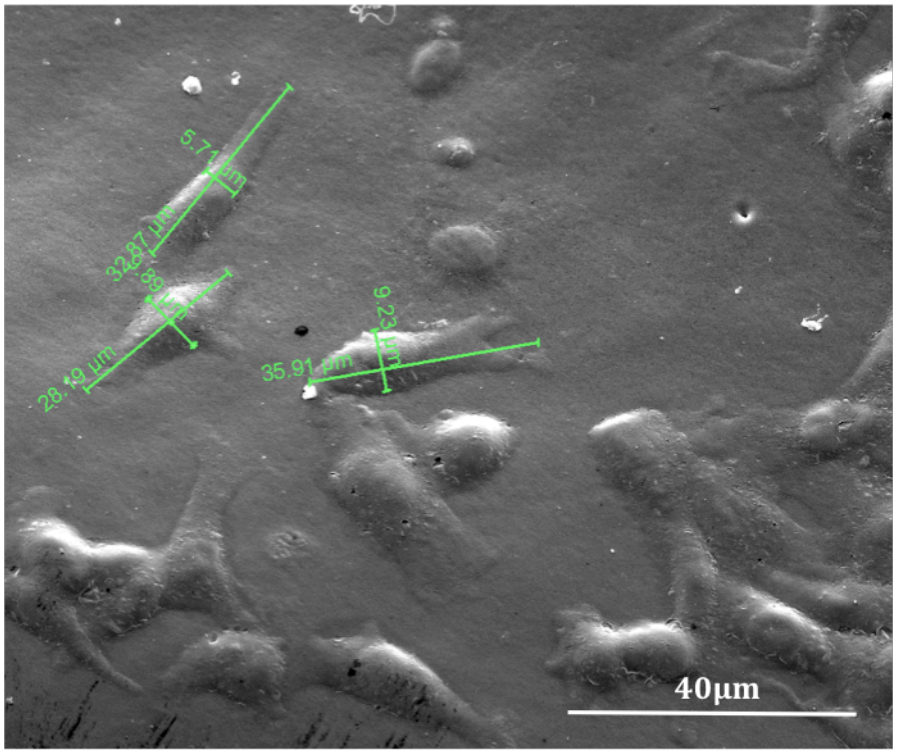

Figure 6.5: Morphology of B50 cells cultured on crosslinked fibrinogen membranes at 18 h of incubation.

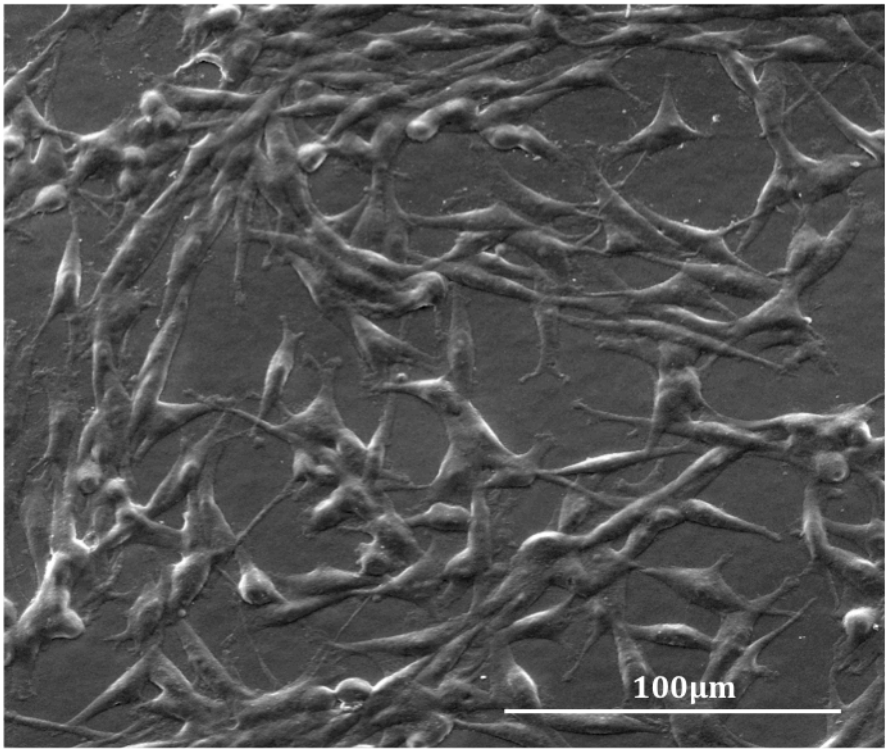

Figure 6.6: Morphology of B50 cells cultured on crosslinked fibrinogen membranes at 24 h of incubation.

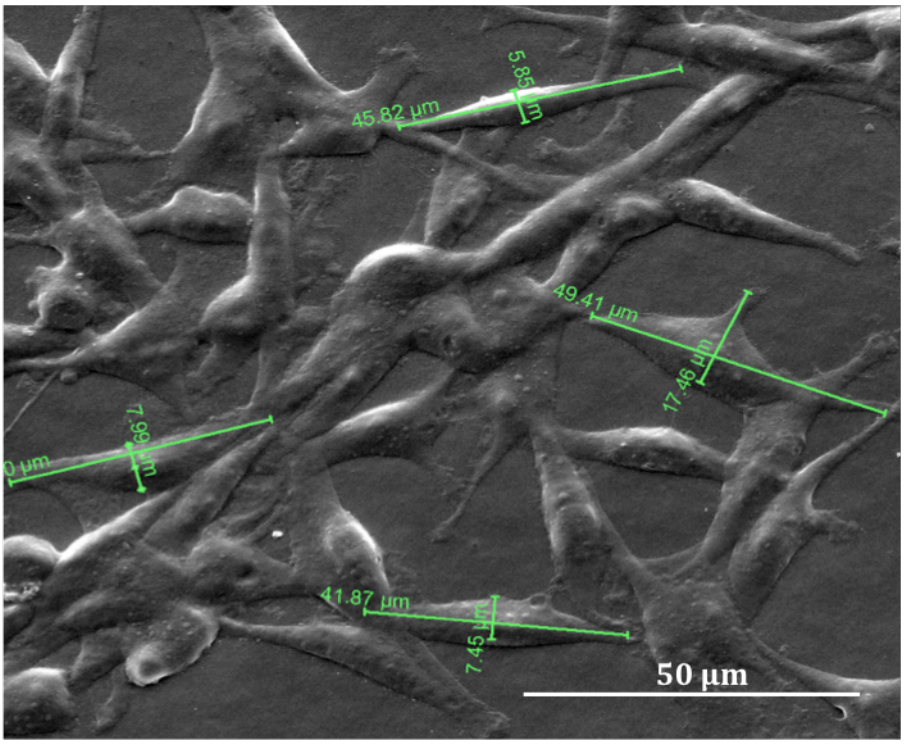

Figure 6.7: Morphology of B50 cells cultured on crosslinked fibrinogen membranes at 48 h of incubation.

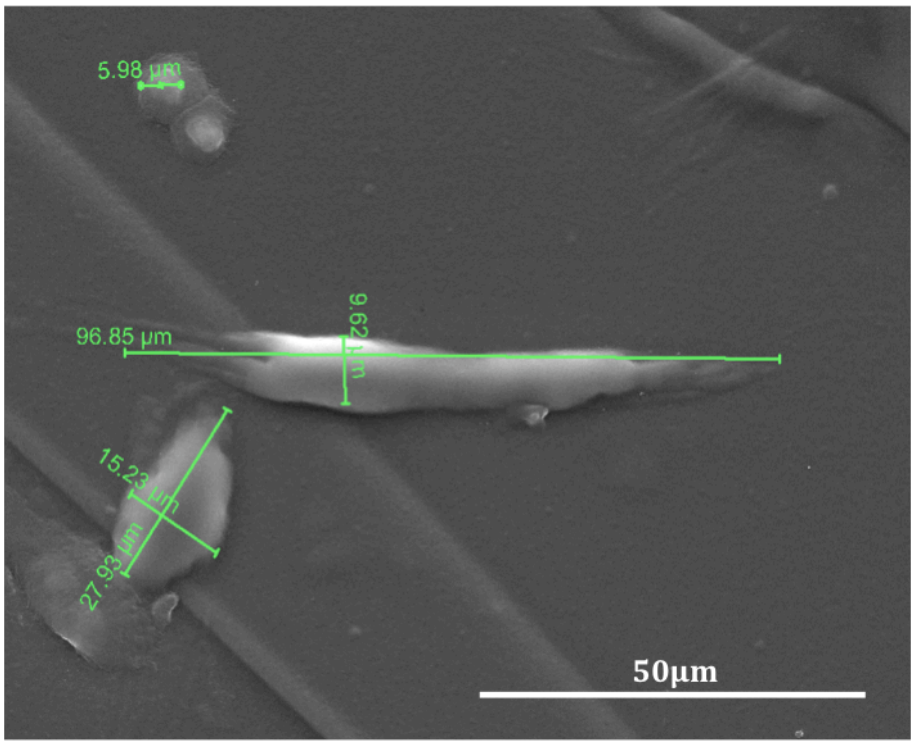

Figure 6.8: Morphology of B50 cells cultured on crosslinked albumin membranes at 6 h of incubation.

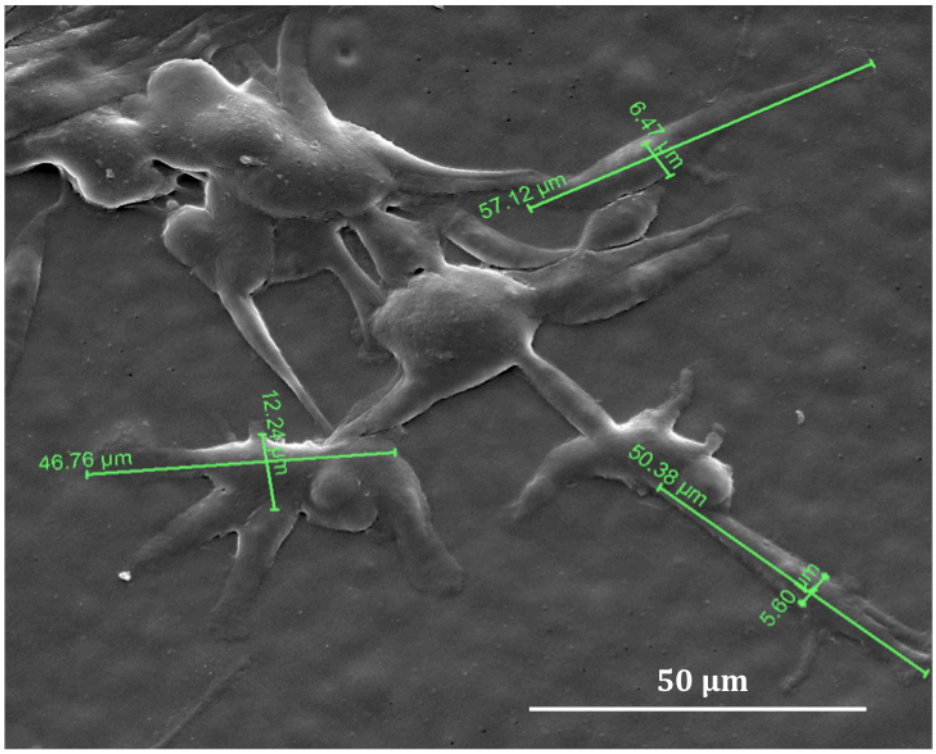

Figure 6.9: Morphology of B50 cells cultured on crosslinked albumin membranes at 18 h of incubation.

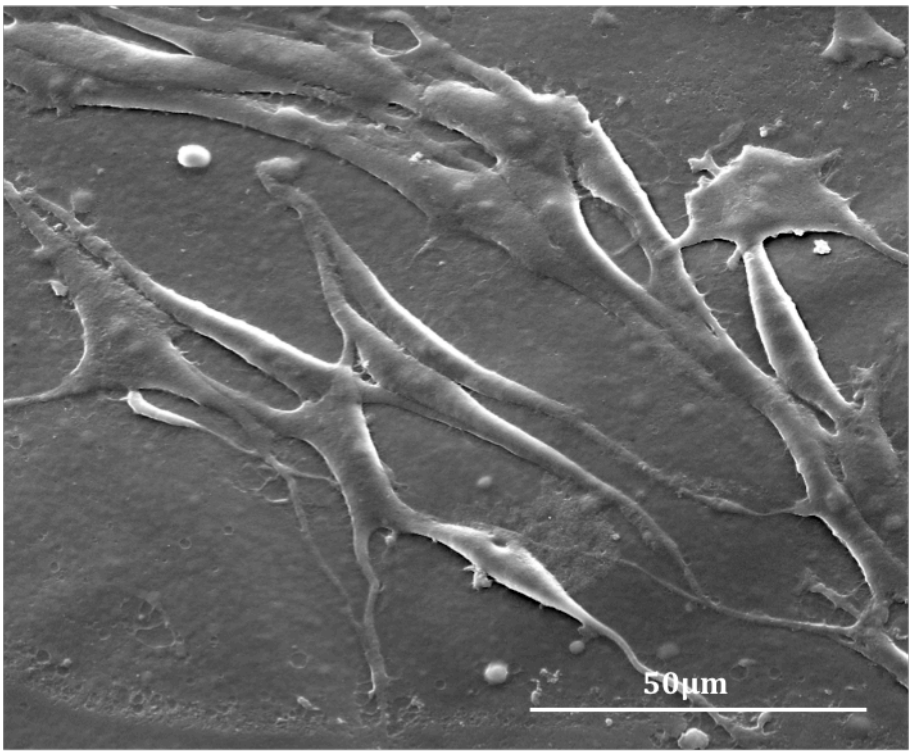

Figure 6.10: Morphology of B50 cells cultured on crosslinked albumin membranes at 24 h of incubation.

SEM imaging of B50 cells cultured on crosslinked protein membranes revealed a change in cell morphology over time. Figure 6.4 at 6 h on fibrinogen membranes (A), the parent cells begin to divide. The average length of cells was 20 μM -25 μM during division, with the width of the cells between 7-10 μM. Some cells present at this time (B) began to elongate to approximately 40 μM. This was similar for albumin membranes (Figure 6.8), however, the cell population was lower compared with the fibrinogen membranes.

At 18 h (Figures 6.5 and 6.9) there was little change in morphology on either membrane through most of the cells had elongated. By 24 h (Figures 6.6 and 6.10) cells were fully-grown to approximately 70% confluence on fibrinogen membranes,

conforming to typical dendrite like neuronal structure. However, the population of cells on albumin membranes was not as dense as on fibrinogen membranes. Figure 6.7 indicates cells on fibrinogen to be more densely distributed with an average cell length of 45-50 μM.

6. 5 Sensor integrated microfluidic channel

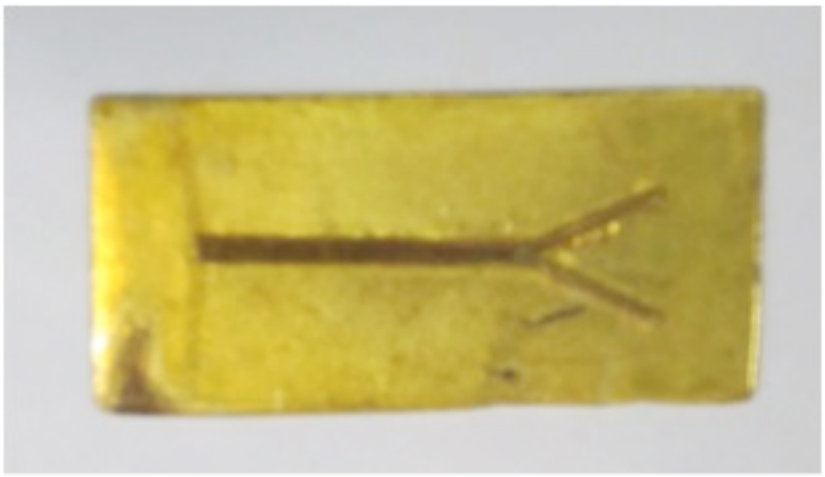

(A)

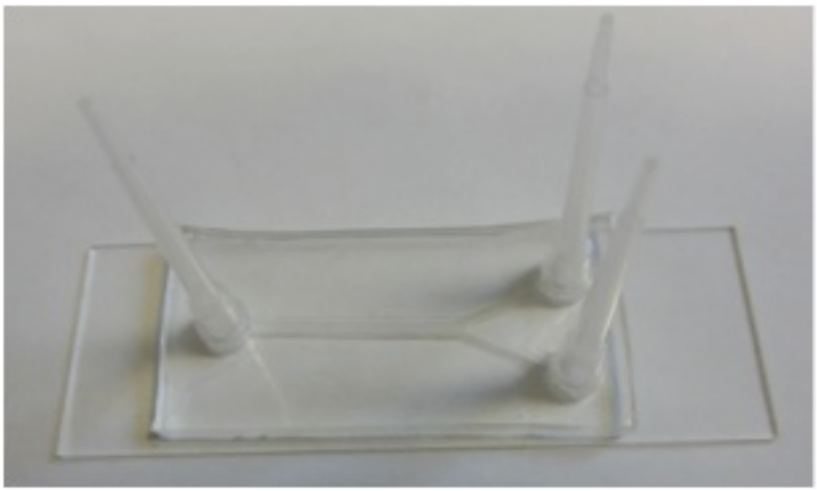

(B)

Figure 6.11: (A) Fabricated brass mould (B) PDMS channel with two 1 mm input channels, main channel diameter 2 mm and 80 μM channel depth.

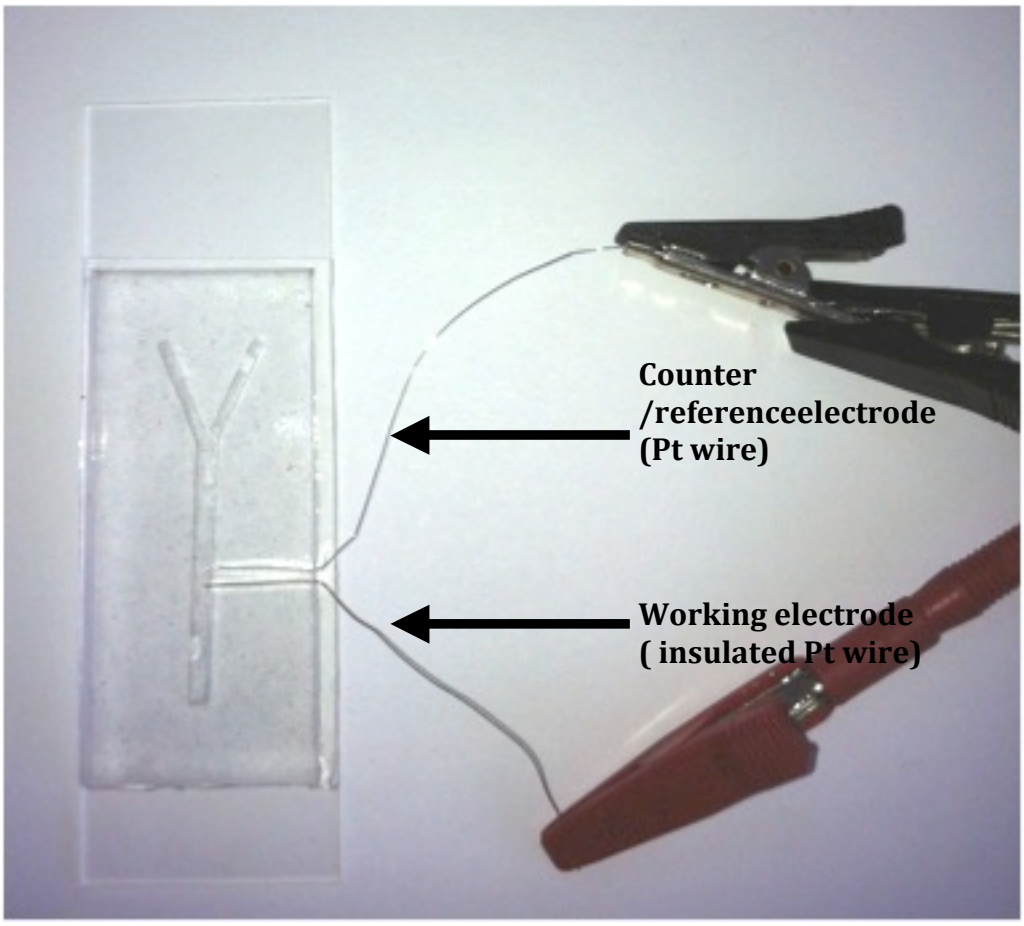

Figure 6.12: Sensor integrated channel, working electrode insulated with polyester (thickness 0.014 mm), conducting diameter 0.125 mm.

The two substrates used from microchannel moulds described in 3.5.3 were of brass and fibreglass PCB board. The brass substrate shown in Figure 6.11 (A) produced a channel depth of 100 μM when cast with PDMS, as where the fibreglass substrate resulted in shallower channels measuring 30 μM in depth making it too limited for sensor integration.

The resulting PDMS cast Figure 6.11 (B) consisted of two input channels of 1mm diameter with the main channel of 2 mm diameter. Input and outputs were formed with Eppendorf tips secured through the PDMS cast. During sensor measurements

these were replaced with needle syringes to generate fluid flow. Working and counter/ reference electrodes comprising insulated and non-insulated Pt wires were embedded adjacent to the main channel (Figure 6.12). During measurements involving the detection of H_2O_2, leakages from the sidewall of the channel in the sensing region were apparent. This resulted in the sensor being unable to detect any increases in H_2O_2 effectively.

6.5.1 Cyclic voltammetry

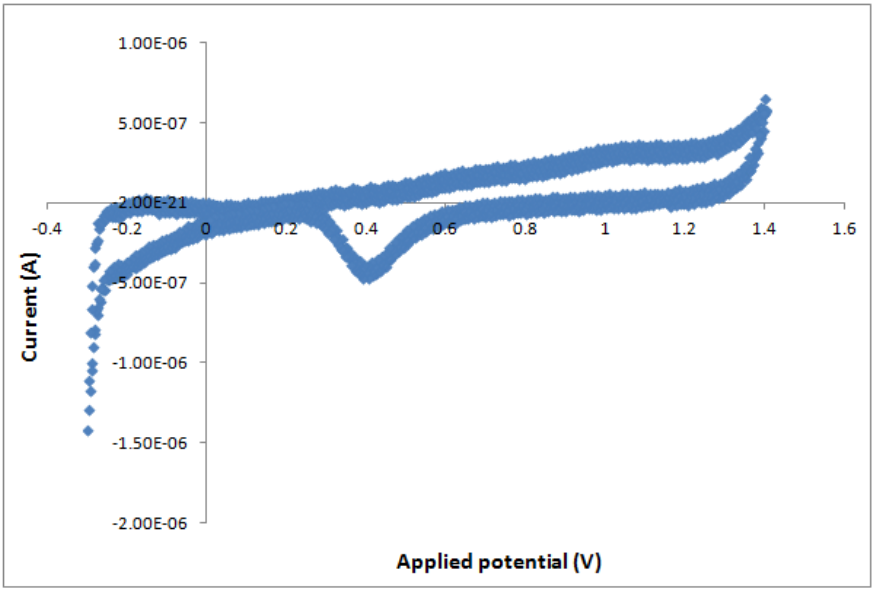

Figure 6.13: Cyclic voltammograph of Pt. electrode cleaning in 0.5 mM sulfuric acid between +1.5 and -0.4 V, Scan rate of 100 mVs^{-1} .

The cyclic voltammogram shown in Figure 6.13 served two purposes. It confirmed the functionality of the electrode circuit, and electrochemically cleaned the surface of the sensing surface. From the voltammogram an increase in current is noted ($5x10^{7}$A) as a high oxidation potential is reached, which then gives a ($-5x10^{-7}$ A) current peak as the electrode surface is reduced.

6.5.2 Detection of Hydrogen peroxide (H_2O_2) in a sensor-integrated microchannel

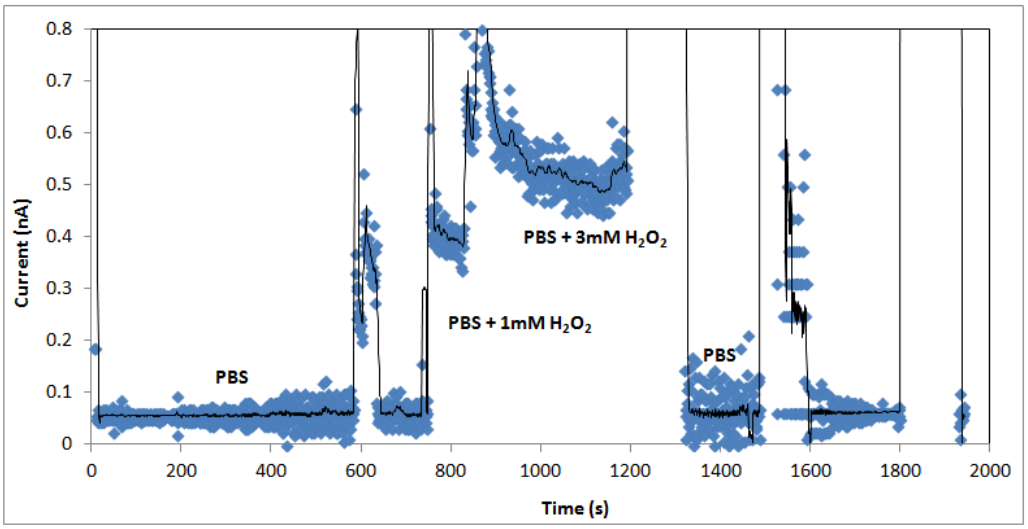

Figure 6.14: Detection of H_2O_2 in microchannel using integrated Pt. wire

Between 0-600 s a stable response is noted, after the increase in concentration leakages in the flow cell cause a unstable response between 1400-1600 s.

Amperometric measurements of H_2O_2 were carried out within the microchannel by first conditioning the sensing region in phosphate buffered saline (PBS). This was achieved by flowing the PBS through one input channel until a stabilized response was achieved. Following this, H_2O_2 was introduced and the concentration gradually increased through a series of stepwise additions of H_2O_2 at 1,3,5 mM through the second input channel. Figure 6.14 demonstrates the initial stabilized response between 0-600 s. Following the addition of H_2O_2 to achieve a concentration of 1mM H_2O_2, an increase in current is noted from approximately 0.1nA to 0.4 nA. After the stabilisation at 1 mM H_2O_2, a further increase in response is noted from 0.4 nA to 0.8 nA at a 3 mM H_2O_2 concentration before stabilization between 900-1200 s.

Subsequent measurements with increasing H_2O_2 concentrations were aborted due to leakages at the sidewall of the device at the sensing region due to loss of fluid volume from within the device. As a result of the leakage, the existing concentration of H_2O_2 was further diluted as indicated in the sudden drop in current at 1200 s.

Despite the fabrication limitations imposed by the flow device, when compared with conventional use of sensors as used in Chapter 5, it is apparent that the response time to increasing H_2O_2 concentrations occurs quicker in the flow device. For example, the initial stabilization period using a non-recessed electrode in the detection of H_2O_2 under standard conditions (Figure 5.4) occurs within 2000 s. Within the flow device, this occurs within 600 s. Also, a concentration of 3 mM can result in a stable response between 900-1200 s in the channel device, as where in the non-recessed biosensor this occurs at 3000-4000 s. In addition to this, it is worth noting that the use of channel devices minimises sample consumption making them more cost effective.

6. 6 Additional study: Shear force on B50 cells under microflow conditions

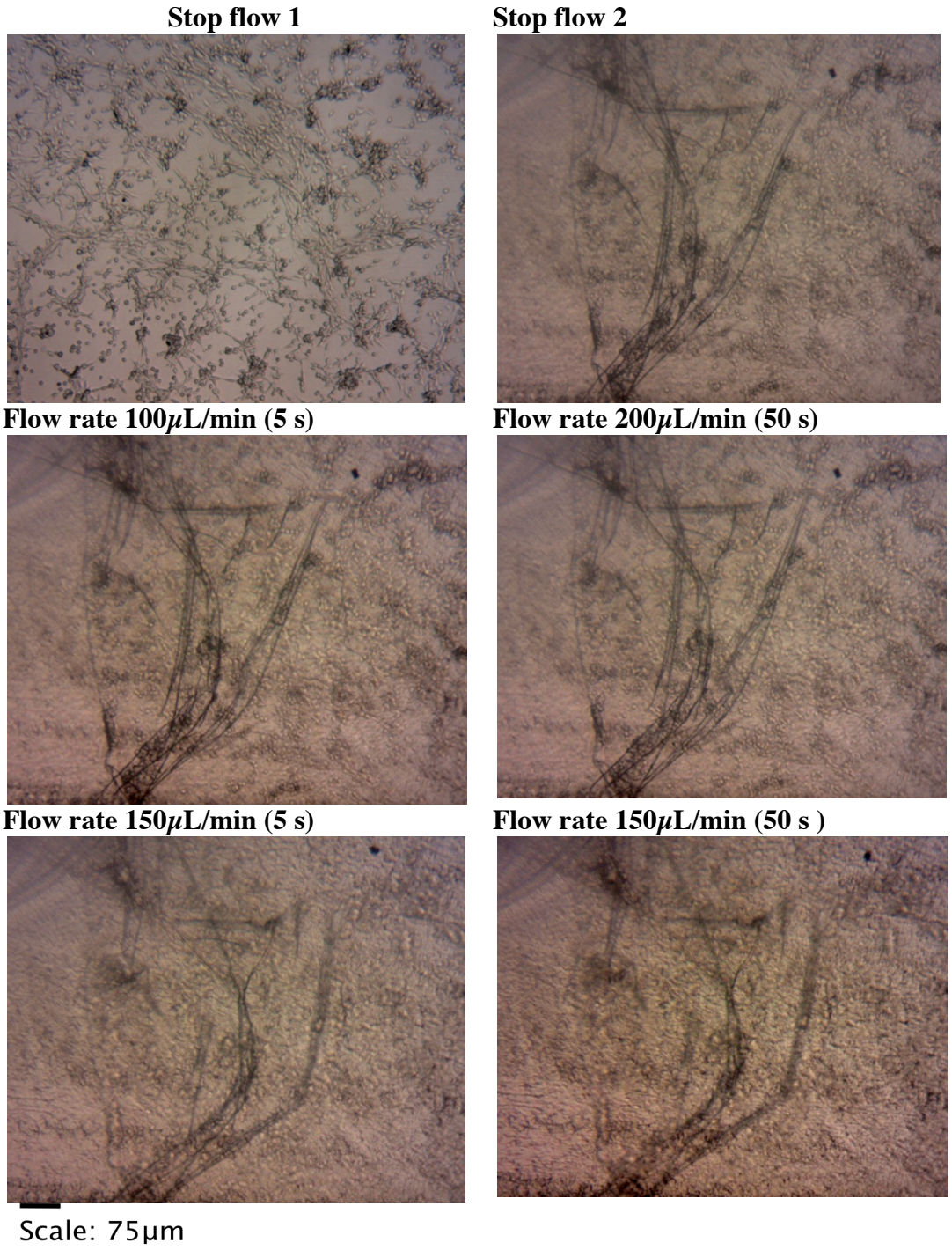

Figure 6.15: Light microscopy images of B50 cells cultured on crosslinked fibrinogen with fibronectin protein membrane, under various flow conditions of Dulbecco's phosphate buffered saline (DPBS).

One of the challenges faced when fabricating the machined flow cell was the ability to fabricate a flow cell that was relatively thin and translucent enough for optical microscopy. Despite the relatively transparent and mechanically stiff nature of Perspex, when machining the Y-shaped channels it was vital to ensure that the block of Perspex to be used was thick enough to withstand the machining process. However, this also meant compromising the visual clarity of the device for microscopy. It required several attempts of sanding and polishing before the flow cell was optimised for use.

Another drawback to the Perspex flow cell was the sterilization of the device. Like most fabricated devices to be used in cell culture application, sterilisation is vital in ensuring the survival of cells. A common method of sterilization used is autoclaving. However due to the high temperatures involved in this process, the flow cell was unable to be sterilized in this manner. As there was the risk of the high temperatures changing the properties of the material. Instead the device was sterilized chemically using isopropanol, alcohol and Biocleanse. This method of sterilization was also not ideal as over time the reagents can erode the material. An alternative method for sterilization that could have been used was antibiotic treatment using penicillin / streptomycin or antimycotic treatment with fungizone.

Figure 6.15 indicates the ability of cells to grow to confluence successfully when cultured on a crosslinked fibrinogen with fibronectin protein membrane across the fluidic flow cell. Increasing the flow rate of D-PBS solution exerted an increase in shear force. It was evident that the number of cells present on the membrane also decreased as result of surface shear. In addition to this, it was noted that the dynamic

force of the solution flow along the channel caused the membrane to peel away slowly from the channel wall. Despite attempts at clamping large sections of planar protein membranes with the O-ring of the Perspex device, the shear force of the liquids being pumped through the channel proved strong enough to break and peel away the membranes even under low flow rates.

In order to fully investigate the effect of shear stress on cells within bioreactor systems, it is vital that a perfused network of nutrient flow is maintained in order for cells to remain viable. Therefore, a system, which also enables the exchange of carbon dioxide and supply of nutrients to cells within fluidic systems, needs to be devised.

6. 7 Summary

Protein membranes formed by spin-coating using TCL crosslinking proved non-toxic to B50 cells cultured on the membranes surface. Crosslinked fibrinogen membranes appeared to enhance cellular adhesion and growth. Fibronectin crosslinked with albumin enhanced the growth of cells relative to albumin alone. Cell viability and morphology data revealed that crosslinked fibrinogen membranes accounted for an increase in proliferation and growth of cells over time.

PDMS microchannel was fabricated with a working integrated sensor, the sensor detected up to 3 mM concentration of H_2O_2 before measurements were aborted due to leakages. The fabricated sensing device proved more rapid in response time compared with conventional needle type sensors.

An additional study into shear force exerted on to B50 cells cultured on crosslinked fibrinogen with fibronectin membranes revealed a decrease in cell numbers as a result of surface shear.

CHAPTER 7

-

Discussion, conclusion and future work

7.0 General discussion

7.1 Cell viability on enzyme encapsulated p(HEMA) *vs* Agarose enzyme gels

In light of the viability data obtained from enzymes immobilized in both p(HEMA) and agarose gels, the findings in Section 4.5 and 4.6 suggest that the possible effect of immobilized enzyme needs to be considered as a factor in cell death leading to an inflammatory response. In general, all agarose gels containing GOx resulted in lower viable cell numbers over time. From the PrestoBlue assay, at 3 h it was noted that all GOx containing agarose gels produced the highest level of cellular metabolic activity. The intracellular reduction of resazurin to resorufin, from the resulting fluorescence values correlate with the metabolic activity of the cells [169]. This is especially the case at 3 h where it can be assumed that all the cells present were viable. This finding was confirmed by a visual analysis of cells and by the trypan blue exclusion.

In comparison with p(HEMA) gels the detrimental effect of GOx on B50 cells in agarose gels seemed to occur more rapidly (Figure 5.13), suggesting that the structure of agarose could account for rapid leeching of the encapsulated enzyme. Enzyme leeching from agarose gels was also observed by Lasch and Koelsch [178] who immobilized leucine aminopeptidase with multiple and single anchoring bonds, conjugated with co-enzymes in agarose. Their findings suggested that the co-immobilisation of enzymes resulted in decoupling causing enzyme leakages high enough to prohibit long-term use of agarose as immobilization matrix for routine work at room temperature.

The amperometric detection of hydrogen peroxide produced by agarose encapsulated GOx gels in Chapter 5 discussed in more detail later, suggest that GOx remains active in H_2O_2 production until approximately 3.5 h, after which the enzyme is saturated and no longer producing H_2O_2. Therefore cells are subject to the cytotoxic effect of H_2O_2 from 3.5 h. The findings relate to the studies conducted by Whittemore *et al* [179] who concluded that the production of H_2O_2 induced apoptotic cell death in neuronal culture within 3 h of H_2O_2 exposure. This correlates with decrease in cell viability noted in all GOx containing agarose gels after 6 h. Similarly to the method used for determining cell viability on p(HEMA) enzyme gels, the study by Whittemore, assessed cell viability by visual counts in conjunction with trypan Blue exclusion. Following this, they also measured the ability of the cortical cultures to reduce MTT coloured formazan to assess mitochondrial activity and cellular oxidative capacity. In contrast to our study, Whittemore *et al* [179] exposed cells to various concentration of H_2O_2 ranging from 10, 30 and 100 μM at incubation periods of 3,6 and 12 h. It was demonstrated that H_2O_2 stimulated a close and time dependant decline in both viable cell number and cellular oxidative capacity. Whittemore *et al* [179] also investigated the effect of H_2O_2 directly on the DNA of cells via DNA fragmentation analysis. They further concluded that there was DNA damage as a result of apoptotic cell death. In this respect, the present study was more limited, as cell damage; only by means of the morphological analysis of whole cells was investigated. This also proved difficult, as imaging of cells on agarose gels samples was problematic due to the low mechanical stiffness of agarose, particularly with regards to fixation of cells. Because of this, cells tended to detach very easily from the surface of agarose, making it difficult for processing samples without cell loss. Based on preliminary studies, B50 cells tend to fully develop after 48 h on

agarose samples. Therefore it is difficult to assess any changes in cell morphology prior to 48 h of cell incubation, therefore further studies into live cell imaging without the need for cell fixation should be investigated to reveal any changes in cell morphology on enzyme gels.

Both the present and Whittemore *et al* [179] studies show evidence that the exposure to H_2O_2 causes cell damage. In the study by Whittemore *et al* [179] the exposure of H_2O_2 is direct, whereas in this study, H_2O_2 exposure is the result of an indirect progressive product of the catalytic reaction between GOx and glucose. The clinical significance of the use of B50 neuronal cells is that they can serve as a model for the mechanism of oxidative injury in the central nervous system and useful in developing protective strategies for the prevention of neurodegenerative diseases associated with oxidative damage or stress [180].

On comparison of cell viability between p(HEMA) and agarose gels, GOx –SOD p(HEMA) gels resulted in the highest number of viable cells at 6 h. This was also the case for GOx-SOD agarose gels at the 3 h study, however by 6 h it was apparent that GOx-SOD agarose gels produced the second lowest number of viable cells of all the enzyme gels studied. Studies by Trivic *et al* [181] investigated the formation of enzyme-catalysed free radicals. They found that the product of GOx reduction undergo a dismutation reaction with the parent compound forming free radicals. They also concluded that in some cases, at appropriate pH values, free radical transformation was quantitative. The free radicals remained stable for several minutes in aqueous solutions under physiological conditions. The role of SOD designed into the enzyme gels was to eliminate any superoxide and peroxide radicals

that may have been formed as a by-product of the GOx reaction. However the presence of SOD within enzyme gels did not, have any significant protective role in preventing cell death as a result of H_2O_2 exposure. A similar finding was illustrated by Savazyan *et al* [182] who evaluated the role of CuZn containing SOD (CuZnSOD) in oxidant induced injury to rat cardiac myocytes. In this study myocytes were exposed to either reagent H_2O_2 or oxidants generated by an extracellular GOx and glucose reaction as in the present study. The results showed that the CuZnSOD treated and untreated cells were equally susceptible to an H_2O_2 effect; hence SOD did not provide a protective role against H_2O_2 induced injury.

In neuroscience studies SOD has been known to catalyze the formation of peroxyynitrate, which is a contributing factor to neuronal injury in motor neuron disease [158]. Cookson *et al* [159] compared the biological and morphological response of neuronal cells to peroxynitrate and H_2O_2 mediated cell death in vitro. Their findings confirmed reduced cell viability in H_2O_2 treated cells with noted change in the morphology of cells showing some cell shrinkage and membrane blubbing at 4 h. By 6 h these changes increased and by 24 h cells were completely damaged with very few left intact, suggesting that H_2O_2 toxicity could account for the late stages of apoptosis and tissue necrosis. The morphological changes noted by Cookson *et al* [159] appear somewhat similar to the morphology of both B50 and RMS12 cells cultured on GOx gels in the present work. The addition of SOD with GOx could be potentially beneficial when used in crosslinked hydrogel structures such as p(HEMA) more so than that of GOx and catalase combined. In agarose gels however SOD provides no real benefit in reducing the cytotoxicity of the GOx effect.

Gels containing only catalase accounted for a consistent increase in cell viability in both agarose and p(HEMA) hydrogels. Based on data from the viability assays, at 12 and 24 h as indicated in Figures (4.10), (4.12) and (4.14), catalase alone produced the most viable cells in both hydrogels relative to enzyme free controls. In the light of the MTT assay data on p(HEMA) gels (Figure 4.8) , it is apparent that the co-immobilization of catalase with GOx does not counteract the harmful effect of H_2O_2 produced in the reaction of GOx with extracellular glucose in the cell culture media. This finding differs from agarose gels where the addition of catalase to GOx gels improved cell viability over time. The co-immobilization of GOx with catalase has been reported to significantly improve the activity and reusability of both enzymes [183]. GOx is inactivated by H_2O_2, and the concentration of this is especially increased because of high enzyme catalytic turnover of glucose reported as K_m of 33-110mM [184]. H_2O_2 induced cell damage can be reduced by catalase as this reduces H_2O_2 concentration eventually removing it from the system if significantly high catalase amounts are used. From this reaction some oxygen is also recovered, which is beneficial to cells. In the present study, the concentration of glucose in the media is ~4.5 mg/ml with the unit of activity of GOx 953.4 units/g solid. The catalytic turnover of catalase is 2.25 $X10^7 s^{-1}$ [184] of which 3809 mg/solid is used in the study.

In general, cells require glucose for metabolism, which is reduced by the presence of GOx that competes with cells for glucose present in the culture media (DMEM). Similarly, oxygen is also required for cells which low levels caused by the presence of GOx or oxygen supply from the gas phase may be inadequate in relation to the depth of incubation over the gels. H_2O_2 has been reported to alter the physical state

and function of plasma membranes of endothelia cells *in vitro*, leading to alterations in the fluidity and leakiness of the membrane as a result to damage to the lipid bilayer of the membrane [185]. The two main mechanisms of apoptosis existing are extrinsic and intrinsic in addition to a perforin / granzyme pathway. Each pathway is triggered by different signals that initiate caspases to activate cellular execution. The extrinsic pathway uses a ligand/ receptor, which detects cell death. This then initiates Caspase-8 to activate the execution pathway. In the intrinsic pathway, toxins hypoxia, radiation etc. cause mitochondrial changes that induce apoptosome formation. This then initiates Caspase-9 to activate and follow the execution pathway. However, the perforin / granzyme pathway uses cytotoxic t-cells initiate granzyme A and B. Granzyme A causes DNA cleavage, whilst granzyme B activates Caspase-1) which then initiates the execution pathway. During the execution stage, nuclear and cytoskeletal proteins are degraded leading to cytoskeletal reorganisation along with chromosomal DNA damage. This then causes cytomorphological changes such as chromatin and cytoplasmic condensation known as blebs, nuclear fragmentation; which results in the formation of apoptotic bodies [186]. Images in Figure. 4.16 (C) obtained using DiOc18(3) stained B50 cells on agarose enzyme gels did confirm the formation of apoptotic blebs in GOx containing gels.

A limiting factor in the study of cell viability on p(HEMA) gels was the use of different methods to evaluate the viable cell number present. In the present study, the concept of cell death was explored via analysis of cell metabolism using both PrestoBlue and the MTT assay. The results of the assays indicated various points at which cell metabolism was active and when it stopped, thus concluding its viability on each gel type.

Unlike the agarose gels where cell viability was determined solely by the PrestoBlue viability assay, the p(HEMA) gels were subject to counting of viable cells using the Trypan Blue exclusion method. This method can be subject to human error and the accuracy of the data obtained can be compromised. Also the method involved the trypsinzation of cells from the surface of the hydrogel. Prolonged exposure of cells to trypsin may be damaging to cells [187]. In comparison with the MTT assay, PrestoBlue offers an increase in sensitivity for cell metabolism with as little as 12 cells/well being detected in contrast to 1000 cells/well as observed by the MTT assay [168]. Furthermore, PrestoBlue allows for the live detection of cells with as little as 10 min reagent incubation, whereas the MTT assay is an endpoint cell lysis assay requiring 2-4 h of reagent incubation. However a limitation for the use of the resazurin based viability reagent was the concern that both GOx and resazurin undergo redox reactions, which could account for false positive results. However an additional control outlined in Section 3.2.5 revealed in there to be a minimal interaction between GOx containing gels and the PrestoBlue reagent as fluorescence values did not deviate much from those obtained from the media blank. This may be due to the concentration of the enzyme used, as lager concentrations of the enzyme could have accounted for a higher fluorescence.

7.2 Comparison of recess and non-recess disc electrodes for glucose measurement - stabilization effect of agarose gels.

7.2.1 Detection of hydrogen peroxide (H_2O_2)

Results for the detection of H_2O_2 revealed a notable difference in sensitivity of non-recess *vs*. recessed disk electrodes. Non-recessed electrodes elicited measurements with higher sensitivity and faster reaction. This can be explained by the reduced diffusional transport of H_2O_2 within the internal space of a recess. A similar finding was reported by A. Kacanovska et al [156]. This work showed that non-recessed electrodes were almost 50 times more sensitive for H_2O_2 than recessed electrodes, which is dependent on the recess depth.

A maximum linear range for both electrode types was noted in the present study of 12 mM H_2O_2, which was extended to up to 50 mM for non-recessed electrodes. Thus, although non-recessed electrodes have higher sensitivity, signal to noise ratio was better in recessed electrodes.

The 0.5% (w/v) agarose filled recess electrodes resulted in no notable difference in measurements obtained in the detection of H_2O_2, which indicated that filling the recess with a gel layer did not have any effect on the response of the electrode thus resulting in a stabilized response.

The use of gels has also been studied to improve the performance and storage of amperometric biosensors. One such study by Wang et al [188] explored the use of sol-gel chitosan as an immobilisation matrix for the detection of H_2O_2. Chitosan was crosslinked with 3-aoryloxypropyl dimethoxymethyslaine to produce a gel film used to immobilize peroxidase (HRP) on gold disk electrodes. The results concluded a

typical Michaelis -Menten mechanism, with the biosensor retaining 75% of original activity after 60 days of storage in PBS at 4ºC.

7.2.2 Detection of glucose

Non-recess electrodes for the detection of glucose were found to exhibit faster responses compared with recess electrodes. This is due to the shorter diffusion path of the analyte to the anode, as well as hemispherical diffusion on non-recess electrodes as opposed to purely linear diffusion in recessed electrodes. Figure 5.8 shows glucose measurement on a recessed electrode with a depth of 850 μM. As can be seen, response time of glucose was greater compared with Figure 5.7 that has a smaller recess length of 45 μM. A similar outcome was reported by A. Kacanovska *et al* and S. Anastasova e*t al* [117][156], where an increase in the recess depth lead to longer response time. Despite the increase in sensitivity and shorter response time demonstrated in non-recess electrodes, the recess electrodes proved to be more stable as they provide a protective layer between the sensing tip and improve response instability associated with sample stirring [115].

The use of hydrogels to enhance the stability of enzyme such as GOx and to provide good optical properties was successfully achieved by Psoma and Turner [189], with optode for glucose detection using simultaneous fluorescence quenching of two indicators: (2,2- bipyridyl) ruthenium (II) chloride, hexahydrate and 1-hydroxypyrene – 3,6,8- trisulfonic acid. Overall, it can be concluded that the presence of the gel can provide a more stable device without air being trapped within a recess giving stable responses and not adversely affecting the performance of the electrode.

7.2.3 Selectivity measurements using recess and non-recess electrodes

Electrochemical methods are very sensitive, however, they lack selectivity. Thus, any electrochemically active substance present can contribute to the signal. Interfering substances such as ascorbic acid (AA), acetaminophen (AC) and uric acid (UA) that are present in physiological samples can contribute to the signal and thus compromise the accuracy of measurements. [190]. There are many ways to increase selectivity of a biosensors, such as use of a selective semi permeable membrane, which are highly permeable to analytes of interest, such as H_2O_2, but impermeable to interferents. Examples of commonly used membranes include Sulphonated polyesther ether sulphone – polyether sulphone (SPEES/PES) [191], and polyphenylenediamines [192].

Selectivity measurements revealed a decrease in the level of interference present with recess electrodes compared with non-recess electrodes. This was also noted in a previously conducted study by Anastasova et al [117], which confirmed that an increase in recess depth result in a decrease in interference. A plausible explanation for this observation could be due to a surface charge effect from the silica glass surface of the electrode. This was supported by the observation that interferants such as catechol and ascorbic acid in anionic, not neutral showed no difference between recess and non-recess electrodes.

7.2.4 Additional Study: Detection of H_2O_2 from enzyme encapsulated agarose gels using platinised electrodes

The use of Pt electrodes in the detection of H_2O_2 produced from the reaction of GOx encapsulated within agarose gels, with free glucose present in DMEM revealed a

difference in H_2O_2 concentration for gels with and without cells. The calibration of H_2O_2 in DMEM achieved a linear range of 1-20 mM. In the absence of cells, the highest concentration of H_2O_2 observed in GOx only gels was 8 mM. In contrast GOx gels with cells seeded, resulted in a 14 mM concentration of H_2O_2. The noted difference in H_2O_2 concentration with and without cells is difficult to explain and requires further study, but could have been due to the volume uptake by cells reducing the gel volume within which the H_2O_2 could be distributed. Another possibility is a cell protective effect for example, masking of impurities or catalytic components in the gel that degraded the H_2O_2. In addition to this theory, H_2O_2 known to produce hydrogen *peroxide*-induced apoptosis and lysis of the B50 cells [193]. B50 cells are similar to *PC12* cells [26] for which it is well know that peroxide induces such apoptosis and lysis [170]. Hydrogen peroxide is an example of reactive oxygen species (ROS). ROS are products of cell metabolism; H_2O_2 formed from converted superoxide in the mitochondria during cellular metabolism can leak into surrounding tissues [194].

The observed increase in H_2O_2 at the platinized platinum electrode may then be due to any of the following three factors:

i) The death of these cells may have produced interfering substances such as ascorbate and citrate that are interfering substances at 0.65 V.

ii) The release of enzymes that generate peroxide (any oxidoreductase) and/or

iii) The release of glucose that increases the production of hydrogen peroxide.

In the absence of cells, the enzyme saturated past 200 min. This may be due to the lack of substrate available for the enzyme, in particular the lack of free glucose

consumed by both cells and the enzyme. With cells the enzyme began to saturate as early as 50 min and by 350 min was fully saturated. In GOx-CAT gels there was no H_2O_2 detected, confirming the active role of catalase in the degradation of H_2O_2.

7.3 B50 cell attachment and viability on crosslinked protein membranes

Crosslinked membranes formed by spin coating revealed no imparted toxic effect of the crosslinking agent on cell growth and attachment [165]. Results determined using the PrestoBlue viability assay indicated that the growth and proliferation of cells was favoured on crosslinked fibrinogen membranes. The co-immobilization of fibronectin, despite its specific RGD cell-binding motif with fibrinogen had no effect on cell morphology or density [25]. However in the presence of BSA, cell growth was enhanced.

Cell viability data on crosslinked BSA and Fibrinogen membranes formed by interfacial crosslinking [165] resulted in the gradual increase in cell proliferation relative to control samples of cells seeded on non tissue culture treated well plates as indicated in Figure 6.2. However, BSA membranes did not support long term viability of B50 cells past 24 h as cells were no longer able to proliferate, where as B50 cells on fibrinogen membranes remained viable with double the number of viable cells present at 24 h. The improved adhesion of B50 cells on fibrinogen membranes can be attributed to surface chemical motifs and pore morphology, these results are similar to those observed on other porous surfaces [27]. The non-toxic adhesive nature of the proteins, and the ability to facilitate cell growth make it favourable for the crosslinked membranes to be used as potential bioreactor surfaces.

7.4 Sensor integrated microfluidic channel

Amperometric detection of H_2O_2 within the fabricated microchannel resulted in a response to H_2O_2 concentration of up to 3 mM. However during measurements, leakages from the sidewall of the channel in the sensing region were apparent. This resulted in the sensor being unable to detect any further increase in H_2O_2 effectively with subsequent measurements being aborted. Following the analysis of the leaking device, it was apparent that the leakages were a result to poor bonding between PDMS and the glass microscope slide. This was due to the surface of the PDMS containing residues of brass from the substrate mould that was unable to be removed despite vigorous cleaning.

Fabricated microdevices with integrated sensors have been of particular interest in biogical and chemical analysis [132], with a wide range of substrates used in the fabrication of these devices. Hu *et al* [195] fabricated and tested planar chalcogenide waveguide integrated microfluidic sensors in PDMS. They reported a linear response observed for the waveguide of sensor to varying concentrations of N-methylaniline. In contrast to the present study, silicon wafers were used as a substrate for the microfluidic device in addition to using traditional lithography fabrication techniques. A glass substrate was used in the fabrication of a microfluidic electro-wetting set up by Srinivasan *et al* [196], they devised a fully integrated and reconfigurable droplet based lab on a chip device for clinical diagnostics on human physiological fluids.

Despite the limitations that the fabricated device imposed in the present study, the response time to H_2O_2 was considerably faster than conventional biosensors

described in Chapter 5. The use of the microchannel still managed to minimize reagent consumption proving cost effective.

7.5 Conclusions

This thesis demonstrated the effect of oxidoreductase enzymes such as glucose oxidase immobilized within biologically derived agarose and biomimetic p(HEMA) hydrogels on cell viability. The results confirmed the presence of GOx to be detrimental to cell viability. The co-immobilization of catalase with GOx in these constructs did not counteract the harmful peroxide effect on cells, nor did the presence of SOD improve viability of cells. However, both gel types showed that a long-term effect of catalase alone was a benefit to cell proliferation. The effect of enzyme leeching in agarose gels was quantified by amperometric detection of peroxide, which revealed cell induced hydrogen peroxide production.

The stabilization of recessed electrodes using agarose was also investigated, which the ease in sensor handing enabled for prevention of air entrapment. Within gels this led to the fabrication of a microfluidics integrated sensor that provided faster amperometric detection of peroxide compared with conventional biosensors. Finally, B50 cell viability was determined on different crosslinked protein membranes from by in situ interfacial crosslinking. Fibrinogen membranes were concluded to improve cell growth and viability.

7.6 Future work

7.6.1 *In vivo* study of p(HEMA) and agarose filled recess electrodes

The uses of recess implantable sensors *in vivo* have been previously reported [156], these sensors were found to improve response instability and reduce protein bio fouling [117]. The recess gap was found to provide a protective area, which protected the sensing region from mechanical damage or protein contamination. Gel filled recess proved beneficial in the current *in vitro* study in the stabilization of the electrode. Therefore, the next step would be to test the both synthetic p(HEMA) *vs*. natural agarose filled recess electrodes *in vivo* to establish if the gel layer provides an added protection to the sensing region and further complements stabilization of the electrode in light of adverse biological responses *in vivo*.

7.6.2 Optimization of sensor integrated microfluidic channel for use as bioreactor

Previous studies within this thesis evaluated the biocompatibility of crosslinked protein membranes; the formation of these membranes through interfacial crosslinking has been investigated [130] with the selectivity of these membranes also determined [165]. Therefore the next stage of the research would focus on the development of a microbioreactor with the use of crosslinked protein membranes as a bioreactor surface by the retention of cell growth. These cell systems require a perfused network of nutrient flow to ensure the viability of cells. Therefore the system needs to support gaseous exchange of CO_2 and O_2 whilst ensuring nutrients such as glucose are supplied to the cells. The integrated sensor would enable the analysis of metabolites across such a bioreactor surface. In addition to this, the study

outlined in Chapter 6, into the shear effect on cells within a microchannel can be further extended.

The current fabrication design would therefore need to be adapted to prevent any leakages from occurring. This can be achieved by exploring the use of other substrates such as silicon wafers with standard lithographic techniques or glass substrates in which microchannels can be fabricated through chemical etching.

References

1. Hubbell, J. A. (1995). Biomaterials in tissue engineering. *Nature Biotechnology*, *13*(6), 565-576.

2. Hynes, R. O. (2002). Integrins: bidirectional, allosteric signaling machines. *Cell*, *110*(6), 673-687.

3. Guiseppi-Elie, A. (2010). Electroconductive hydrogels: synthesis, characterization and biomedical applications. *Biomaterials*, *31*(10), 2701-2716.

4. Bickerstaff, G. F. (1997). *Immobilization of enzymes and cells*.

5. Kamath, K. R., & Park, K. (1993). Biodegradable hydrogels in drug delivery. *Advanced drug delivery reviews*, *11*(1), 59-84.

6. Khademhosseini, A., & Langer, R. (2007). Microengineered hydrogels for tissue engineering. *Biomaterials*, *28*(34), 5087-5092.

7. Vinogradov, S. V., Bronich, T. K., & Kabanov, A. V. (2002). Nanosized cationic hydrogels for drug delivery: preparation, properties and interactions with cells. *Advanced drug delivery reviews*, *54*(1), 135-147.

8. Updike, S. J., & Hicks, G. P. (1967). The enzyme electrode. *Nature*, *214*, 986-988.

9. Yu, B., Long, N., Moussy, Y., & Moussy, F. (2006). A long-term flexible minimally-invasive implantable glucose biosensor based on an epoxy-enhanced polyurethane membrane. *Biosensors and Bioelectronics*, *21*(12), 2275-2282.

10. Wilkins, E., Atanasov, P., & Muggenburg, B. A. (1995). Integrated implantable device for long-term glucose monitoring. *Biosensors and Bioelectronics*, *10*(5), 485-494.

11. Onuki, Y., Bhardwaj, U., Papadimitrakopoulos, F., & Burgess, D. J. (2008). A review of the biocompatibility of implantable devices: current challenges to overcome foreign body response. *J Diabetes Sci Technol*, *2*(6), 1003-1015.

12. Thévenot, D. R. (1982). Problems in adapting a glucose-oxidase electrochemical sensor into an implantable glucose-sensing device. *Diabetes Care*, *5*(3), 184-189.

13. Yu, J., Liu, S., & Ju, H. (2003). Glucose sensor for flow injection analysis of serum glucose based on immobilization of glucose oxidase in titania sol–gel membrane. *Biosensors and Bioelectronics*, *19*(4), 401-409.

14. Wisniewski, N., & Reichert, M. (2000). Methods for reducing biosensor membrane biofouling. *Colloids and Surfaces B: Biointerfaces*, *18*(3), 197-219.

15. Compton, R. G., Eklund, J. C., Page, S. D., Sanders, G. H., & Booth, J. (1994). Voltammetry in the presence of ultrasound. Sonovoltammetry and surface effects. *The Journal of Physical Chemistry*, *98*(47), 12410-12414.

16. Anderson, J. M., & Miller, K. M. (1984). Biomaterial biocompatibility and the macrophage. *Biomaterials*, *5*(1), 5-10.

17. Becker, L. K. W., Kleinsmith, L. J., & Hardin, J. (2002). *World of the Cell with Free Solutions*. Benjamin-Cummings Publishing Company.

18. Langmuir, I., & Blodgett, K. (1946). *A mathematical investigation of water droplet trajectories*. Army Air Forces Headquarters, Air Technical Service Command.

19. Singer, S. J., & Nicolson, G. L. (1972). The fluid mosaic model of the structure of cell membranes. *Landmark Papers in Cell Biology*, 296-307.3

20. Giancotti, F. G., & Ruoslahti, E. (1999). Integrin signaling. *Science*, *285*(5430), 1028-1033.

21. Guan, J. L., & Hynes, R. O. (1990). Lymphoid cells recognize an alternatively spliced segment of fibronectin via the integrin receptor, *Cell*, *60*(1), 53-61.

22. Ylänne, J., Huuskonen, J., O'Toole, T. E., Ginsberg, M. H., Virtanen, I., & Gahmberg, C. G. (1995). Mutation of the Cytoplasmic Domain of the Integrin Subunit differential effects on cell spreading, recruitment to adhesion plaques, endocytosis and phagocytosis. *Journal of Biological Chemistry*, *270*(16), 9550-9557.

23. Theoretical and Computational Biophysics group, NIH Centre for Macromolecular Modeling & Bioinformatics, University of Illinois at Urbana Campaign

24. Ulmer, J., Geiger, B., & Spatz, J. P. (2008). Force-induced fibronectin fibrillogenesis in vitro. *Soft Matter*, *4*(10), 1998-2007.

25. Ruoslahti, E., & Pierschbacher, M. D. (1987). New perspectives in cell adhesion: RGD and integrins. *Science (New York, NY)*, *238*(4826), 491.

26. Schubert, D., Heinemann, S., Carlisle, W., Tarikas, H., Kimes, B., Patrick, J., ... & Brandt, B. L. (1974). Clonal cell lines from the rat central nervous system. *Nature*, *249*(454), 224.

27. Sapelkin, A. V., Bayliss, S. C., Unal, B., & Charalambou, A. (2006). Interaction of B50 rat hippocampal cells with stain-etched porous silicon. *Biomaterials*, *27*(6), 842-846.

28. Jen, A. C., Wake, M. C., & Mikos, A. G. (1996). Review: Hydrogels for cell immobilization. *Biotechnology and Bioengineering*, *50*(4), 357-364.

29. Collaud, S., Warloe, T., Jordan, O., Gurny, R., & Lange, N. (2007). Clinical evaluation of bioadhesive hydrogels for topical delivery of hexylaminolevulinate to Barrett's esophagus. *Journal of Controlled Release*, *123*(3), 203-210.

30. Oxley, H. R., Corkhill, P. H., Fitton, J. H., & Tighe, B. J. (1993). Macroporous hydrogels for biomedical applications: methodology and morphology. *Biomaterials*, *14*(14), 1064-1072.

31. Awad, H. A., Quinn Wickham, M., Leddy, H. A., Gimble, J. M., & Guilak, F. (2004). Chondrogenic differentiation of adipose-derived adult stem cells in agarose, alginate, and gelatin scaffolds. *Biomaterials*, *25*(16), 3211-3222.

32. O'Connor, S. M., Stenger, D. A., Shaffer, K. M., & Ma, W. (2001). Survival and neurite outgrowth of rat cortical neurons in three-dimensional agarose and collagen gel matrices. *Neuroscience letters*, *304*(3), 189-193.

33. Nguyen, K. T., & West, J. L. (2002). Photopolymerizable hydrogels for tissue engineering applications. *Biomaterials*, *23*(22), 4307-4314.

34. Chang, P. L., Shen, N., & Westcott, A. J. (1993). Delivery of recombinant gene products with microencapsulated cells in vivo. *Human gene therapy*, *4*(4), 433-440.

35. Whistler, R. L. (1977). Hydrogels-synthetic and natural. *Journal of the Technical Association of the Pulp and Paper Industry*, *60*(12), 64-67.

36. Ramachandran, G. N., & Kartha, G. (1954). Structure of collagen.

37. Siegel, R. C., & Martin, G. R. (1970). Collagen cross-linking. *Journal of Biological Chemistry*, *245*(7), 1653-1658.

38. Chen, G., Ushida, T., & Tateishi, T. (2001). Development of biodegradable porous scaffolds for tissue engineering. *Materials Science and Engineering: C*, *17*(1), 63-69.

39. Laurent, T. C. (1970). Structure of hyaluronic acid. *Chemistry and molecular biology of the intercellular matrix*, *2*, 703-732.

40. Baier Leach, J., Bivens, K. A., Patrick Jr, C. W., & Schmidt, C. E. (2003). Photocrosslinked hyaluronic acid hydrogels: natural, biodegradable tissue engineering scaffolds. *Biotechnology and bioengineering*, *82*(5), 578-589.

41. Luo, Y., Kirker, K. R., & Prestwich, G. D. (2000). Cross-linked hyaluronic acid hydrogel films: new biomaterials for drug delivery. *Journal of Controlled Release*, *69*(1), 169-184.

42. Berger, J., Reist, M., Mayer, J. M., Felt, O., Peppas, N. A., & Gurny, R. (2004). Structure and interactions in covalently and ionically crosslinked chitosan hydrogels for biomedical applications. *European Journal of Pharmaceutics and Biopharmaceutics*, *57*(1), 19-34.

43. Arnott, S., Fulmer, A. S. W. E., Scott, W. E., Dea, I. C. M., Moorhouse, R., & Rees, D. A. (1974). The agarose double helix and its function in agarose gel structure. *Journal of molecular biology*, *90*(2), 269-284.

44. Sakai, S., Hashimoto, I., & Kawakami, K. (2007). Agarose–gelatin conjugate for adherent cell-enclosing capsules. *Biotechnology letters*, *29*(5), 731-735.

45. Geckil, H., Xu, F., Zhang, X., Moon, S., & Demirci, U. (2010). Engineering hydrogels as extracellular matrix mimics. *Nanomedicine*, *5*(3), 469-484.

46. Sreejalekshmi, K. G., & Nair, P. D. (2011). Biomimeticity in tissue engineering scaffolds through synthetic peptide modifications—Altering

chemistry for enhanced biological response. *Journal of Biomedical Materials Research Part A*, *96*(2), 477-491.

47. Crompton, K. E., Goud, J. D., Bellamkonda, R. V., Gengenbach, T. R., Finkelstein, D. I., Horne, M. K., & Forsythe, J. S. (2007). Polylysine-functionalised thermoresponsive chitosan hydrogel for neural tissue engineering. *Biomaterials*, *28*(3), 441-449.

48. Wichterle, O., & Lim, D. (1960). Hydrophilic gels for biological use.

49. Wichterle, O., Lim, D., & Dreifus, M. (1961). On the problem of contact lenses]. *Ceskoslovenská oftalmologie*, *17*, 70.

50. Montheard, J. P., Chatzopoulos, M., & Chappard, D. (1992). 2-Hydroxyethyl methacrylate (HEMA): chemical properties and applications in biomedical fields. *Journal of Macromolecular Science, Part C: Polymer Reviews*, *32*(1), 1-34.

51. Gursel, I., Balcik, C., Arica, Y., Akkus, O., Akkas, N., & Hasirci, V. (1998). Synthesis and mechanical properties of interpenetrating networks of polyhydroxybutyrate-co-hydroxyvalerate and polyhydroxyethyl methacrylate. *Biomaterials*, *19*(13), 1137-1143.

52. Abraham, S., Brahim, S., Ishihara, K., & Guiseppi-Elie, A. (2005). Molecularly engineered p (HEMA)-based hydrogels for implant biochip biocompatibility. *Biomaterials*, *26*(23), 4767-4778.

53. Abdur Rahman, A. R., Justin, G., & Guiseppi-Elie, A. (2009). Towards an implantable biochip for glucose and lactate monitoring using microdisc electrode arrays (MDEAs). *Biomedical microdevices*, *11*(1), 75-85.

54. Kotanen, C. N., & Guiseppi-Elie, A. (2012, August). Bioactive Electroconductive Hydrogels Yield Novel Biotransducers for Glucose. In

Macromolecular Symposia (Vol. 317, No. 1, pp. 187-197). WILEY-VCH Verlag.

55. Kotanen, C. N., Wilson, A. N., Wilson, A. M., Ishihara, K., & Guiseppi-Elie, A. (2012). Biomimetic hydrogels gate transport of calcium ions across cell culture inserts. *Biomedical microdevices*, 1-10.

56. Guiseppi-Elie, A., Dong, C., & Dinu, C. Z. (2012). Crosslink density of a biomimetic poly (HEMA)-based hydrogel influences growth and proliferation of attachment dependent RMS 13 cells. *Journal of Materials Chemistry*, *22*(37), 19529-19539.

57. Lehninger, A.L.; Nelson, D.L.; Cox, M.M. (2005). *Lehninger principles of biochemistry*. New York: W.H. Freeman.

58. Fersht, A. (1998). *Structure and mechanism in protein science: a guide to enzyme catalysis and protein folding*. WH Freeman.

59. Cornish-Bowden, A., & Cornish-Bowden, A. (1979). *Fundamentals of enzyme kinetics* (Vol. 73). London: Butterworths.

60. G Wohlfahrt, S Witt, J Hendle, D Schomburg, H M Kalisz, H J Hecht *Acta Crystallogr. Sect D* 1999, 55, 969

61. Mehmet Şenel, Cevdet Nergiz, Novel amperometric glucose biosensor based on covalent immobilization of glucose oxidase on poly(pyrrole propylic acid)/Au nanocomposite, Current Applied Physics, Volume 12, Issue 4, July 2012, Pages 1118-1124, ISSN 1567-1739, 10.1016/j.cap.2012.02.004.

62. Weibel, M. K., & Bright, H. J. (1971). The glucose oxidase mechanism interpretation of the pH dependence. *Journal of Biological Chemistry*, *246*(9), 2734-2744.

63. Nakane, P. K., & Watanabe, (1984). Distribution of oncodevelopmental markers in neoplastic cells: therapeutic implications. *Journal of Histochemistry & Cytochemistry*, *32*(8), 894-898.

64. Christofidou-Solomidou, M., Pietra, G. G., Solomides, C. C., Arguiris, E., Harshaw, D., Fitzgerald, G. A. & Muzykantov, V. R. (2000). Immunotargeting of glucose oxidase to endothelium in vivo causes oxidative vascular injury in the lungs. *American Journal of Physiology-Lung Cellular and Molecular Physiology*, *278*(4), L794-L805.

65. Lai, G., Yan, F., & Ju, H. (2009). Dual signal amplification of glucose oxidase-functionalized nanocomposites as a trace label for ultrasensitive simultaneous multiplexed electrochemical detection of tumor markers. *Analytical chemistry*, *81*(23), 9730-9736.

66. Pickup, J. C., Shaw, G. W., & Claremont, D. J. (1989). In vivo molecular sensing in diabetes mellitus: an implantable glucose sensor with direct electron transfer. *Diabetologia*, *32*(3), 213-217.

67. Bankar, S. B., Bule, M. V., Singhal, R. S., & Ananthanarayan, L. (2009). Glucose oxidase—an overview. *Biotechnology advances*, *27*(4), 489-501.

68. Rando, D., Kohring, G. W., & Giffhorn, F. (1997). Production, purification and characterization of glucose oxidase from a newly isolated strain of Penicillium pinophilum. *Applied microbiology and biotechnology*, *48*(1), 34-40.

69. Hecht, H. J., Kalisz, H. M., Hendle, J., Schmid, R. D., & Schomburg, D. (1993). Crystal Structure of Glucose Oxidase from Aspergillus niger Refined at 2· 3 Å Reslution. *Journal of molecular biology*, *229*(1), 153-172.

70. Kadish, A. H., Litle, R. L., & Sternberg, J. C. (1968). A new and rapid method for the determination of glucose by measurement of rate of oxygen consumption. *Clinical Chemistry*, *14*(2), 116-131.

71. Wolfbeis, O., Reisfeld, R., & Oehme, I. (1996). Sol-gels and chemical sensors. *Optical and Electronic Phenomena in Sol-Gel Glasses and Modern Application*, 51-98.

72. Witt, S., Singh, M., & Kalisz, H. M. (1998). Structural and Kinetic Properties of Nonglycosylated Recombinant Penicillium amagasakienseGlucose Oxidase Expressed in Escherichia coli. *Applied and environmental microbiology*, *64*(4), 1405-1411.

73. Re, R., Pellegrini, N., Proteggente, A., Pannala, A., Yang, M., & Rice-Evans, C. (1999). Antioxidant activity applying an improved ABTS radical cation decolorization assay. *Free Radical Biology and Medicine*, *26*(9), 1231-1237.

74. Karmali, P. P., & Simberg, D. (2011). Interactions of nanoparticles with plasma proteins: implication on clearance and toxicity of drug delivery systems. *Expert Opinion on Drug Delivery*, *8*(3), 343-357.

75. Fita, I., & Rossmann, M. G. (1985). The active center of catalase. *Journal of molecular biology*, *185*(1), 21-37.

76. Klotz, M. G., Klassen, G. R., & Loewen, P. C. (1997). Phylogenetic relationships among prokaryotic and eukaryotic catalases. *Molecular biology and evolution*, *14*(9), 951-958.

77. Chelikani, P., Fita, I., & Loewen, P. C. (2004). Diversity of structures and properties among catalases. *Cellular and molecular life sciences*, *61*(2), 192-208.

78. Margoliash, E., & Novogrodsky, A. (1958). A study of the inhibition of catalase by 3-amino-1: 2: 4-triazole. *Biochemical Journal*, *68*(3), 468.

79. Ho, Y. S., Xiong, Y., Ma, W., Spector, A., & Ho, D. S. (2004). Mice lacking catalase develop normally but show differential sensitivity to oxidant tissue injury. *Journal of Biological Chemistry*, *279*(31), 32804-32812.

80. Laszlo, G., Peter, R., & Aniko, P. (2004). Catalase enzyme mutations and their association with diseases. *Molecular Diagnosis*, *8*(3), 141-149.

81. Rao, P. S., Yamada, Y., & Leung, K. Y. (2003). A major catalase (KatB) that is required for resistance to H2O2 and phagocyte-mediated killing in Edwardsiella tarda. *Microbiology*, *149*(9), 2635-2644.

82. McCord JM, Fridovich I (1988). "Superoxide dismutase: the first twenty years (1968-1988)". *Free Radic. Biol. Med.* 5 (5–6): 363–9.

83. Antonyuk SV, Strange RW, Marklund SL, Hasnain SS (May 2009). "The structure of human extracellular copper-zinc superoxide dismutase at 1.7 A resolution: insights into heparin and collagen binding". *J. Mol. Biol.* 388 (2): 310–26.

84. Muller FL, Lustgarten MS, Jang Y, Richardson A, Van Remmen H (August 2007). "Trends in oxidative aging theories". *Free Radic. Biol. Med.* 43 (4): 477–503.

85. Van Remmen H, Ikeno Y, Hamilton M, Pahlavani M, Wolf N, Thorpe SR, Alderson NL, Baynes JW, Epstein CJ, Huang TT, Nelson J, Strong R, Richardson A (December 2003). Life-long reduction in MnSOD activity results in increased DNA damage and higher incidence of cancer but does not accelerate aging. *Physiol. Genomics* 16 (1): 29–37.

86. Zelko IN, Mariani TJ, Folz RJ (2003). Superoxide dismutase multigene family: a comparison of the CuZn-SOD (SOD1), Mn-SOD (SOD2), and EC-SOD (SOD3) gene structures, evolution, and expression. *Free Radic. Biol. Med.* 33 (3): 337–49.

87. Bickerstaff, G. F. (1997). *Immobilization of enzymes and cells*.

88. Woodward, J. (Ed.). (1985). *Immobilised cells and enzymes: a practical approach*. IRL press.

89. Chibata, I., Tosa, T., & Shibatani, T. (1992). The industrial production of optically active compounds by immobilized biocatalysts. *Chirality in Industry*, *19*, 351-370.

90. Sheldon, R. A. (2007). Enzyme immobilization: the quest for optimum performance. *Advanced Synthesis & Catalysis*, *349*(8-9), 1289-1307.

91. Garcia, G. A., & Goodenough-Lashua, D. M. (1998). Mechanisms of RNA-modifying and-editing enzymes. *Modification and Editing of RNA*, 135-168.

92. Mao, L. C., Xu, Y. Q., & Que, F. (2007). Maintaining the quality of sugarcane juice with blanching and ascorbic acid. *Food chemistry*, *104*(2), 740-745.

93. Li, S., Hu, J., & Liu, B. (2004). Use of chemically modified PMMA microspheres for enzyme immobilization. *Biosystems*, *77*(1), 25-32.

94. Garcia III, A., Oh, S., & Engler, C. R. (1989). Cellulase immobilization on Fe3O4 and characterization. *Biotechnology and bioengineering*, *33*(3), 321-326.

95. Pollak, A., Blumenfeld, H., Wax, M., Baughn, R. L., & Whitesides, G. M. (1980). Enzyme immobilization by condensation copolymerization into crosslinked polyacrylamide gels. *Journal of the American Chemical Society*, *102*(20), 6324-6336.

96. Cosnier, S. (1999). Biomolecule immobilization on electrode surfaces by entrapment or attachment to electrochemically polymerized films. A review. *Biosensors and Bioelectronics*, *14*(5), 443-456.

97. Anwar, A., Qader, S. A. U., Raiz, A., Iqbal, S., & Azhar, A. (2009). Calcium alginate: A support material for immobilization of proteases from newly isolated strain of Bacillus subtilis KIBGE-HAS. *World Appl Sci J*, *7*(10), 1281-6.

98. Chang, T. (1971). Stablisation of enzymes by microencapsulation with a concentrated protein solution or by microencapsulation followed by cross-linking with glutaraldehyde. *Biochemical and biophysical research communications*, *44*(6), 1531-1536.

99. Caruso, F., Trau, D., Möhwald, H., & Renneberg, R. (2000). Enzyme encapsulation in layer-by-layer engineered polymer multilayer capsules. *Langmuir*, *16*(4), 1485-1488.

100. Betancor, L., & Luckarift, H. R. (2008). Bioinspired enzyme encapsulation for biocatalysis. *Trends in biotechnology*, *26*(10), 566-572.

101. Wang, Y., & Caruso, F. (2004). Enzyme encapsulation in nanoporous silica spheres. *Chemical Communications*, (13), 1528-1529.

102. McDowell, E. M., & Trump, B. F. (1976). Histologic fixatives suitable for diagnostic light and electron microscopy. *Archives of pathology & laboratory medicine*, *100*(8), 405.

103. Migneault, I., Dartiguenave, C., Bertrand, M. J., & Waldron, K. C. (2004). Glutaraldehyde: behavior in aqueous solution, reaction with proteins, and application to enzyme crosslinking. *BioTechniques*, *37*(5), 790-806.

104. Bigi, A., Cojazzi, G., Panzavolta, S., Rubini, K., & Roveri, N. (2001). Mechanical and thermal properties of gelatin films at different degrees of glutaraldehyde crosslinking. *Biomaterials*, *22*(8), 763-768.

105. Cheung, D. T., Perelman, N., Ko, E. C., & Nimni, M. E. (1985). Mechanism of crosslinking of proteins by glutaraldehyde III. Reaction with collagen in tissues. *Connective tissue research*, *13*(2), 109-115.

106. Yonath, A., Sielecki, A., Moult, J., Podjarny, A., & Traub, W. (1977). Crystallographic studies of protein denaturation of renaturation. 1. Effects of denaturants on volume and x-ray pattern of crosslinked triclinic lysozyme crystals. *Biochemistry*, *16*(7), 1413-1417.

107. Kowal, R., & Parsons, R. G. (1980). Stabilization of proteins immobilized on Sepharose from leakage by glutaraldehyde crosslinking. *Analytical biochemistry*, *102*(1), 72-76.

108. Lowe, C. R. (1985). An introduction to the concepts and technology of biosensors. *BIOSENSORS.*, *1*(1), 3-16.

109. McArthur, K. T., Clark, L. C., Lyons, C., & Edwards, S. (1962). Continuous recording of blood oxygen saturation in open-heart operations. *Surgery*, *51*(Jan), 121-126.

110. Guilbault, G. G., & Montalvo Jr, J. G. (1969). Urea-specific enzyme electrode. *Journal of the American Chemical Society*, *91*(8), 2164-2165.

111. Davis, G. (1985). Electrochemical techniques for the development of amperometric biosensors. *Biosensors*, *1*(2), 161-178.

112. Shichiri M, Kawamori R, Yamasaki Y, Hakui N, Abe H. Wearable Artificial Endocrine Pancreas with Needle-type Glucose Sensor. Lancet 1982; 20: 1129 – 1131.

113. Wilkins E, Atanasov P. Glucose Monitoring: State of the Art and Future Possibilities. Med. Eng. Phys. 1996; 18: 273 – 288.

114. Cass, A. E., Davis, G., Green, M. J., & Hill, H. A. O. (1985). Ferricinium ion as an electron acceptor for oxido-reductases. *Journal of electroanalytical chemistry and interfacial electrochemistry*, *190*(1), 117-127.

115. Judge, K., Morrow, L., Lastovich, A. G., Kurisko, D., Keith, S. C., Hartsell, J., ... & Hompesch, M. (2011). Continuous glucose monitoring using a novel glucose/galactose binding protein: results of a 12-hour feasibility study with the becton dickinson glucose/galactose binding protein sensor. *Diabetes Technology & Therapeutics*, *13*(3), 309-317.

116. Wisniewski, N., & Reichert, M. (2000). Methods for reducing biosensor membrane biofouling. *Colloids and Surfaces B: Biointerfaces*, *18*(3), 197-219.

117. Anastasova, S., Spehar-Délèze, A. M., & Vadgama, P. (2012). Oxygen Detection Using Different Types of Membranes Deposited on Needle Based Platforms. *ECS Transactions*, *41*(20), 43-48.

118. Maines, A., Ashworth, D., & Vadgama, P. (1996). Enzyme electrodes for food analysis. *Food Technology and Biotechnology*, *34*(1).

119. Rong, Z., Cheema, U., & Vadgama, P. (2006). Needle enzyme electrode based glucose diffusive transport measurement in a collagen gel and validation of a simulation model. *Analyst*, *131*(7), 816-821.

120. Pfeiffer, D., Möller, B., Klimes, N., Szeponik, J., & Fischer, S. (1997). Amperometric lactate oxidase catheter for real-time lactate

monitoring based on thin film technology. *Biosensors and Bioelectronics*, *12*(6), 539-550.

121. Wilson, G. S., Bindra, D. S., Hill, B. S., Thevenot, D. R., Sternberg, R., Reach, G., & Zhang, Y. (1992). *U.S. Patent No. 5,165,407*. Washington, DC: U.S. Patent and Trademark Office.

122. Chen, C. Y., Gotoh, M., Makino, H., Su, Y. C., Tamiya, E., & Karube, I. (1992). Amperometric needle-type glucose sensor based on a modified platinum electrode with diminished response to interfering materials. *Analytica chimica acta*, *265*(1), 5-14.

123. Moussy, F., Harrison, D. J., & Rajotte, R. V. (1994). A miniaturized Nafion-based glucose sensor: in vitro and in vivo evaluation in dogs. *International Journal of Artificial Organs*, *17*(2), 88-99.

124. Rong, Z., Leitao, E., Popplewell, J., Alp, B., & Vadgama, P. (2008). Needle Enzyme Electrode for Lactate Measurement. *Sensors Journal, IEEE*, *8*(1), 113-120.

125. Kamholz, A. E., Schilling, E. A. & Yager, P. Optical measurement of transverse molecular diffusion in a microchannel. Biophysical Journal 80, 1967-1972 (2001).

126. Whitesides, G. M. (2006). The origins and the future of microfluidics. *Nature*, *442*(7101), 368-373.

127. Dittrich, P. S., & Manz, A. (2006). Lab-on-a-chip: microfluidics in drug discovery. *Nature Reviews Drug Discovery*, *5*(3), 210-218.

128. Srinivasan, V., Pamula, V. K., & Fair, R. B. (2004). An integrated digital microfluidic lab-on-a-chip for clinical diagnostics on human physiological fluids. *Lab Chip*, *4*(4), 310-315.

129. Ziaie, B., Baldi, A., Lei, M., Gu, Y., & Siegel, R. A. (2004). Hard and soft micromachining for BioMEMS: review of techniques and examples of applications in microfluidics and drug delivery. *Advanced Drug Delivery Reviews*, *56*(2), 145-172.

130. Gargiuli, J., Shapiro, E., Gulhane, H., Nair, G., Drikakis, D., & Vadgama, P. (2006). Microfluidic systems for in situ formation of nylon 6, 6 membranes. *Journal of membrane science*, *282*(1), 257-265.

131. Lion, N., Rohner, T. C., Dayon, L., Arnaud, I. L., Damoc, E., Youhnovski, N., ... & Girault, H. H. (2003). Microfluidic systems in proteomics. *Electrophoresis*, *24*(21), 3533-3562.

132. Seong, G. H., Heo, J., & Crooks, R. M. (2003). Measurement of enzyme kinetics using a continuous-flow microfluidic system. *Analytical chemistry*, *75*(13), 3161-3167.

133. Song, H., Chen, D. L., & Ismagilov, R. F. (2006). Reactions in droplets in microfluidic channels. *Angewandte chemie international edition*, *45*(44), 7336-7356.

134. Whitesides, G. M., & Stroock, A. D. (2001). Flexible methods for microfluidics. *Physics today*, *54*, 42.

135. Zimmerman, W. B. J. (2006). Microfluidics: History. *Theory and Applications*.

136. Inglis, D. W., Riehn, R., Sturm, J. C., & Austin, R. H. (2006). Microfluidic high gradient magnetic cell separation. *Journal of Applied Physics*, *99*(8), 08K101-08K101.

137. Hansen, C. L., Skordalakes, E., Berger, J. M., & Quake, S. R. (2002). A robust and scalable microfluidic metering method that allows protein

crystal growth by free interface diffusion. *Proceedings of the National Academy of Sciences*, *99*(26), 16531-16536.

138. Kamholz, A. E., Weigl, B. H., Finlayson, B. A., & Yager, P. (1999). Quantitative analysis of molecular interaction in a microfluidic channel: the T-sensor. *Analytical Chemistry*, *71*(23), 5340-5347.

139. Regehr, K. J., Domenech, M., Koepsel, J. T., Carver, K. C., Ellison-Zelski, S. J., Murphy, W. L., ... & Beebe, D. J. (2009). Biological implications of polydimethylsiloxane-based microfluidic cell culture. *Lab Chip*, *9*(15), 2132-2139.

140. Purcell, E. M. (1977). Life at low Reynolds number. *Am. J. Phys*, *45*(1), 3-11.

141. Collins, R. E. (1961). Flow of fluids through porous materials.

142. Brody, J. P., & Yager, P. (1997). Diffusion-based extraction in a microfabricated device. *Sensors and Actuators A: Physical*, *58*(1), 13-18.

143. Chan, E. Y., Goncalves, N. M., Haeusler, R. A., Hatch, A. J., Larson, J. W., Maletta, A. M., ... & Gilmanshin, R. (2004). DNA mapping using microfluidic stretching and single-molecule detection of fluorescent site-specific tags. *Genome research*, *14*(6), 1137-1146.

144. Beebe, D. J., Mensing, G. A., & Walker, G. M. (2002). Physics and applications of microfluidics in biology. *Annual review of biomedical engineering*, *4*(1), 261-286.

145. Satyanarayana, S., Karnik, R. N., & Majumdar, A. (2005). Stamp-and-stick room-temperature bonding technique for microdevices. *Microelectromechanical Systems, Journal of*, *14*(2), 392-399.

146. Jia, Z. J.; Fang, Q.; Fang, Z. L. Anal. Chem. 2004, 76, 5597-5602

147. Xia, Y., & Whitesides, G. M. (1998). Soft lithography. *Annual review of materials science*, *28*(1), 153-184.

148. Leclerc, E., Sakai, Y., & Fujii, T. (2003, January). A multi-layer PDMS microfluidic device for tissue engineering applications. In *Micro Electro Mechanical Systems, 2003. MEMS-03 Kyoto. IEEE The Sixteenth Annual International Conference on* (pp. 415-418). IEEE.

149. Fujii, T. (2002). PDMS-based microfluidic devices for biomedical applications. *Microelectronic Engineering*, *61*, 907-914.

150. Tirrell, M. (1996). Measurement of interfacial energy at solid polymer surfaces. *Langmuir*, *12*(19), 4548-4551.

151. MacDonald, J.C.; Duffy, D.C.; Anderson, J.R,; Chui, D.T,; Wu, H.; Schueller, O.J.A.; Whitesides, G.M. Fabrication of Microfluidic sytems in Poly(dimethylsiloxane). Electrophoresis 2000, 21, 27-40

152. Chiu, D. T., Jeon, N. L., Huang, S., Kane, R. S., Wargo, C. J., Choi, I. S., ... & Whitesides, G. M. (2000). Patterned deposition of cells and proteins onto surfaces by using three-dimensional microfluidic systems. *Proceedings of the National Academy of Sciences*, *97*(6), 2408-2413.

153. G. Kyriacou, P. Vadgama, W.Wang, Characterization of a laminar flow cell for the prevention of biosensor fouling. J. Medical Engineering & Physics, 2006, 28, 989- 998

154. Ishihara, K., Ueda, T., & Nakabayashi, N. (1990). Preparation of phospholipid polymers and their properties as polymer hydrogel membranes. *Polymer Journal*, *22*(5), 355-360.

155. Ahmed, S., Dack, C., Farace, G., Rigby, G., & Vadgama, P. (2005). Tissue implanted glucose needle electrodes: early sensor stabilisation and

achievement of tissue-blood correlation during the run in period. *Analytica chimica acta*, *537*(1), 153-161.

156. Kacanovska, A., Rong, Z., Schmidt, M., Russell, P. S. J., & Vadgama, P. (2010). Bio-sensing using recessed gold-filled capillary amperometric electrodes. *Analytical and bioanalytical chemistry*, *398*(4), 1687-1694.

157. Eichenmüller, M., Hemmerlein, B., Von Schweinitz, D., & Kappler, R. (2010). Betulinic acid induces apoptosis and inhibits hedgehog signalling in rhabdomyosarcoma. *British journal of cancer*, *103*(1), 43-51.

158. Gurney, M. E., Pu, H., Chiu, A. Y., Dal Canto, M. C., Polchow, C. Y., Alexander, D. D., ... & Siddique, T. (1994). Motor neuron degeneration in mice that express a human Cu, Zn superoxide dismutase mutation. *Science New York then Washington*, 1772-1772.

159. Cookson, M. R., Ince, P. G., & Shaw, P. J. (1998). Peroxynitrite and Hydrogen Peroxide Induced Cell Death in the NSC34 Neuroblastoma× Spinal Cord Cell Line: Role of Poly (ADP-Ribose) Polymerase. *Journal of neurochemistry*, *70*(2), 501-508.

160. O'Brien J, Wilson I, Orton T, Pognan F. Investigation of the Alamar Blue (resazurin) fluorescent dye for the assessment of mammalian cell cytotoxicity. Eur J Biochem 2000;267:5421–6.

161. Zhang HX, Du GH, Zhang JT. Assay of mitochondrial functions by resazurin in vitro. Acta Pharmacol Sin 2004;25:385–9.

162. Maeda, H., Matsu-Ura, S., YAMAUCHI, Y., & OHMORI, H. (2001). Resazurin as an Electron Acceptor in Glucose Oxidase-Catalyzed Oxidation of Glucose. *Chemical and pharmaceutical bulletin*, *49*(5), 622-625.

163. Strober, W. (2001). Trypan blue exclusion test of cell viability. *Current Protocols in Immunology*, A-3B.

164. Using a Hemacytometer, Cascade biologics Inc. Doc107.0

165. Chang, H., Khan, R., Rong, Z., Sapelkin, A., & Vadgama, P. (2010). Study of albumin and fibrinogen membranes formed by interfacial crosslinking using microfluidic flow. *Biofabrication*, *2*(3), 035002.

166. Rubartelli, A., & Lotze, M. T. (2007). Inside, outside, upside down: damage-associated molecular-pattern molecules (DAMPs) and redox. *Trends in immunology*, *28*(10), 429-436.

167. Badylak, S. F., & Gilbert, T. W. (2008, April). Immune response to biologic scaffold materials. In *Seminars in immunology* (Vol. 20, No. 2, pp. 109-116). Academic Press.

168. O'Brien, J., Wilson, I., Orton, T., & Pognan, F. (2003). Investigation of the Alamar Blue (resazurin) fluorescent dye for the assessment of mammalian cell cytotoxicity. *European Journal of Biochemistry*, *267*(17), 5421-5426.

169. Anoopkumar-Dukie, S., Carey, J. B., Conere, T., O'sullivan, E., Van Pelt, F. N., & Allshire, A. (2005). Resazurin assay of radiation response in cultured cells. *British journal of radiology*, *78*(934), 945-947.

170. Satoh, T., Sakai, N., Enokido, Y., Uchiyama, Y., & Hatanaka, H. (1996). Free radical-independent protection by nerve growth factor and Bcl-2 of PC12 cells from hydrogen peroxide-triggered apoptosis. *Journal of biochemistry*, *120*(3), 540-546.

171. Schneiderman, G., & Goldstick, T. K. (1978). Oxygen electrode design criteria and performance characteristics: recessed cathode. *Journal of applied physiology*, *45*(1), 145-154.

172. Yoon, K., Kim, K., Wang, X., Fang, D., Hsiao, B. S., & Chu, B. (2006). High flux ultrafiltration membranes based on electrospun nanofibrous PAN scaffolds and chitosan coating. *Polymer*, *47*(7), 2434-2441.

173. Widmer, M. S., & Mikos, A. G. (1998). *Fabrication of biodegradable polymer scaffolds for tissue engineering* (pp. 107-120). Elsevier Sciences: New York.

174. Riboldi, S. A., Sampaolesi, M., Neuenschwander, P., Cossu, G., & Mantero, S. (2005). Electrospun degradable polyesterurethane membranes: potential scaffolds for skeletal muscle tissue engineering. *Biomaterials*, *26*(22), 4606-4615.

175. Tanaka, M., & Sackmann, E. (2005). Polymer-supported membranes as models of the cell surface. *Nature*, *437*(7059), 656-663.

176. J. Raedler, E. Sackmann, (1998).Functionalization of solids by ultrathin soft polymer films and polymer/lipid film composites: modelling of cell surfaces and cell recognition processes Curr. Opin. Solid State Mater. Sci., 2, pp. 330–336

177. Berti, W. R., Wolstenholme, B. W., Kozlowski, J. J., Sobocinski, R. L., & Freerksen, R. W. (2006). Hydrolytic stability of terephthaloyl chloride and isophthaloyl chloride. *Environmental science & technology*, *40*(20), 6330-6335.

178. Lasch, J., & Koelsch, R. (2008). Enzyme Leakage and Multipoint Attachment of Agarose-Bound Enzyme Preparations. *European Journal of Biochemistry*, *82*(1), 181-186.

179. Whittemore, E. R., Loo, D. T., Watt, J. A., & Cotman, C. W. (1995). A detailed analysis of hydrogen peroxide-induced cell death in primary neuronal culture. *Neuroscience*, *67*(4), 921.

180. Barnham, K. J., Masters, C. L., & Bush, A. I. (2004). Neurodegenerative diseases and oxidative stress. *Nature Reviews Drug Discovery*, *3*(3), 205-214.

181. Trivić, S., Leskovac, V., Zeremski, J., Vrvić, M., & Winston, G. W. (2002). Bioorganic mechanisms of the formation of free radicals catalyzed by glucose oxidase. *Bioorganic chemistry*, *30*(2), 95-106.

182. Sarvazyan, N., Askari, A., Klevay, L. M., & Huang, W. H. (1995). Role of intracellular SOD in oxidant-induced injury to normal and copper-deficient cardiac myocytes. *American Journal of Physiology-Heart and Circulatory Physiology*, *268*(3), H1115-H1121.

183. Ozyilmaz, G., & Tukel, S. S. (2007). Simultaneous co-immobilization of glucose oxidase and catalase in their substrates. *Applied Biochemistry and Microbiology*, *43*(1), 29-35.

184. Sigma Aldrich & Co.

185. Block, E. R. (1991). Hydrogen peroxide alters the physical state and function of the plasma membrane of pulmonary artery endothelial cells. *Journal of cellular physiology*, *146*(3), 362-369.

186. Elmore, S. (2007). Apoptosis: a review of programmed cell death. *Toxicologic pathology*, *35*(4), 495-516.

187. Faith, R. E., Luster, M. I., & Kimmel, C. A. (1979). Effect of chronic developmental lead exposure on cell-mediated immune functions. *Clinical and experimental immunology*, *35*(3), 413.

188. Wang, G., Xu, J. J., Chen, H. Y., & Lu, Z. H. (2003). Amperometric hydrogen peroxide biosensor with sol–gel/chitosan network-like film as immobilization matrix. *Biosensors and Bioelectronics*, *18*(4), 335-343.

189. Setford, S. J., & Newman, J. D. Enzyme biosensors. *Microbial Enzymes and Biotransformations (2004)*.

190. Lowry, J. P., & O'Neill, R. D. (1992). Homogeneous mechanism of ascorbic acid interference in hydrogen peroxide detection at enzyme-modified electrodes. *Analytical chemistry*, *64*(4), 453-456.

191. Benmakroha, Y., Christie, I., Desai, M., & Vadgama, P. (1996). Poly (vinyl chloride), polysulfone and sulfonated polyether-ether sulfone composite membranes for glucose and hydrogen peroxide perm-selectivity in amperometric biosensors. *Analyst*, *121*(4), 521-526.

192. Garjonyte, R., & Malinauskas, A. (1999). Amperometric glucose biosensor based on glucose oxidase immobilized in poly phenylenediamine layer. *Sensors and Actuators B: Chemical*, *56*(1), 85-92.

193. Iwata, E., Miyazaki, I., Asanuma, M., Iida, A., & Ogawa, N. (1998). Protective effects of nicergoline against hydrogen peroxide toxicity in rat neuronal cell line. *Neuroscience letters*, *251*(1), 49-52.

194. Bayr, H. (2005). Reactive oxygen species. *Critical care medicine*, *33*(12), S498-S501.

195. Hu, J., Tarasov, V., Agarwal, A., Kimerling, L., Carlie, N., Petit, L., & Richardson, K. (2007). Fabrication and testing of planar chalcogenide waveguide integrated microfluidic sensor. *Opt. Express*, *15*(5), 2307-2314.

196. Srinivasan, V., Pamula, V. K., & Fair, R. B. (2004). An integrated digital microfluidic lab-on-a-chip for clinical diagnostics on human physiological fluids. *Lab Chip*, *4*(4), 310-315.

Appendix

Publications

Chang, H., Khan, R., Rong, Z., Sapelkin, A., & Vadgama, P. (2010). Study of albumin and fibrinogen membranes formed by interfacial crosslinking using microfluidic flow. *Biofabrication*, *2*(3), 035002.

Khan, R, Guiseppi-Elie, A, Vadgama P, Hydrogel encapsulated Glucose Oxidase: effect on cell viability (In submission)

Presentations / Abstracts

- School of engineering and materials science (QMUL) research showcase (2008-2011)
- BMES Annual Meeting 2010 – Austin Texas
- ICCA-LRI & Health Canada Workshop June 2011 - Québec City